M. D

WASHINGTON UNIVERSITY
SEVER INSTITUTE OF TECHNOLOGY

MODELING THE PROCESS CYCLE OF THERMOPLASTIC COMPOSITES WITH EXPERIMENTAL VERIFICATION

by

IN SEON YOON

Prepared under the direction of

Professors J.L.Kardos & M.P. Duduković

A dissertation presented to the Sever Institute of
Washington University in partial fulfillment
of the requirements for the degree of

DOCTOR OF SCIENCE

May, 1990

Saint Louis, Missouri

WASHINGTON UNIVERSITY
SEVER INSTITUTE OF TECHNOLOGY

ABSTRACT

MODELING THE PROCESS CYCLE OF THERMOPLASTIC COMPOSITES WITH EXPERIMENTAL VERIFICATION

by In Seon Yoon

ADVISORS: Professors J.L. Kardos & M.P. Duduković

May, 1990

Saint Louis, Missouri

The formation of voids and undesirable resin content gradients within composite laminates ha~~s~~ve been repeatedly recognized as ~~a~~ limitations to the widespread application of this material to aircraft structures. Avoidance of these problems clearly requires a thorough understanding of the basic phenomena, which can help build a master model to control and optimize the manufacturing process.

This study is focused on experimental verification of two important submodels of the master model for the processing of thermoplastic polyimide composite materials. These include: 1) devolatilization with heat transfer, 2) resin flow during consolidation of the prepreg. The devolatilization model is experimentally verified by measuring the total and component volatile fluxes out of the laminates. The resin flow model based on soil consolidation theory is also verified with resin pressure measurements using miniature pressure transducers. The phenomenon of crack formation and healing is addressed and examined with optical microscopy studies.

TABLE OF CONTENTS

LIST OF FIGURES

MODELING THE PROCESS CYCLE OF THERMOPLASTIC COMPOSITES WITH EXPERIMENTAL VERIFICATION

1. INTRODUCTION

Continuous fiber thermoset composites made mainly from epoxies have been used extensively for aerospace applications. However, they have some inherent deficiencies. These include limited shelf life, low toughness, sensitivity to solvent, and lack of reprocessability. Also they usually perform poorly when subjected to out-of-plane loads.

One of the major needs of the aerospace composites industry in recent years has been the development of a matrix resin which would be significantly tougher and could tolerate exposure to higher temperatures than the brittle epoxies. This is necessary to meet the requirements of damage tolerance and high temperature stability for high performance laminates. A second goal of the aerospace industry is the development of lower cost fabrication techniques. Suitable for this purpose is a prepreg with the thermoplastic matrix resin because of the simplicity of the process and reprocessability of the molded parts [1] *.

---

*The numbers in brackets in the text indicate references in the Bibliography.

One polymer which can meet the requirements described above is a thermoplastic polyimide such as K-polymer [2]. Carbon fiber reinforced laminates based on K-polymer impregnated tape have been shown to have good strength, impact damage tolerance, and environmental resistance.

The most-used production process for fabrication of high performance structural laminates is the autoclave/vacuum degassing (AC/VD) laminating process. In this process, individual prepreg plies are laid up in a prescribed orientation to form a laminate. The laminate is laid against a smooth tool surface and covered with successive layers of release cloth, glass bleeder fabric, occasionally a caul plate, combination glass breather cloths, and finally a vacuum bag. A typical entire sandwich is shown schematically in Figure 1.1 for a unidirectional laminate. Autoclave pressure is applied from the vertical direction to the plane of the laminate through a caul plate. Bleeder bag pressure is applied through ports located within the space enclosed by the bag.

In fabricating the thermoplastic polyimide composite, there are two major processes. One is devolatilization and the other consolidation.

The devolatilization process is absolutely necessary because the polyimide composite is produced in situ by the reaction of an aromatic diethylester diacid with an aromatic diamine dissolved in a high-boiling solvent such as N-methyl-2-pyrrolidone (NMP). One particular combination results in Avimid K-III (Trademark of Du Pont Co.) polyimide. It should be noted that the solvent such as NMP must be removed to fabricate the high performance composite. With the evolution of volatile condensation by-products such as ethanol and water, the formation of the imide linkage occurs. It is difficult to remove volatile components

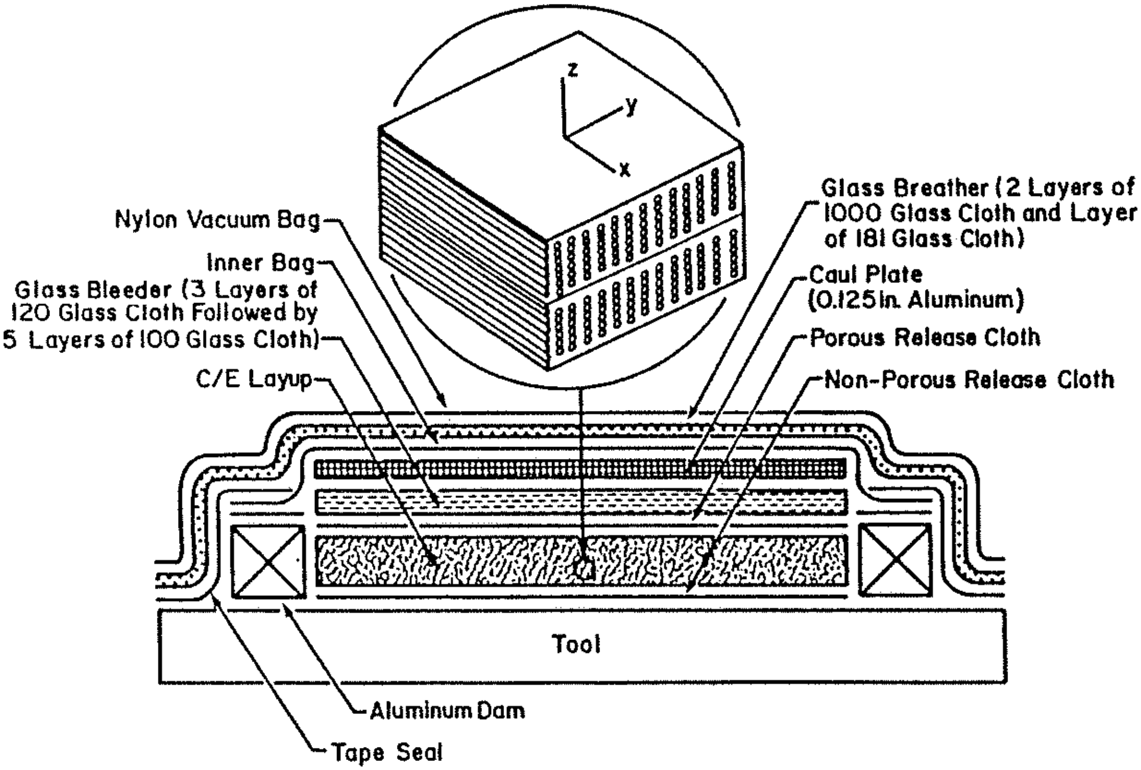

Figure 1.1: Schematic of a laminate lay-up. Insert shows a microscopic view of the fiber orientation within the laminate.

at once which causes formation of voids. The multiple volatiles evolved as a result of reaction also make the control of the devolatilization process complicated. It is emphasized that the devolatilization process is related to void formation which badly degrades the mechanical performance of the part. Therefore, one cannot prepare void-free composites unless the devolatilization process is fully-understood and well-controlled. All voids must be eliminated before the process cycle ends.

The consolidation process is described as follows: An external load transverse to the laminate plane is applied during the process cycle. The applied pressure is intended to squeeze air or volatiles and resin out, to minimize the void content, and to make uniform the fiber volume fraction distribution in the laminate. Also, the applied load is selected together with the shape of the tool and surface materials to determine the final dimensions and surface finish of the molded part. The magnitude of the applied pressure affects the quality of the finished product. This process is called consolidation.

In order to fabricate a composite of high quality, a model describing the entire process (so-called master model) is required for understanding and controlling the polymerization process. Figure 1.2 depicts the development of a state-of-the-art manufacturing process for structural composite parts. The first step in developing an optimized process would be the establishment of a master process model. Then, combining with a process simulator and sensors interfaced with the process, one would be able to optimize and real-time control the manufacturing process. The master model includes submodels involving kinetics, viscosity, devolatilization, heat transfer, resin flow (consolidation), and void formation and growth. The master model can be used to establish the relations between process cycle parameters and the presence or absence of voids as well as the residual resin

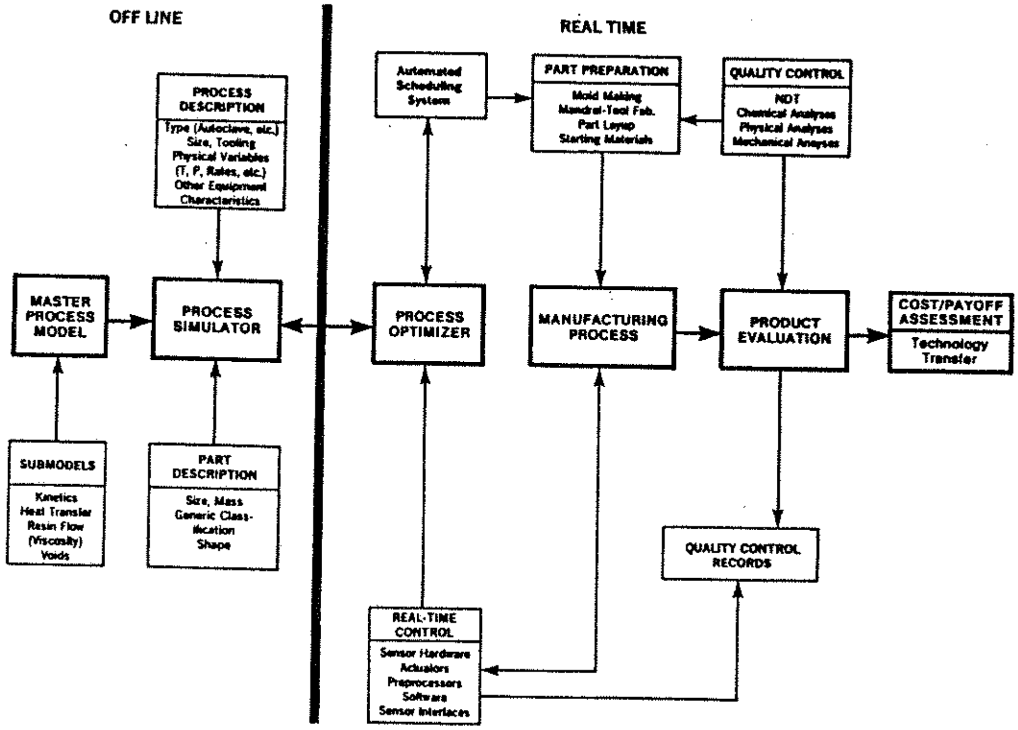

Figure 1.2: Development of a state-of-the-art manufacturing process for advanced composite materials.

content.

A submodel for describing the devolatilization of thermoplastic polyimide composites has been proposed. Also, a submodel for the consolidation process (i.e., resin flow model) has been proposed using soil consolidation theory [3, 4].

In this study, the problems of devolatilization and consolidation of thermoplastic polyimide composites are addressed in terms of modeling and experimental verification of the proposed models.

objectives ?

2. BACKGROUND

2.1. DEVOLATILIZATION

The devolatilization model for the thermoplastic polyimide composite has been proposed as a submodel and is explained in the following sections.

2.1.1. Physical Situation

Figure 2.1 illustrates the configuration of a three-phase system which is considered as a model of the Avimid K-III composite material. An inert, rigid, solid phase, represented as the σ phase, is surrounded by both gas and liquid phases. These are identified as the γ and β phase, respectively. It is assumed that the gas phase is continuous throughout the composite during the devolatilization step. This assumption is based on the phenomenon of crack formation which will be discussed later.

The transport of heat, mass, and momentum in the system shown in Figure 2.1 can be described by the appropriate laws of continuum physics. Although we can not solve the complete transport equations because of the complex unknown geometry exhibited by any porous medium, we can apply the theory of heat and mass transfer to the K-III composite system and can obtain solvable equations

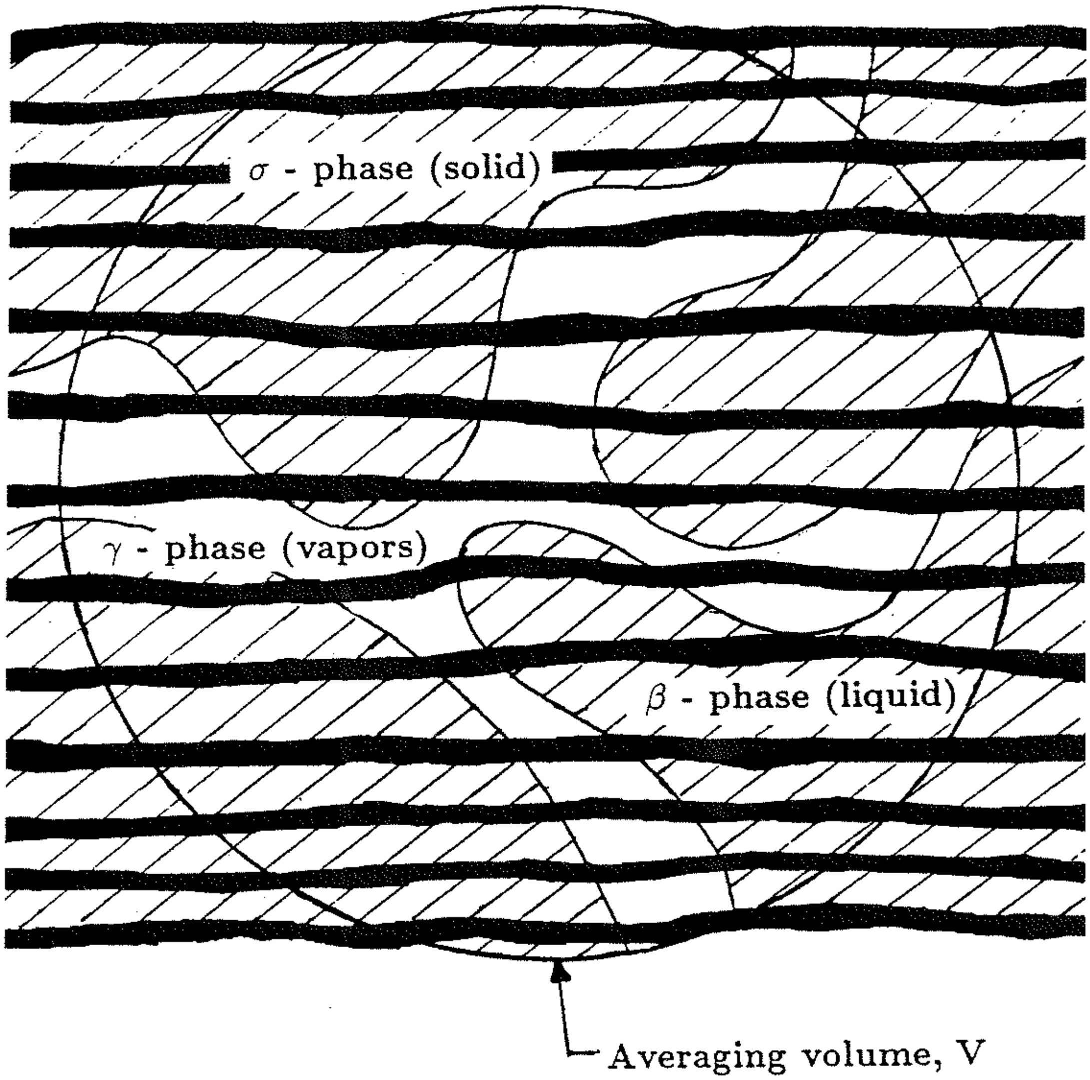

Figure 2.1: A model of the Avimid K-III thermoplastic composite material

by the method of volume averaging [5]. The volume averaging provides a formal route from the point equations, which are applicable in discontinuous regions, to the volume averaged equations, which are valid for the continuous representation of the composite material.

2.1.2. Development of the Model Equations

The following mathematical model can be applied only to the early stage of devolatilization. First, the basic equations of mass, momentum, and energy transport are established as the governing point equations. The volume-averaging method [5] is then used to get a tractable model of heat and mass transport in the K-III composite system.

The following unsteady state, one-dimensional forms of energy, mass, and momentum transport equations are obtained for the devolatilization of the thermoplastic material.

Energy Equation. It is assumed that local thermal equilibrium exists among the phases at each point in order to develop the energy transport equation. This makes a heat transfer model between fluid (resin) and solid (fiber) unnecessary and provides an unambiguous definition of the temperature at a given point.

$$\rho_m C_{pm}\frac{\partial T}{\partial t} + \rho_\gamma C_{p\gamma} V_\gamma \frac{\partial T}{\partial x} + \sum_{i=1}^{3} \Delta H_{vap,i}\dot{m}_i = k_{eff}\frac{\partial^2 T}{\partial x^2} \qquad (2.1)$$

$$I.C. \quad t = 0, \quad T = T_0 \;\; for \;\; all \;\; x \qquad (2.2)$$

$$B.C.\ 1 \quad x = 0, \quad T = T_0(t) \qquad (2.3)$$

$$B.C.\ 2 \quad x = L, \quad -k_{eff}\frac{\partial T}{\partial x} = h(T - T_\infty) \qquad (2.4)$$

Equation (2.1) represents the conservation of energy in the composite. The first term on the left-hand side of equation (2.1) accounts for the rate of change of internal energy per unit volume. The second term is the convective thermal transport of gases through the composite. The third term is energy loss due to the evaporation of the volatile species. The right-hand side of equation (2.1) accounts for the heat transport by thermal conduction.

Two boundary conditions are needed at the composite surfaces. Equation (2.3) represents the heating ramp at the tool surface, assuming a negligible contact resistance between the tool and the composite. The boundary condition (2.4) is based on the assumption that heat transfer from the composite to the bleeder surface is by convection.

Gas Phase Equation of Motion. Darcy's Law is used to describe the relation between the gas phase velocity and pressure drop. It is known that the permeability of the porous matrix, K_γ, depends solely on the property of the solid matrix and the effect of the fluid's properties is reflected through the viscosity, μ_γ.

$$V_\gamma = -\frac{K_\gamma(\alpha)}{\mu_\gamma}\frac{\partial P_\gamma}{\partial x} \tag{2.5}$$

$$B.C. \quad x = 0, \quad V_\gamma = 0 \tag{2.6}$$

As the composite is solidified, the permeability of the solid matrix changes. The permeability, K_γ, of the composite may be assumed to be a linear function of the extent of reaction, α, (degree of polymerization). This simplest assumption is justified until more data become available. The gravitational force is neglected.

Overall Gas Phase Mass Balance. The gas diffusion is neglected in the early stage of devolatilization compared to the convective flux of gas driven by the pressure gradient.

$$\frac{\partial}{\partial t}(\rho_\gamma \epsilon_\gamma) + \frac{\partial}{\partial x}(\rho_\gamma V_\gamma) = \sum_{i=1}^{3} \frac{\dot{m}_i}{M_{Wi}} \tag{2.7}$$

$$I.C. \quad t = 0, \quad \rho_\gamma = \rho_{\gamma 0} = \frac{P_{vac}}{RT} \tag{2.8}$$

$$B.C. \quad x = L, \quad \rho_\gamma = \rho_{\gamma vac} \tag{2.9}$$

The boundary condition (2.9) simply asserts that certain level of vacuum is maintained at the bleeder surface. A separate submodel could relate that to the vacuum pump rate and properties of the bleeder cloth, liners etc.

Gas Component Mass Balance.

$$\frac{\partial}{\partial t}(\rho_{\gamma i} \epsilon_\gamma) + \frac{\partial}{\partial x}(\rho_{\gamma i} V_\gamma) = \frac{\dot{m}_i}{M_{Wi}} \tag{2.10}$$

$$I.C. \quad t = 0, \quad \rho_{\gamma i} = \rho_{\gamma i 0} \tag{2.11}$$

$$B.C. \quad x = L, \quad \rho_{\gamma i} = Y_i \rho_{\gamma vac} \tag{2.12}$$

Monomers Mass Balance in Liquid. The mass balance on monomer is needed to monitor the degree of polymerization and the volatile generation rate. The diffusion term is neglected due to small diffusivities in the liquid. Liquid convective motion is also assumed small.

$$\frac{\partial}{\partial t}(\epsilon_\beta C_A) = -R_A \epsilon_\beta \tag{2.13}$$

$$I.C. \quad t = 0, \quad C_A = C_{A0} \tag{2.14}$$

Liquid Mass Balance.

$$\frac{\partial(\epsilon_\beta \rho_\beta)}{\partial t} = -\sum_{i=1}^{N} \dot{m}_i \tag{2.15}$$

$$I.C. \quad t = 0, \quad \epsilon_\beta = 1 - \epsilon_{\sigma 0} - \epsilon_{\gamma 0} \tag{2.16}$$

Mass Balance on Volatiles in Liquid.

$$\frac{\partial}{\partial t}(\epsilon_\beta C_i) = R_i \epsilon_\beta - \frac{\dot{m}_i}{M_{Wi}} \tag{2.17}$$

$$I.C. \quad t = 0, \quad C_i = C_{i0} \tag{2.18}$$

Constitutive Equation. The constitutive equation for the rate of mass transfer is based on the assumption that there is a mass transfer resistance on the liquid side to the transport of volatile species from the liquid to the gas phase. In the first approximation constant volumetric mass transfer coefficients, $K_{mi}A_{\beta\gamma}$, are assumed. However, $K_{mi}A_{\beta\gamma}$ is expected to ~~be~~ change~~d~~ and considered as a function of temperature and time.

$$\dot{m}_i = K_{mi}A_{\beta\gamma}(\phi_i \gamma_i P_i^{sat} - Y_i P_\gamma) \tag{2.19}$$

where γ_i is the activity coefficient of i^{th} volatile component, ϕ_i is the volume fraction of species i in the liquid phase, and P_i^{sat} is the saturation vapor pressure of pure component i.

The results of preliminary computer simulations suggest that the mass transfer coefficient, permeability and heating rate are the three most important parameters during the devolatilization process in the processing of thermoplastic polyimide composite materials. Note that in the devolatilization process, the primary concern is the devolatilization rate out of the composite. It has been shown [6] that experimentally observed devolatilization rate can be calculated by properly adjusting the mass transfer coefficient of the constitutive equation as well as the permeability in the Darcy's law. It was also shown that the devolatilization model qualitatively predicts the devolatilization rate for each component well [6].

In this study, the devolatilization submodel is to be verified with appropriate experiments.

2.2. POLYMERIZATION CHEMISTRY OF THE AVIMID K-III

Avimid K-III polymers are amorphous linear condensation polyimides produced from monomer solutions by the reaction of an aromatic diethylester diacid with an aromatic diamine in NMP solvent. The reaction proceeds with loss of water, ethanol and solvent to form the imide ring (Figure 2.2). However, the repeating unit of the Avimid K-III has not been published yet.

In general, the kinetics of imidization are very complex. The most common explanation is that the material passes through a change in physical state due to solvent loss and cyclization, both of which reduce polymer chain flexibility. "Movement" of the glass transition temperature (T_g) depends both on imidization and solvent loss. Thus, if the reaction temperature is below T_g, the reaction may cease, but solvent loss may continue.

The kinetics of the Avimid K-III have been unknown so far. However, experimental data from Du Pont show that the imide formation reaction begins at about 120 °C and completes at about 180 °C. Strictly speaking, RDS (Rheometrics Dynamic Spectrometer) and mass spectroscopy studies indicate that the reaction of the Avimid K-III has two different maximum peaks. The reaction of the first peak starts at 100 °C and ends at 120 °C. The reaction of the second peak begins at 130 °C and completes at 180 °C.

2

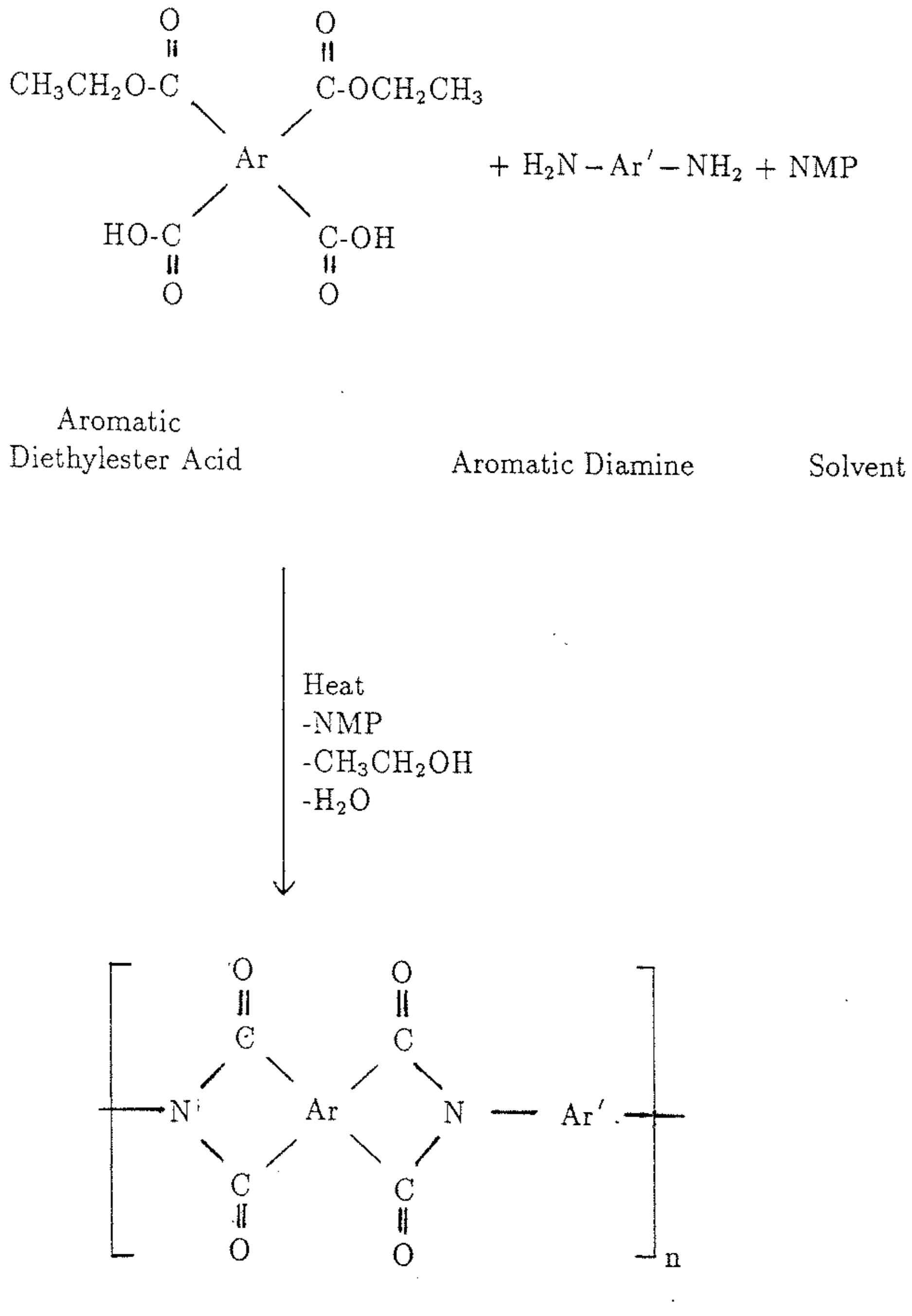

Figure 2.2: Avimid K-III polymerization chemistry

2.3. CONSOLIDATION

Various resin flow models based on Darcy's Law have been so far proposed [3, 7, 12].

Springer et al. [7] modeled consolidation of the composite due to the resin flow as follows: When the resin flow is only in the normal direction then at first only the top layer moves, while resin is being squeezed out from the space between the first and second layers. When the fibers reach the second layer, the first two layers move in unison towards the third layer, squeezing resin out from the space between the second and third layers. This sequence is repeated for the subsequent layers. Thus, the layers are compacted in a wavelike, cascading manner.

Loos and Springer [8] have also modeled the horizontal flow as laminar flow between ply planes with the implicit assumption that a linear pressure gradient exists in the horizontal direction. They showed that the model accurately predicts the resin flow, indicating that the pressure distributions assumed in the calculation are adequate for calculating the resin flow.

However, due to the decoupling of the vertical and horizontal flows, a major disadvantage is that profiles calculated for the two flows could result in different predicted resin pressures at the same point in the laminate. Furthermore, the authors [8] considered that the applied pressure on the laminate is borne solely by the resin. In other words, they modeled the resin flow as the consolidation of layer of porous sheets that lacked deformability. However, Brand et al. [9] and Campbell et al. [10] reported from experiments that the resin pressure at the center of the laminate at the tool surface below the lowest ply decreases with time during processing and does not remain constant under a constant applied stress. It is also pointed out that although the Springer model may have predicted reasonable resin flow values, it is not useful in predicting various other aspects related to resin flow like the consolidation profile of the laminate, the resin content profile and void migration.

Tang et al. [11] work on resin flow does not consider the effect of the resistance of the bleeder. In reality, the bleeder would definitely have an impeding effect on the resin flowing out of the laminate. It is to be expected that the resin pressure distribution is dependent on the resistance of the bleeder and between the prepregs and on the viscosity of the resin. The mode of compaction of prepregs is also affected by the resin pressure distribution. When the resin can not penetrate into the bleeder easily, the mechanism by which the prepregs are compacted is changed in such a way that the resin pressure varies with position continuously. It is noted that Springer and coworkers [7, 8, 11] suggested that the resin is distributed in a nearly discrete manner. Furthermore, the permeabilities S_b and S_c used in the model of Loos and Springer [8] are determined for the perforated steel plate whose properties such as porosity and tortuosity are totally ignored.

Gutowski and coworkers [12, 13] presented a viscoelastic model for the behavior of an aligned fiber composite during the curing cycle. It was found from the application of a constant pressure to a constant viscosity resin/aligned fiber composite that the load rapidly transfers from the resin to the fibers, and in an equally short time, the final fiber volume fraction is obtained. By addressing both the viscous resin flow, as well as the elastic processes, Gutowski's model is capable of predicting the time dependent behavior of curing a laminate.

Gutowski et al. [14, 15] conducted an experiment on the consolidation of special prepregs made of constant viscosity oils and aligned graphite fibers. They used three different kinds of oil which spanned two orders of magnitude in viscosity. The graphite fibers used were Hysol-Grafil XA-S (Courtaulds) fibers and Hercules AS-4 fibers. They measured four quantities; 1) fiber deformation, 2) axial permeability, 3) transverse permeability, 4) resin pressure.

However, they measured the resin pressure only at the tool surface using a recessed pressure transducer (see Fig.2 in *ref* [15]). Furthermore, when calculating axial permeability S_{xx} in the experiment of compression molding of an aligned fiber prepreg, they measured the pressure at the center of the sample (i.e., one point measurement) and calculated the average pressure with an assumption of a parabolic pressure profile. Note that the resin pressure distribution plays an important role in the consolidation process and therefore should be determined accurately. Also it is reported in their experiments that they applied pressure to the composite in the following manner. At the beginning of the test they compressed the sample at a constant crosshead speed, then once the target load was achieved, they held the load constant. However, if you have a bleeder in the sample, before achieving target load, the resin flow occurs through the bleeder and causes consolidation of the composite. Therefore, a knowledge of the bleeder properties should be incorporated in analyzing the resin flow out of the laminate.

In Gutowski's model, there are three parameters which have to be determined experimentally. These include the spring constant A_s, the available fiber volume fraction V_a, and the permeability S_{xx}. A_s and V_a are needed for the relations between the effective stress and void ratio. S_{xx} is found to be a function of the void ratio.

Dave et al. [3] proposed a resin flow model based on soil consolidation theory, which results in a nonlinear pressure gradient in the vertical and horizontal direction of the laminate. When the resin flow model based on consolidation theory is applied to the situation of one-dimensional consolidation under a constant load with one-dimensional seepage in the vertical direction, the resin pressure at the midpoint of the laminate is found to decrease with time.

The advantage of the resin flow model of Dave et al. is that the model does not decouple the flows in different directions. Therefore, the model predicts only one resin pressure at any point in the laminate at any particular instant.

However, Dave et al. assumed free bleeding to exclude the effect of the bleeder on the resin flow behavior (i.e., $p_{r,bc}$ at the top plate = 0 psig). In reality, it is thought that the boundary condition $p_{r,bc}$ at the top plate and near the dam does not remain constant because the applied pressure may affect the boundary resin pressure.

In the resin flow model of Dave et al., there are three parameters which have to be determined experimentally. The relations between the effective stress and void ratio need two parameters. The permeability is the remaining parameter needed to solve the resin pressure equation. Note that the coefficient of volume change m_v is not an independent parameter and can be calculated from the relations between the effective stress and void ratio. Recently, Lam and Kardos [16] obtained the above parameters from experiments using a special permeability tester.

For a better understanding of the role of the applied pressure on the resin pressure and resin content inside the laminate (i.e., resin flow model), the pressure distribution inside the laminate must be known. Campbell et al. [10] measured the resin pressure inside a laminate as a function of position and time by embedding miniature pressure transducers in the laminate and between the bleeder and on the tool surface. However, Campbell and coworkers [10] measured the resin pressure only for one particular type of cure cycle and set of bleeders. So far, the effect of bleeder resistance on the resin pressure inside the laminate has not been investigated. In order to verify which model is correct and best, the term "resin pressure" should be fully understood and measured precisely as a function of position as well as time by using the appropriate pressure transducer. It should be noted that only one point measurement inside the laminate is not sufficient. The influence of various factors on the resin pressure distribution such as applied pressure, bleeder resistance, thickness of the laminate, presence of the dam, etc. has to be more systematically considered. It should be emphasized that the pressure distribution inside the laminate plays an important role in determining the validity of the various models which have been proposed so far.

The purpose of this study is to identify the set of designed experiments which can be used to verify the model for devolatilization and consolidation of the thermoplastic polyimide composite.

3. DEVOLATILIZATION

3.1. ANALYSIS OF NEAT AVIMID K-III RESIN

3.1.1. DSC Measurements

Differential scanning calorimetry (DSC) was performed using a Perkin Elmer DSC-4. Nitrogen gas was used to continuously purge the sample compartments. For each DSC scan, 5-15 mg of sample was used. The sample pan and an empty aluminum reference pan were loaded into the DSC and heated according to the constant heating rate of 1, 2, 5, and 10 °C/min.

The DSC response from typical scans is shown in Figure 3.1. The two different endotherms are attributed to the imidization reaction and the melting of the crystal structures formed during heating and devolatilization, respectively. The DSC measurements with different heating rates show that as the heating rate is increased the range of the endotherm peak is broadened and the peak is shifted to higher temperature. This means that the crystallinity and morphological structure of the formed polyimide are strongly dependent upon the heating rate. In other words, the change of the heating rate leads to the formation of different crystalline phases. This finding is derived from the fact that the shapes and areas of the melting endotherm are different for each heating rate (see Figure 3.1, 3.2

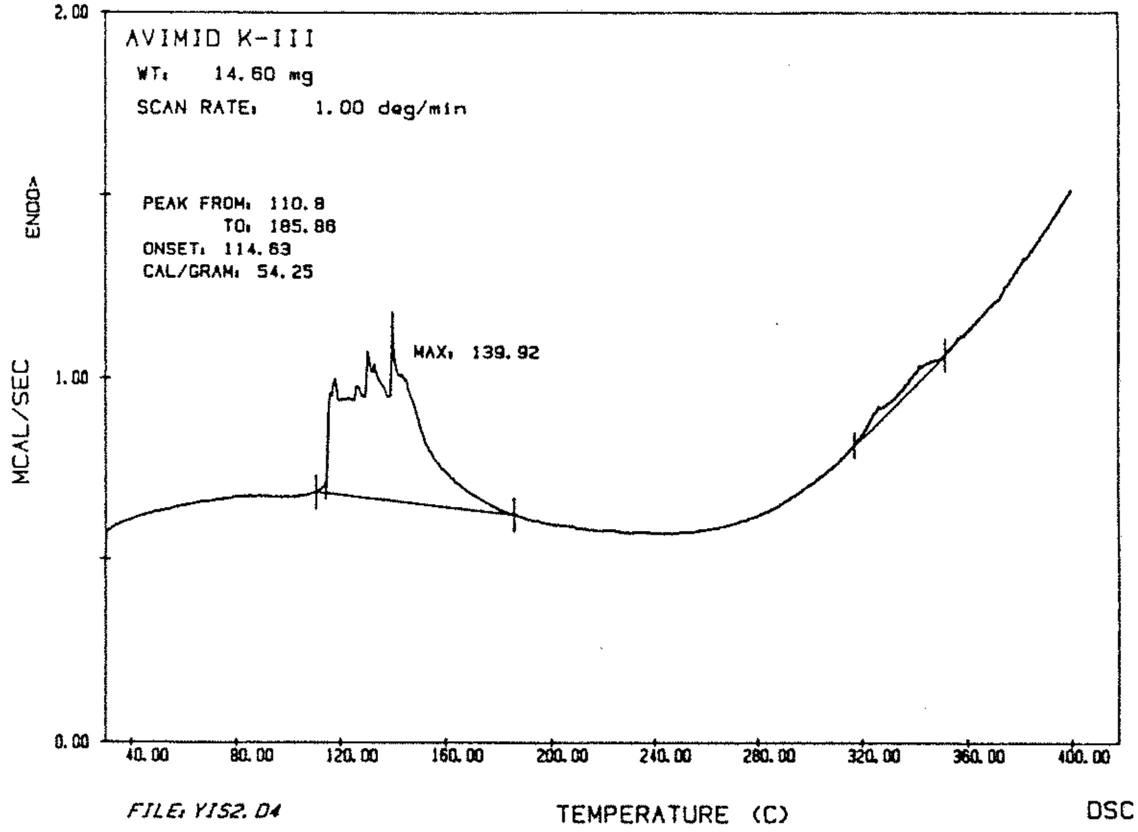

Figure 3.1: DSC heating scans at 1 °C/min of the Avimid K-III neat resin.

and 3.3). The shape and the area of the melting endotherm represent the morphology and degree of crystallinity of the polyimide, respectively.[ ] Wedgewood and Grant [17] also observed that the melting point of Avimid K-III prepregs depends upon the processing history such as applied vacuum level and full vacuum application temperature. The change in melting behavior was explained in terms of a transition between a heat and mass transfer controlled crystallization process.

Therefore, based on the DSC scans, the morphological structure prior to the crystalline melting can be manipulated by controlling the heating rate as well as the holding time at a certain temperature. The DSC results also lead to the suggestion that the gas permeability of the polyimide composite is a function of the heating rate as well as the extent of reaction. It was suggested that changes in the morphology of PMDA (pyromellitic dianhydride) - ODA (oxydianiline) during processing are related to conformational changes associated with the nitrogen-phenyl and ether linkage, allowing denser packing of adjacent chains [18]. In the case of LaRC-TPI, the evidence for the existence of crystalline phases was obtained with the DSC measurements by quenching and rerunning the samples [19].

3.1.2. Thermogravimetric Analysis (TGA)

Thermal stability and weight loss as a function of temperature were determined with the Du Pont 990 Thermal Analyzer at a heating rate of 10 °C/min. A N_2 atmosphere was provided by a continuous gas flow of 150 ml/min. Thermogravimetric analysis shows that the Avimid K-III neat resin contains 35 wt. % volatiles, which are known to be the byproduct (ethanol and water) and the sol-

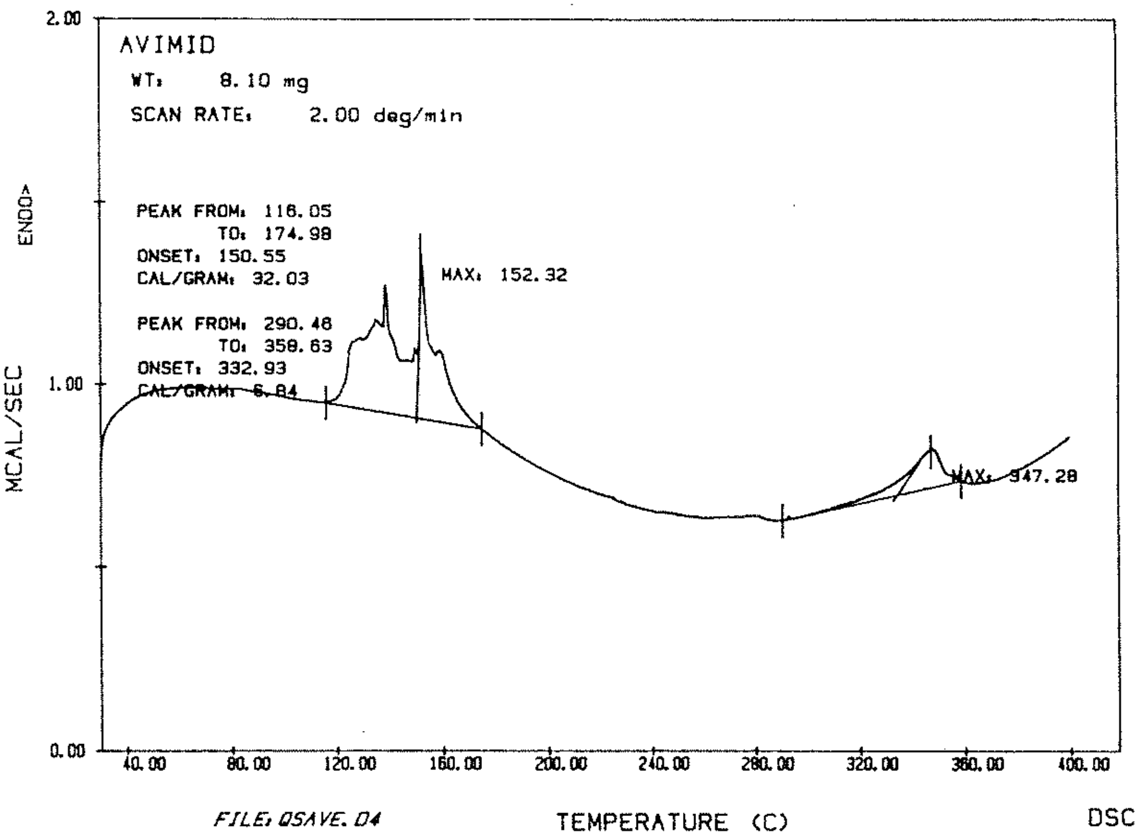

Figure 3.2: DSC heating scans at 2 °C/min of the Avimid K-III neat resin.

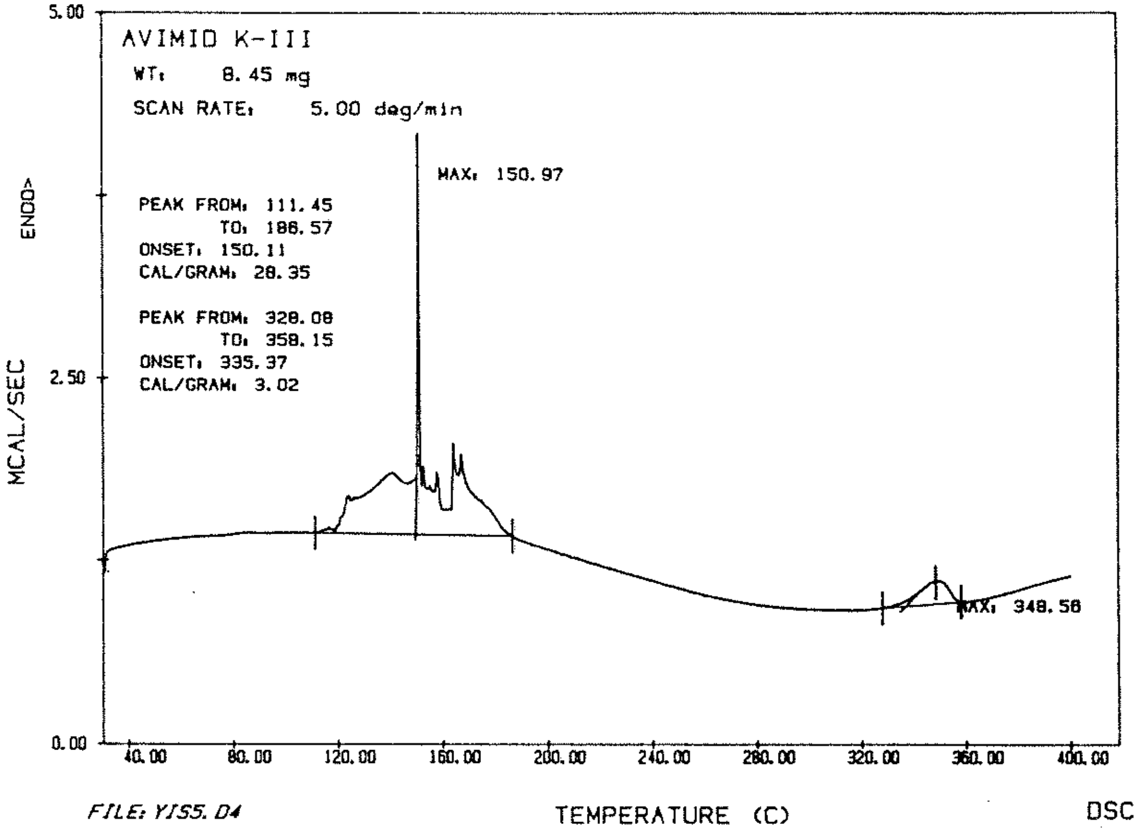

Figure 3.3: DSC heating scans at 5 °C/min of the Avimid K-III neat resin.

vent NMP. Figure 3.4 shows the measured weight loss caused by the imidization reaction, when the Avimid K-III was heated at a rate of 10 °C/min. These results show that weight loss occurred in two steps. Weight loss first occurred in the temperature range of 150 °C to 250 °C and next above 500 °C. First-step weight loss is mainly due to the removal of the byproduct released from the imidization reaction, while the second-step weight loss is assumed to be caused by the thermal decomposition. The char yield at 850 °C is 36 % based on the neat resin.

Thermogravimetric analysis also shows a correlation between the first step weight loss and the observed DSC endotherm prior to melting. In other words, the temperature range of the endotherm coincides with that of the first step weight loss of the TGA thermogram.

3.1.3. IR measurements

Infrared spectrum from 4000 to 400 cm^{-1} was obtained at room temperature using Perkin Elmer IR spectrometer (Model 882). The spectrum shown in Figure 3.5 is very complicated by considerable band overlap. Note that the neat Avimid K-III resin is composed of an aromatic diethyl ester diacid, an aromatic diamine, N-methyl-2-pyrrolidone (NMP), and ethanol.

The IR transmittance bands can be assigned based on the functionality of the Avimid K-III. The 3386 and 3280 cm^{-1} bands are due to N-H stretch of an amine group. The 1726 cm^{-1} band is attributed to the carbonyl C=O stretch of the ester and imide group. The 1641 cm^{-1} band is overlapped by N-H bending of the amine group and C=O stretch of amide. The 1114 cm^{-1} is assigned to C-O stretch of the ester group. The aromatic C-H stretch and out-of-plane bending

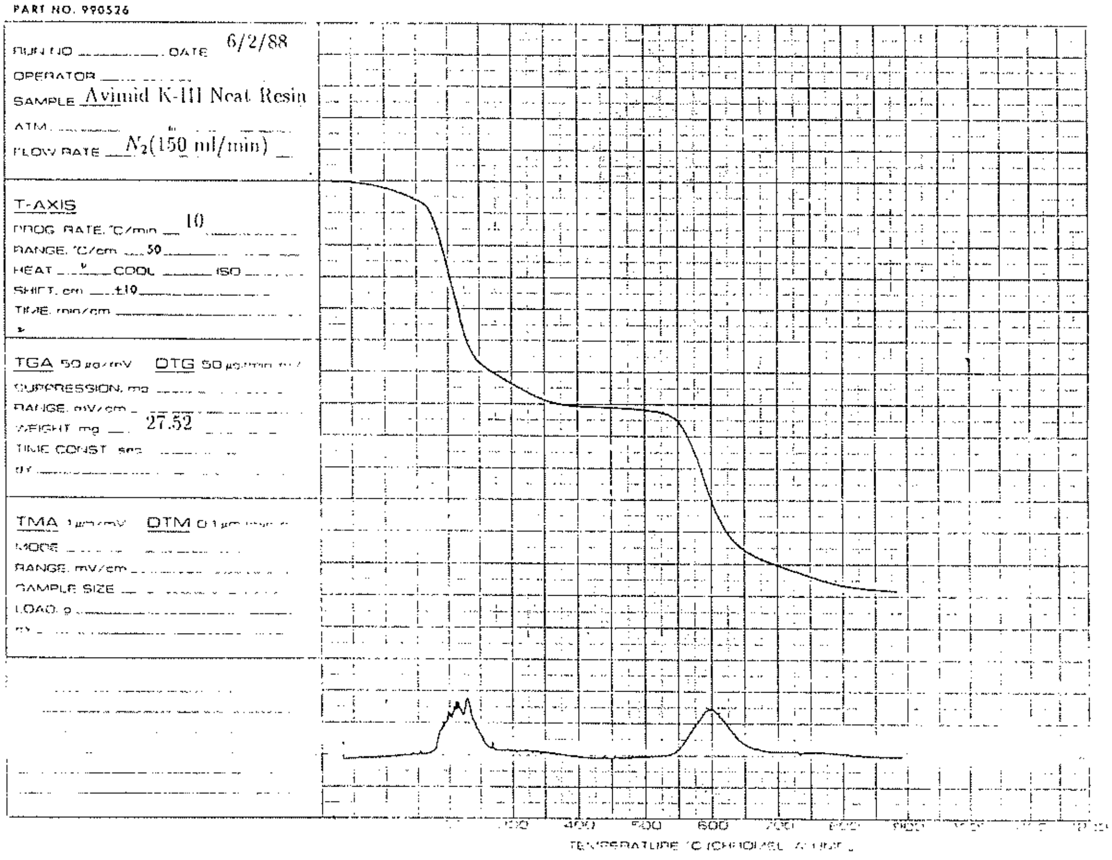

PART NO. 990526

RUN NO ______ DATE 6/2/88

OPERATOR ______

SAMPLE Avimid K-III Neat Resin

ATM. ______

FLOW RATE N$_2$(150 ml/min)

T-AXIS

PROG. RATE, °C/min 10

RANGE, °C/cm 50

HEAT ✓ COOL ______ ISO ______

SHIFT, cm ±10

TIME, min/cm ______

TGA 50 µg/mV DTG 50 µg/min/mV

SUPPRESSION, mg ______

RANGE, mV/cm ______

WEIGHT, mg 27.52

TIME CONST. sec ______

BY ______

TMA 1 µm/mV DTM 0.1 µm/min/mV

MODE ______

RANGE, mV/cm ______

SAMPLE SIZE ______

LOAD, g ______

BY ______

Figure 3.4: Weight loss of the Avimid K-III neat resin as a function of temperature.

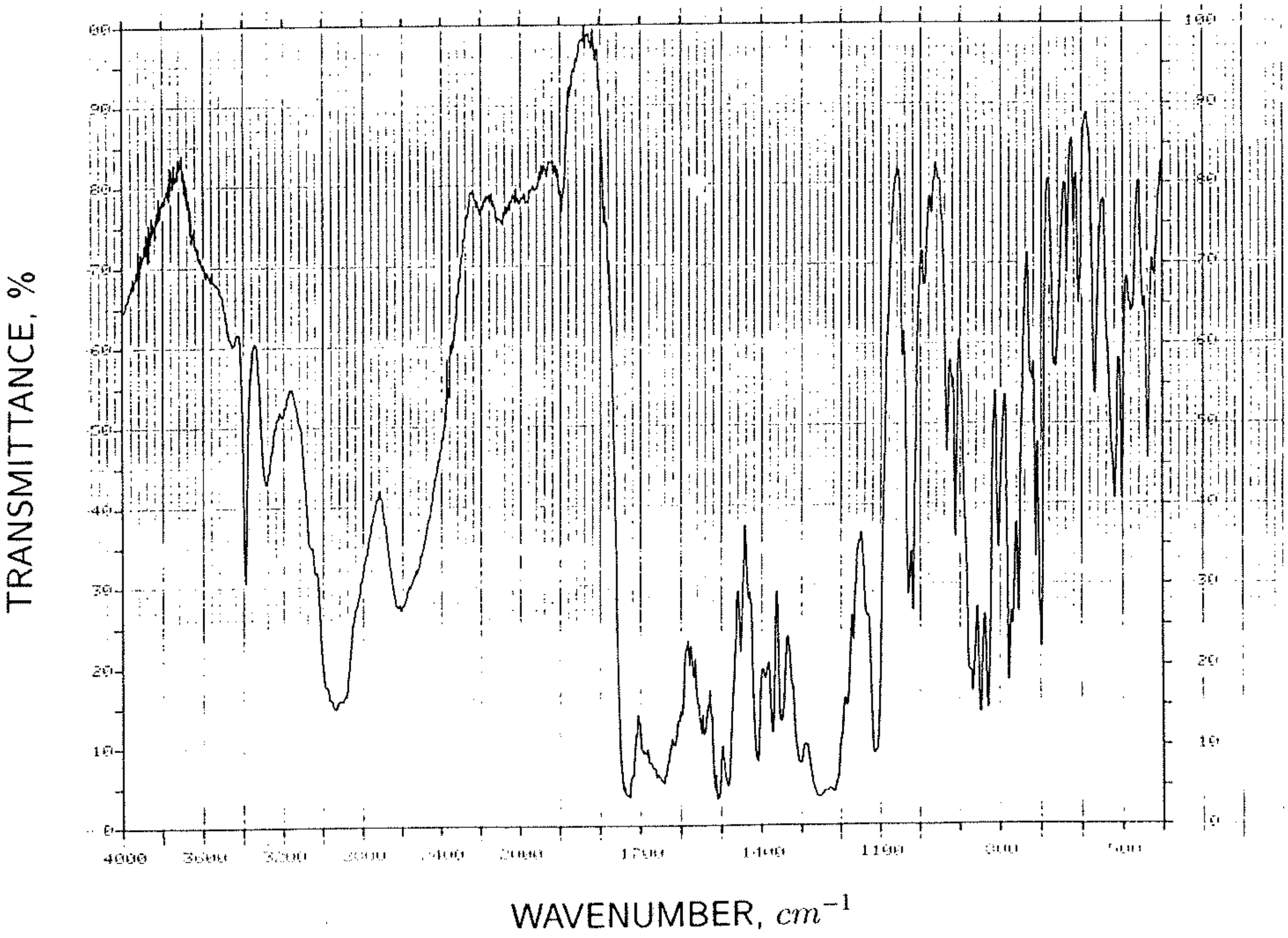

Figure 3.5: IR spectrum of the Avimid K-III neat resin (film on KBr disk).

vibrations are found in the typical band position. It is noted that the OH and NH stretches are overlapped with one another. The NH in-plane bend is also overlapped with an aromatic ring stretch of the aromatic components.

3.2. CRACK FORMATION AND HEALING

Heat and mass transfer phenomena occurring in the Avimid K-III polyimide prepreg are accompanied by morphological changes such as crystallization and melting of the crystalline phase. It is proposed that morphological changes, high processing temperature and consolidation pressure can lead to crack formation and healing. Figure 3.6 shows a typical processing cycle for the Avimid K-III composite material and ranges of temperature where the devolatilization and the consolidation process and the phenomena such as the imide formation reaction, crystallization, and melting of the crystalline phase occur.

Avimid K-III polymer is known as an amorphous polyimide matrix resin. However, the thermal analysis of the Avimid K-III neat resin shows two endotherms. One is ascribed to the imide formation reaction and the other to melting of the crystalline phase which is formed during the reaction. The temperatures employed in the imide formation reaction vary in the range of 120 °C to 180 °C, while the melting temperature of the crystalline phase is found as 347 °C. During the imide formation reaction, the formation of the crystalline phase occurs which causes the matrix resin to shrink in the carbon fiber reinforced thermoplastic composite. Note that the surface of the carbon fiber is known as the active site for the crystallization [20, 21]. Thus, the crystallization becomes a second process that occurs

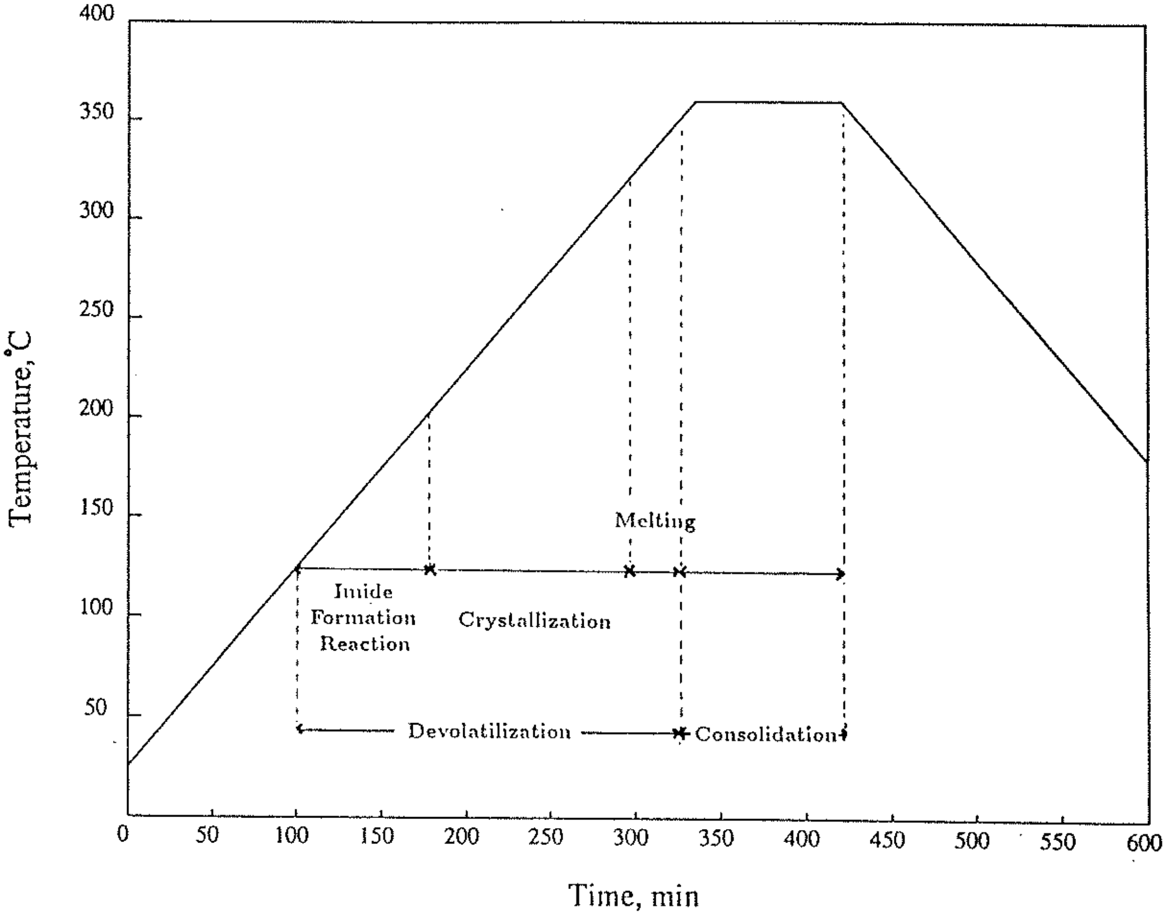

Figure 3.6: A typical process cycle for the Avimid K-III including temperature ranges of various processes

simultaneously with the imidization process. This phenomenon can be explained as reaction-induced crystallization.

With the crystallization, great amounts of volatiles (about 15 wt.%) vaporize to build high gas pressure because of the extremely high reaction temperature. The high gas pressure has to be released by venting the gas out of the composite through certain paths.

When these two phenomena occur simultaneously in the fiber reinforced composite, it is reasonable to propose that some kind of cracks are formed to accommodate both the shrinkage phenomenon and the release of the high vapor pressure.

3.2.1. Optical Microscopy Study (Polarized Light)

Optical microscopy was used to investigate the morphology change and crack formation of the Avimid K-III neat resin during heating. The Avimid K-III neat resin was placed between two slide glasses and heated using a hot-stage optical microscope (Leitz) with a heating rate of 2.5 °C/min. Photomicrographs were taken in transmitted polarized light (magnifications: 300×). The polarizer and analyzer have their electric vectors at 90° at each other.

Figure 3.7 shows a bubble which was formed by the evaporation of the volatiles (black circle), and that the as-received Avimid K-III neat resin is not completely an isotropic material. It should be noted that a polyamic acid, poly(4,4′-methylene diphenylene pyromellitic acid), crystallizes in N-methyl pyrrolidone (NMP) [22]. When the sample was heated up to 120 °C, the image became black. This means

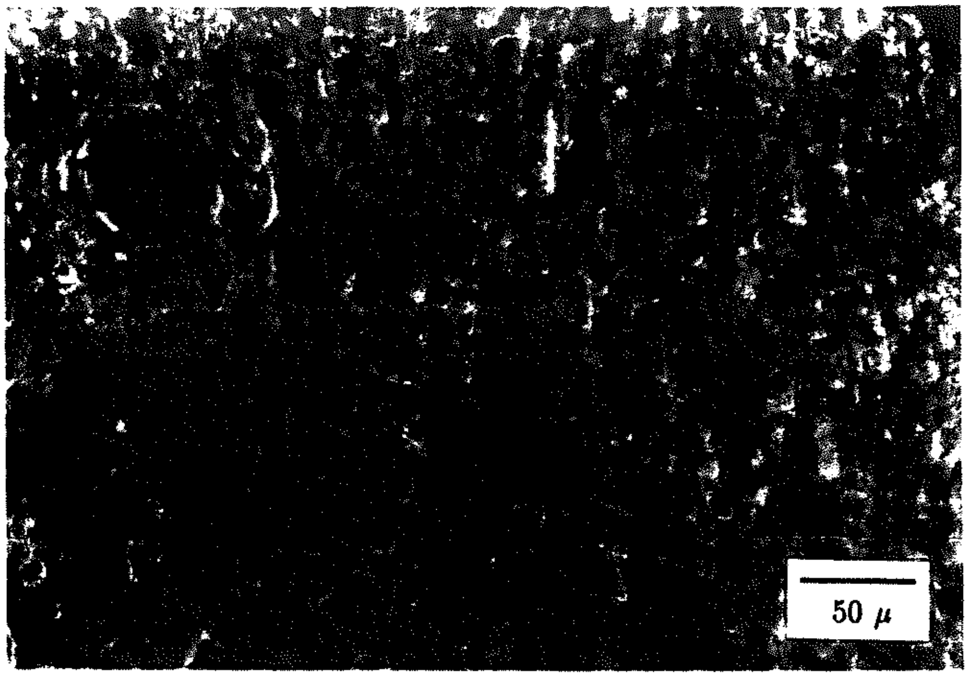

Figure 3.7: Optical micrograph of the Avimid K-III neat resin at room temperature (300× magnification).

that the structure of the Avimid K-III resin is disturbed and it becomes optically isotropic. As the heating was continued, the crystallites were formed as a form of spherulites as shown in Figure 3.8. As the temperature was close to 330 °C, the image was gradually getting dark and finally turned black. This means that the Avimid K-III becomes amorphous with the melting of the crystallites. It can be concluded that the crystallites do form during heating and disappear after melting. These optical microscopy results are consistent with the interpretation of the DSC thermograms which were shown earlier.

It has been proposed that morphological changes including crystallization lead to crack formation. The microscopy was utilized to observe cracks. Figure 3.9 shows the cracks which were formed during the heating cycle. As the processing temperature increases, the crack density increases. It is also found that the formed cracks were growing and gradually interconnected. Theses linked cracks

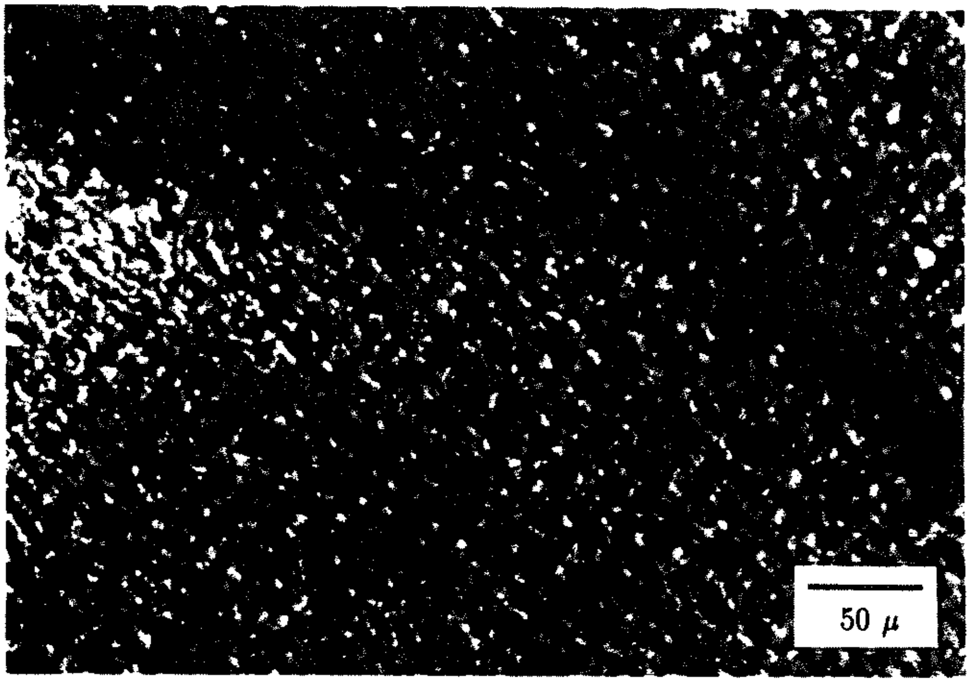

Figure 3.8: Optical micrograph of the Avimid K-III neat resin at 220 °C (300 × magnification).

can serve as a path through which the vaporizing volatiles can migrate. This phenomenon can support the assumption that the gas phase is continuous in developing the devolatilization submodel. Note that this assumption plays an important role in deriving the transport equation for calculating the volatile flux at the bleeder surface. It was observed that the processed polyimide resin (Skybond^R) that exhibited cracks contained the crystalline phase, which was detected with X-ray diffraction technique [23]. It was shown (refer to Figure 9 of [23]) that the crystalline (brickdust) phase was composed of a network of resin nodules with interconnected porosity, providing numerous sites for initiation of cracks. The cracks was were also shown to provide a path for volatile release for a Skybond 703/T300 graphite fabric prepreg which contains a condensation type polyimide matrix [24].

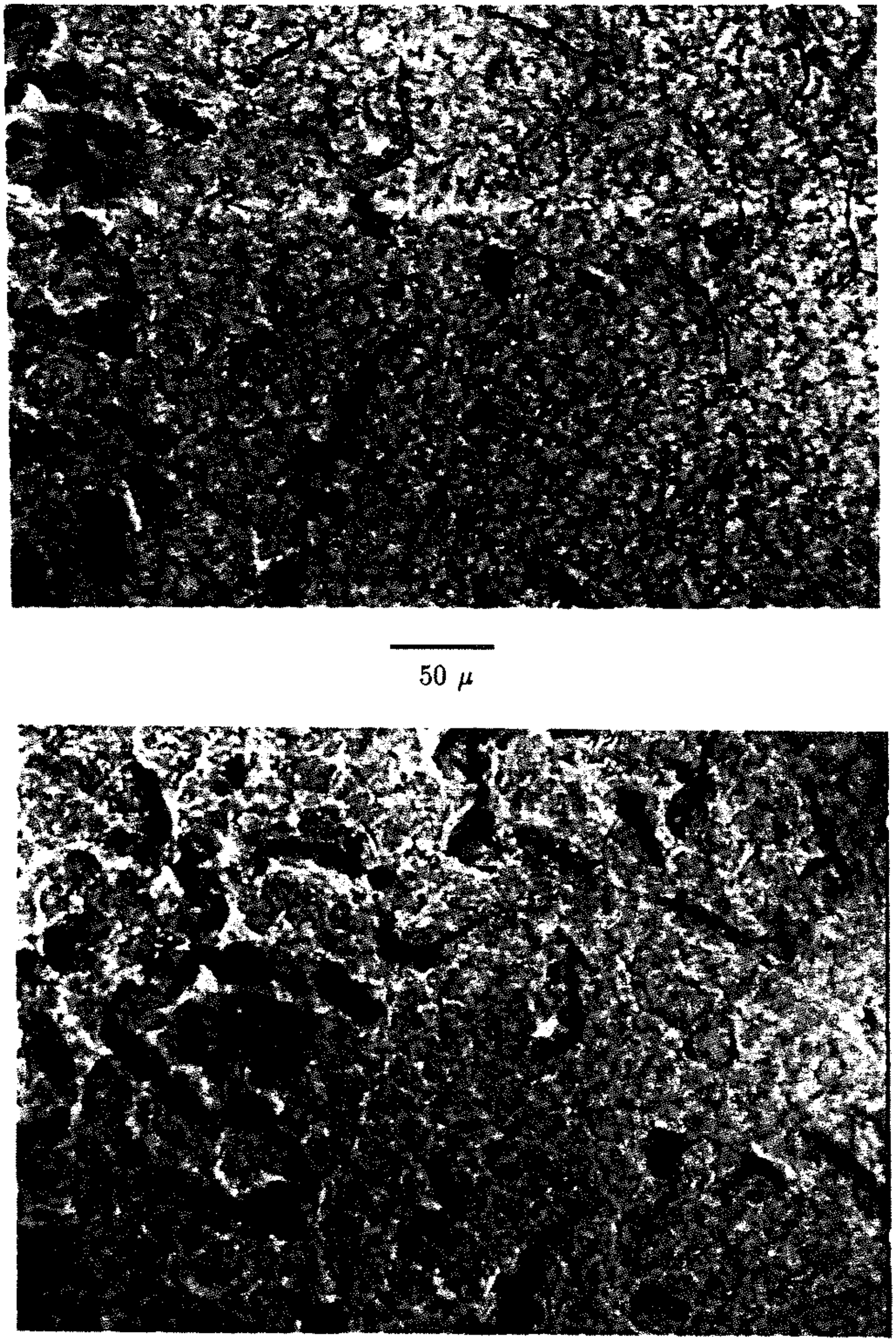

Figure 3.9: Growing microcracks of the Avimid K-III neat resin during heating (300× magnification).

3.2.2. Microscopy Study

Six neat resin samples were prepared by heating to various temperatures up to 200 °C, followed by quenching in either ice water or room temperature air. Figure 3.10 shows the progressive appearance of neat resin film as the temperature is raised at a constant rate of 3°C/min. The film remained a consistent dark brown color up to 200 °C, but it changed from transparent to opaque. Observations of the film morphology before and after quenching were noted as follows for micrographs A-F in Figure 3.10.

- A-120°C: Small bubbles begin to appear in the film. There is no change in morphology upon quenching into water.
- B-140°C: The bubbles become larger and more clear at 140°C. Again, no change is observed upon quenching into water.
- C-155°C: Bubbles are now large as a result of coalescence and massive volatile evolution. The few cracks on the left of the photo appear only after quenching into water.
- D-165°C: Large bubbles continue to evolve. Cracks now appear at 165°C prior to quenching in air. The transparent film becomes opaque between 155°C and 165°C, presumably due to crystallization. There is no effect of quenching into air.
- E-175°C: New bubbles cease to be formed. More cracks form between 165°C and 175°C. The film becomes more opaque. There is no effect of quenching into air.

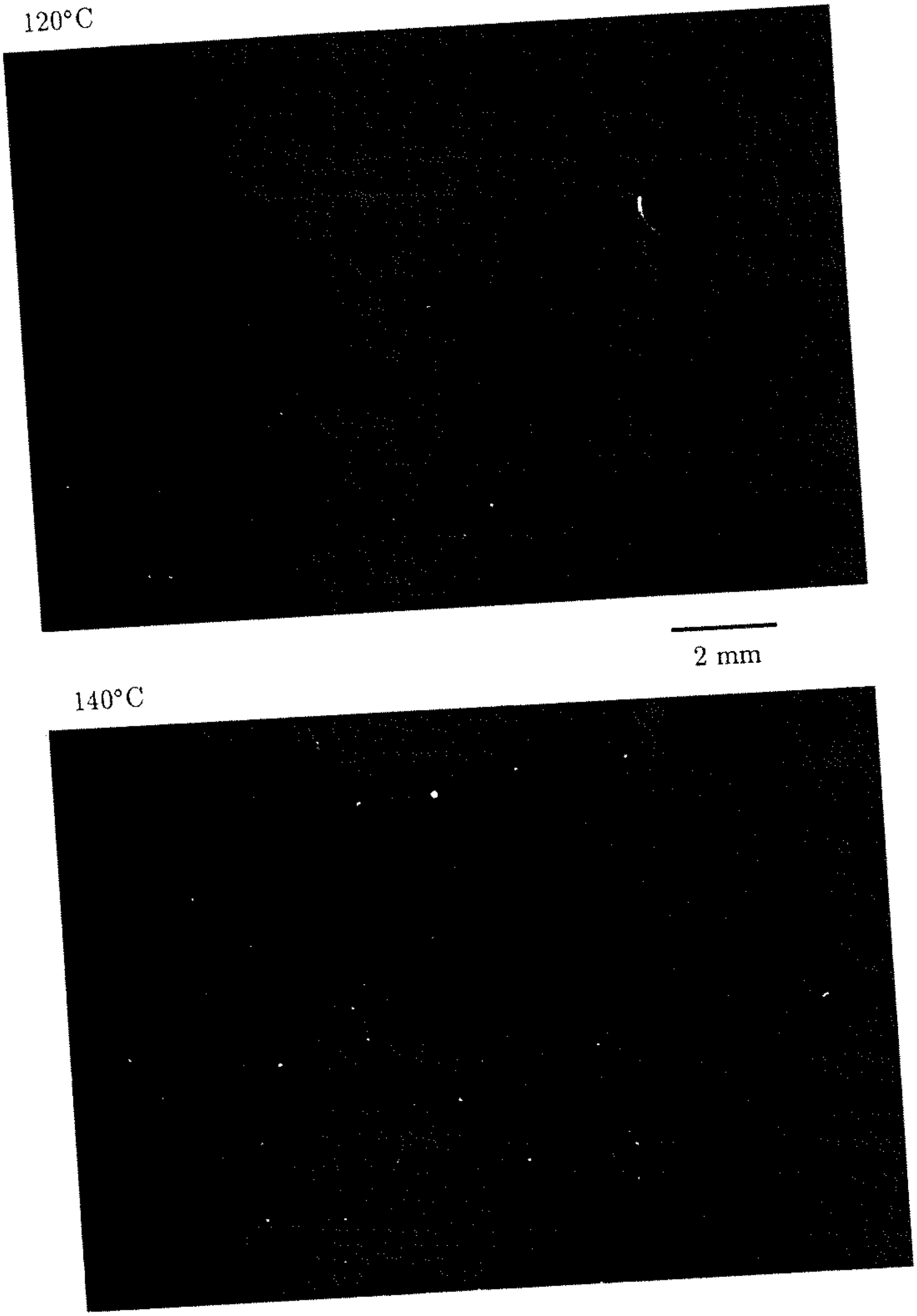

Figure 3.10: Changes in sample morphology with temperature (8× magnification).

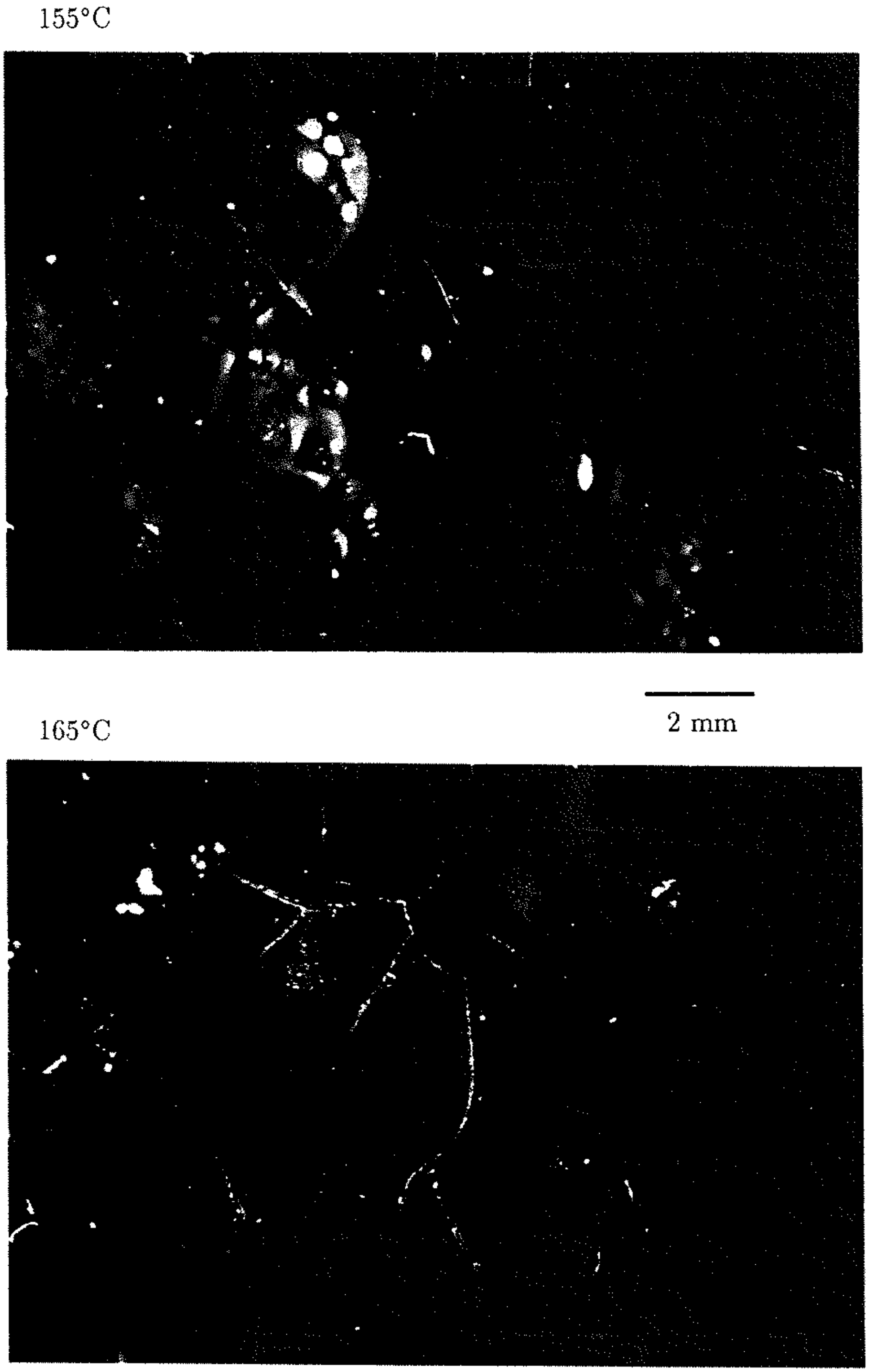

(continued)
Figure 3.10: Changes in sample morphology with temperature (8× magnification).

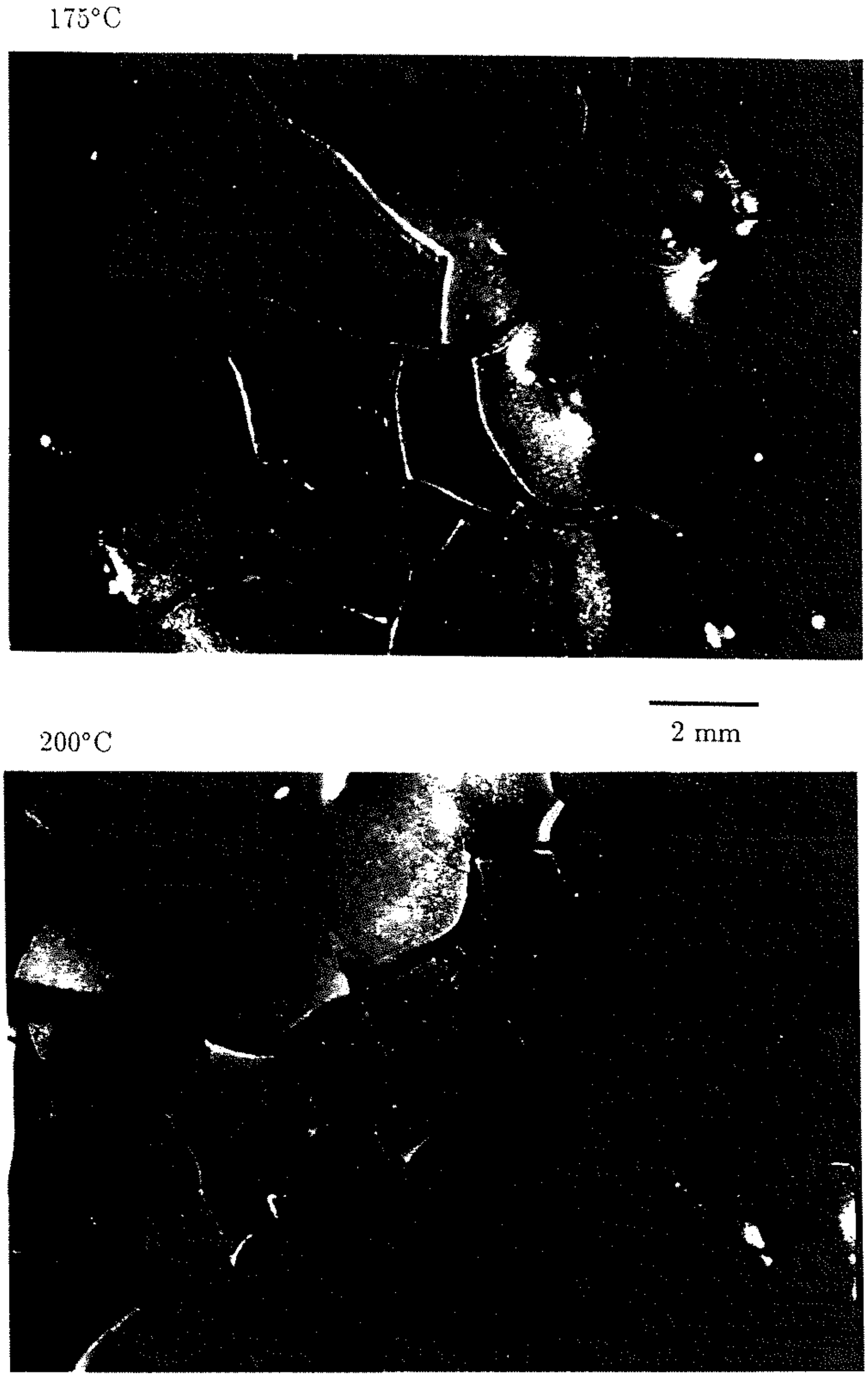

(continued)
Figure 3.10: Changes in sample morphology with temperature (8× magnification).

- F-200°C: There is no apparent change from the 175°C morphology. There does seem to be some overall film buckling presumably from shrinkage stress due to crystallization. There is no effect of quenching into air.

It is clear that major morphological changes occur which will affect volatile evolution and consolidation in a composite laminate. In particular, the cracks allow devolatilization, but they will also have to "heal" in order for viable structural laminates to be produced.

3.3. PROCESSING OF AMIMID K-III/IM-6 LAMINATE

3.3.1. Thermogravimetric Analysis on Avimid K-III/IM-6 Prepreg

A small amount of the Avimid K-III/IM-6 prepreg sample (30-40 mg) was set on a precision thermobalance (Rigaku) and heated in air to 360 °C with three different heating rates (1.25, 2.5, and 5 °C/min).

Figure 3.11 shows the weight loss of the prepreg as a function of temperature and heating rate. As the heating rate is increased, the curves shift to higher temperatures, and the temperature at which the maximum rate of the weight loss occurs is also increased. The shifts are clearly seen from the derivative curves, indicating a kinetic effect. This dependency of the weight loss on the heating rate can be utilized in estimating the volumetric mass transfer coefficient which is an input parameter for the devolatilization model. Figure 3.11 also indicates that while a very small amount of weight loss occurred for temperatures under 120 °C, the maximum rate of weight loss occurred in the range 130 - 180 °C. The weight

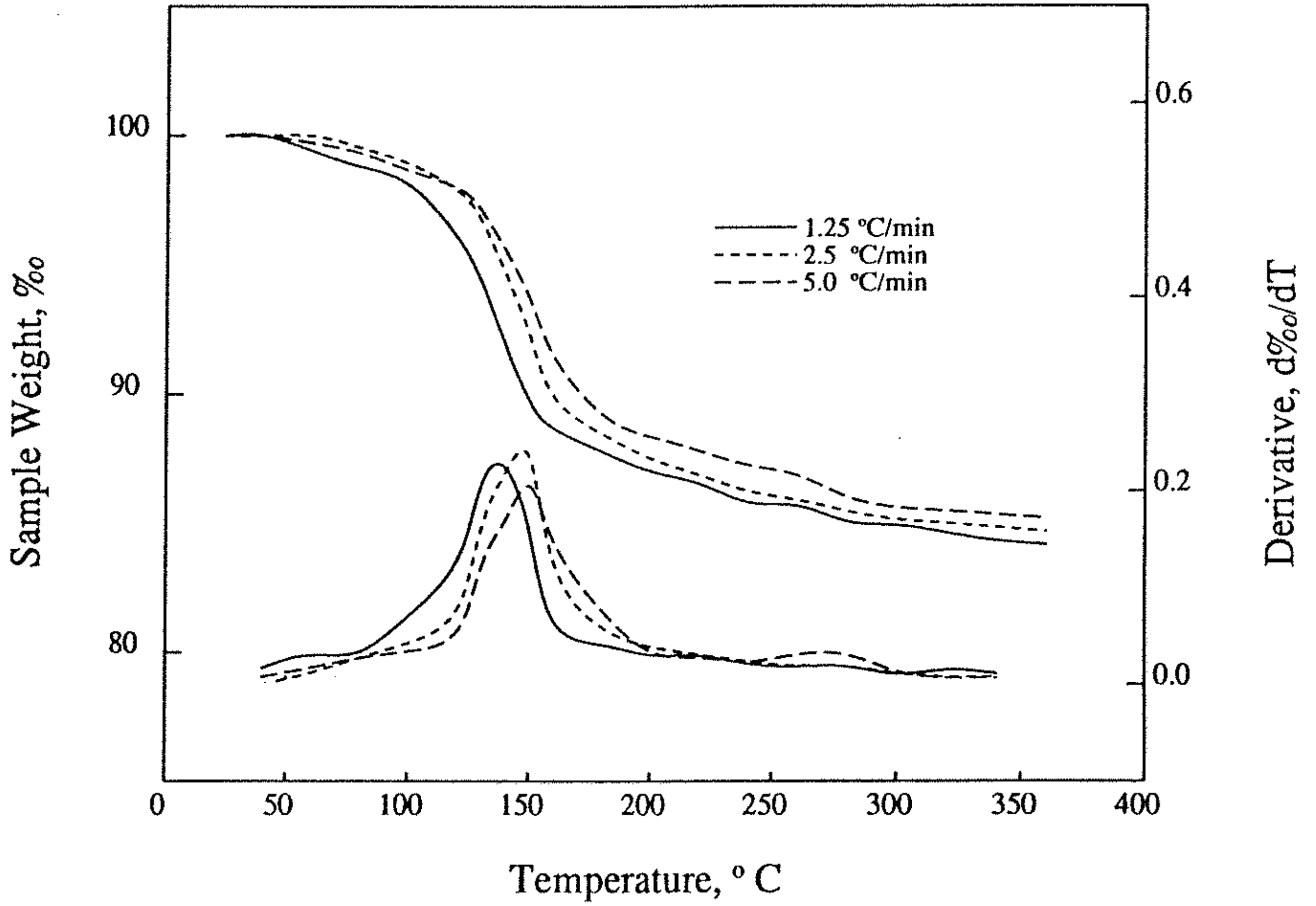

Figure 3.11: Weight loss of the Avimid K-III/IM-6 prepreg as a function of temperature and heating rate.

loss in this latter range is due to the imidization reaction which produces the volatile by-products ethanol and water. The DSC scan supports this interpretation. The additional weight loss after 180 °C is mainly caused by the evaporation of the solvent NMP.

The weight loss percentage due to heating up to 360 °C for the Avimid K-III/IM-6 prepreg was found to be 15.4 %.

3.3.2. Description of a Miniclave

An instrumented miniclave apparatus, shown in Figure 3.12, has been constructed and pressure tested. The miniclave can accept laminate up to 6 × 6 inches lateral dimensions and 3/4 inch thickness. The heavily bolted top plate (see Figure 3.12) contains a pressure control line and a pressure sensor. The large knobs protruding horizontally from the rectangular chamber are entry ports for thermocouples or other pressure sensor probes. In the foreground are the data acquisition equipment and heating rate controllers. The unit is designed to simultaneously maintain pressure and collect volatiles. The miniclave is heated from the bottom with embedded electrical heaters to simulate a heated tool.

3.3.3. Processing Cycle

In order to process the Avimid K-III/IM-6 laminate, 1 mil thick release film (A4000RP3) was laid on the tool surface. Then, a number of Avimid K-III/IM-6 prepreg plies were laid up and followed by a peel ply (Bleeder Lease B). Bleeder Lease B is a high temperature fabric coated with a non-transferring release agent.

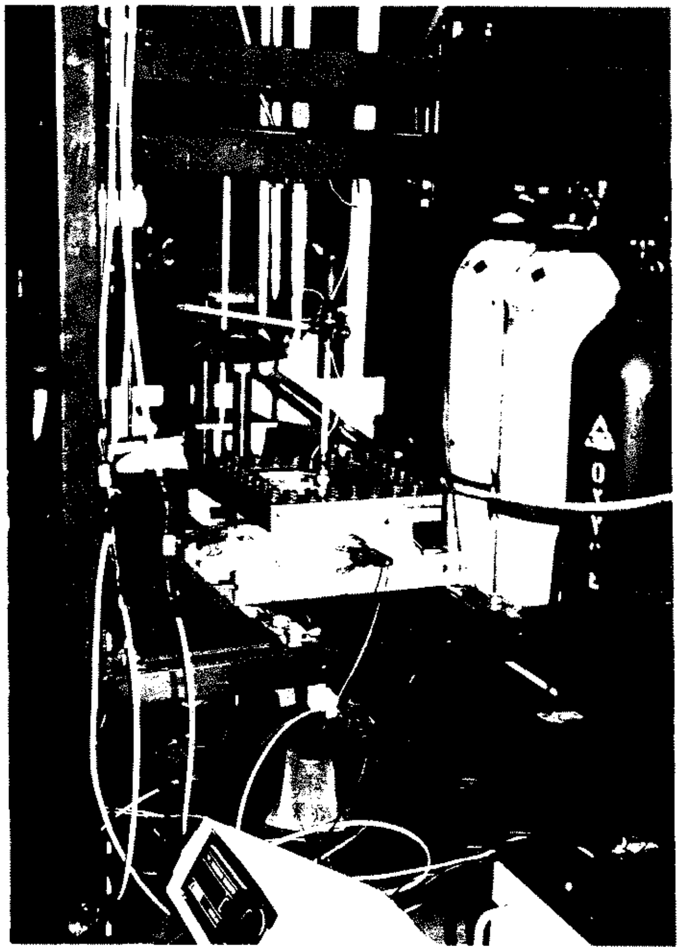

Figure 3.12: Instrumented miniclave apparatus.

One ply of the bleeder (Airweave N-10) was placed on the peel ply. The tool temperature was controlled with a programmable controller (CN-1020, Omega) which can adjust the heating rate. The initial vacuum was applied from the beginning of the cycle ($\leq$ 100 mmHg). When the temperature at the tool reached 130 °C, full vacuum was introduced ($\leq$ 0.5 mmHg). The processing was stopped at the desired temperature by removing both vacuum and heat. All the layups were uniaxial.

3.3.4. Processing without a Caul Plate

In order to check the effect of the caul plate, 24 plies of Avimid K-III/IM-6 prepregs were unidirectionally laid up and processed at a heating rate of 2.2 °C/min without a caul plate and without any compressive force in the thickness direction (open mold). The processing was stopped at 220 °C by removing both vacuum and heat.

It is found that the width (perpendicular direction to fiber axis) of the laminate shrank from 5.75 to 5.25 inches after processing. The percent of shrinkage is 8.7 %. This remarkable shrinkage is attributed to both volatile removal and the condensation reaction which presumably includes crystallization of a polyimide. However, the length (parallel to the direction of the fiber axis) was not changed due to restraint by the carbon fibers.

Needle-shaped cracks were also observed on the top surface, running in the longitudinal (fiber) direction. This is because the carbon fiber serves as a nucleating site for the crystallization and the crystallites grow on the surface of the carbon fibers. The large transverse shrinkage is likely related to these cracks.

The final thickness of the laminate increased tremendously from 5 mm to 10 mm. This increase arises because there was no compressing force on the laminate and because the volatiles caused ply lofting throughout the laminate. The longitudinal cross section becomes oval-shaped after quenching at 220 °C. This implies that there is a pressure buildup at the center and in the middle of the laminate. It was observed that large voids were formed, especially between plies. Volatile transport at this point in the process can occur much more readily between the plies horizontally than through the plies in the vertical direction.

3.3.5. Processing with a Caul Plate

In order to prevent the laminate from expanding due to the pressure build-up, 12 plies of Avimid K-III/IM-6 prepregs were laid up and processed with an aluminum caul plate under vertical compressive load. The process cycle was the same as the case without the caul plate.

It was found that the volatile weight loss due to vacuum and heating up to 220 °C is 11.63 % based on the original weight of the prepregs. Because of the force on the caul plate, no shrinkage along the transverse direction (perpendicular to the fiber alignment) was observed. However, the surface was wrinkled, which probably arises as a complex result of the shrinkage phenomenon perpendicular to the fiber alignment as well as the prevention of lofting. Again, needle-shaped cracks were observed along the fiber alignment direction with about the same frequency as before, even though a caul plate was used, as shown in Figure 3.13.

In order to examine the morphology change during processing, 12 layers of the Avimid K-III/IM-6 prepregs were processed with a caul plate and quenched at

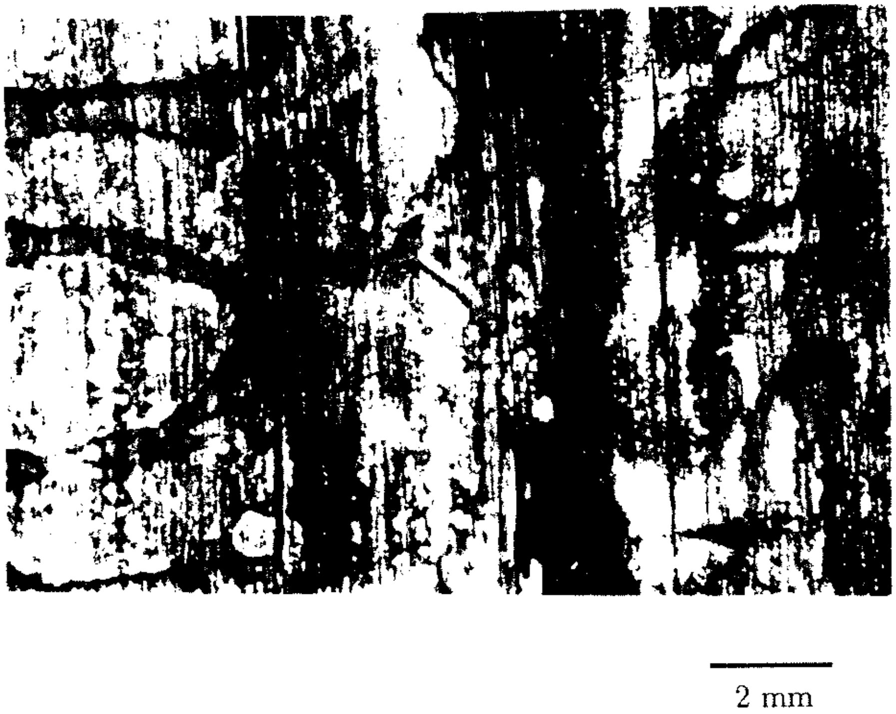

Figure 3.13: Photomicrograph of the Avimid K-III/IM-6 laminate processed to 220 °C (facing the tool surface).

140 °C. The surface at the tool is wrinkled and the top surface below the peel ply again has small needle-shaped cracks running along the fibers as shown in Figure 3.14. The crack density was much less than for the laminate which was processed and quenched at 220 °C. This supports the observation in the neat resin that more cracks are generated as the reaction proceeds. The laminate processed up to 170 °C and quenched has a crack density in between that at 220 °C and at 140 °C as shown in Figure 3.15. This trend coincides with the optical microscopy study. This crack density is an input parameter in estimating the volumetric mass transfer coefficient.

The crack density can be represented by the bulk density of a laminate. The bulk density was calculated from the weight and volume measurement. Figure

Figure 3.14: Photomicrograph of the Avimid K-III/IM-6 laminate processed to 140 °C (facing the tool surface).

3.16 shows the bulk density as a function of processing temperature. As the processing temperature increases, the bulk density is decreasing. This means that the interfacial area due to cracks is increasing with the processing temperature. These bulk density data can be correlated to the overall averaged density as well as the volume fraction of the gas phase from the devolatilization submodel.

3.3.6. Devolatilization Experiments

The effects of both heating rate and laminate thickness on the weight loss of the Avimid K-III/IM-6 laminate were examined under the predescribed process cycle. A caul plate was used to prevent warpage of the laminate during the

Figure 3.15: Photomicrograph of the Avimid K-III/IM-6 laminate processed to 170 °C (facing the tool surface).

devolatilization process.

Effect of Heating Rate. Figure 3.17 shows the cumulative weight losses (ethanol, water, and NMP) of the laminate having 12 plies as a function of tool temperature at heating rates of 0.6, 1.2 and 2.2 °C/min. The weight loss value at 100 °C is assumed to zero since the condensation reaction starts at 100 °C. As the heating rate is increased, the cumulative weight loss curves are shifting to higher temperatures. This means that the devolatilization process is strongly dependent upon the heating rate. The dependency of the devolatilization process on the heating rate is increasing as the laminate thickness is increased (see Figure 3.18). The experimental results are consistent with and verify the predictions

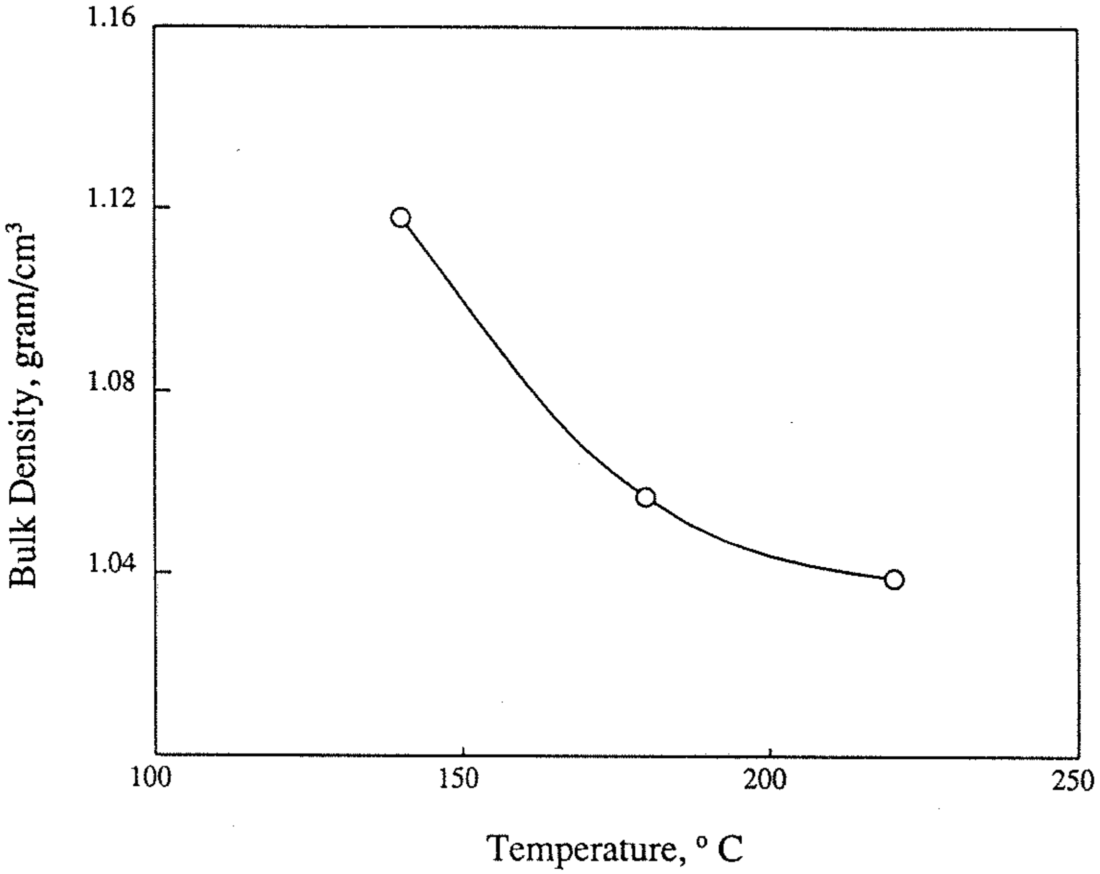

Figure 3.16: Bulk density of the Avimid K-III/IM-6 laminate as a function of processing temperature.

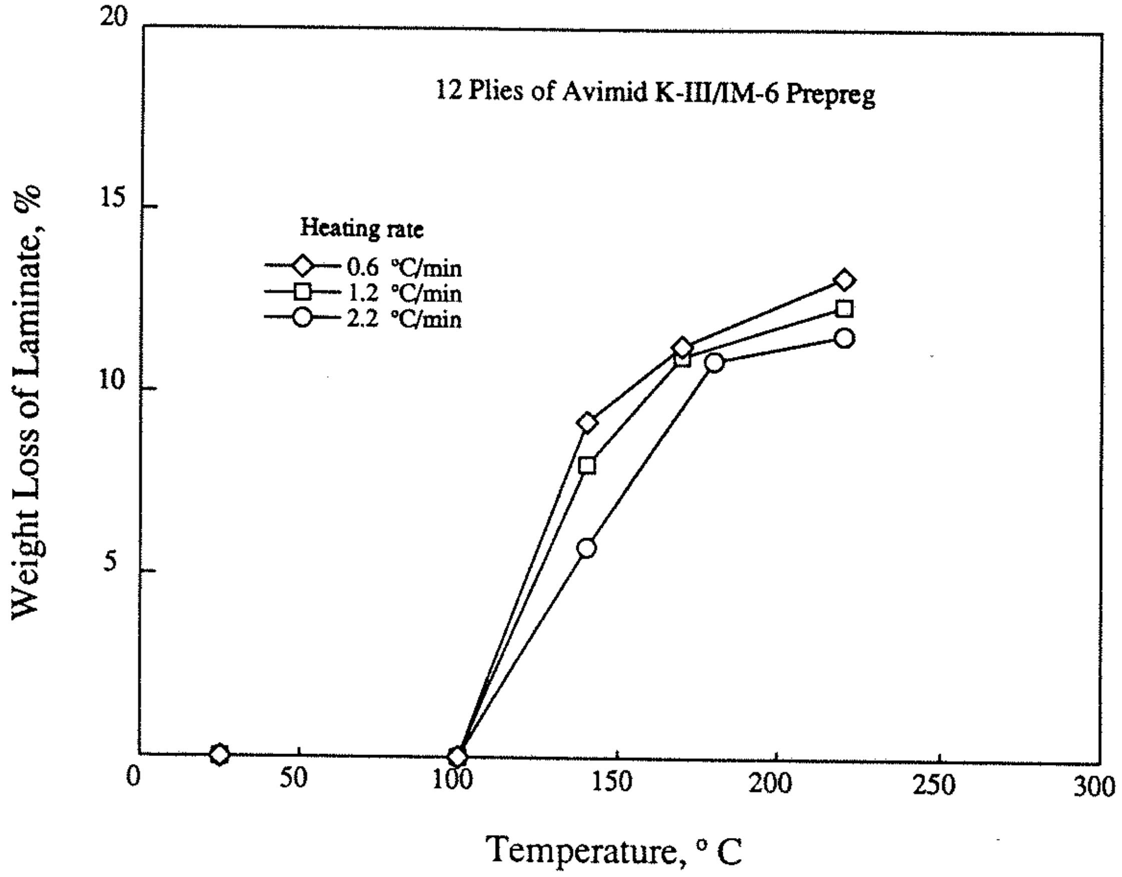

Figure 3.17: Weight loss of the Avimid K-III/IM-6 laminate of 12 plies as a function of temperature and heating rate.

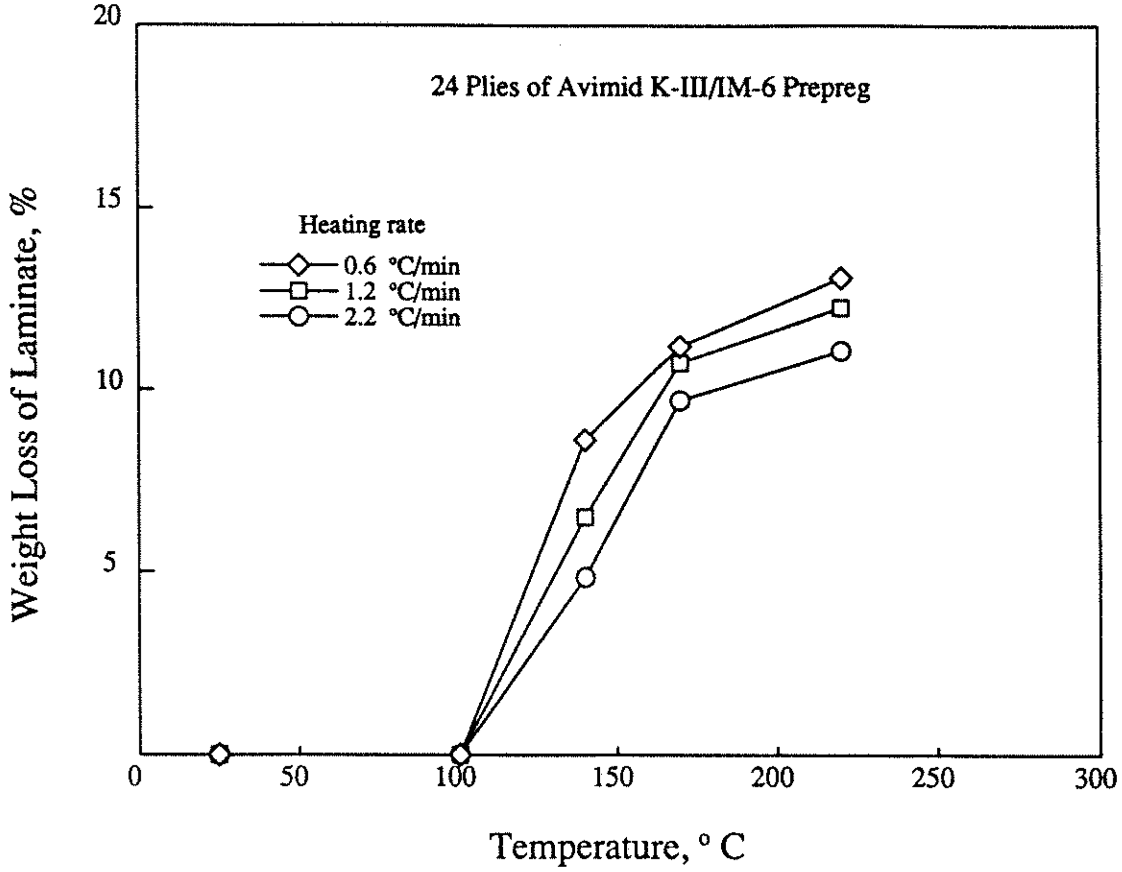

Figure 3.18: Weight loss of the Avimid K-III/IM-6 laminate of 24 plies as a function of temperature and heating rate.

which suggest that the lower heating rate is needed to completely remove the high-boiling point solvent, NMP [25].

Effect of Laminate Thickness. Figure 3.19 shows the weight losses as a function of tool temperature for two different thicknesses of 12 and 24 plies with a heating rate of 2.2 °C/min. The weight losses for the 24-ply laminate are always less than those for the 12-ply one. However, when the heating rate is decreased to 1.2 °C/min, the weight losses after 170 °C are close for both thicknesses as shown in Figure 3.20. The weight losses for the 0.6 °C/min heating rate are nearly identical (see Figure 3.21). This indicates that a lower heating rate is better in processing a thicker laminate. The experimental data also verify the prediction that the mass flux peaks occur at higher tool surface temperatures for thicker composites [25].

3.3.7. Volatile Analysis

In order to know the component volatile flux as a function of processing temperature, volatiles were collected with a cold trap and analyzed with gas chromatography technique.

A Hewlett-Packard GC unit (5890 Series II) with an area integrator was used with a capillary column (liquid phase: SE-30) installed. n-Butanol was used as an internal standard to quantitatively analyze the compositions of the condensate since water, which is one component of the condensate, can not be detected with a flame ionization detector.

The volatiles were collected for the 24-ply Avimid K-III/IM-6 laminates which

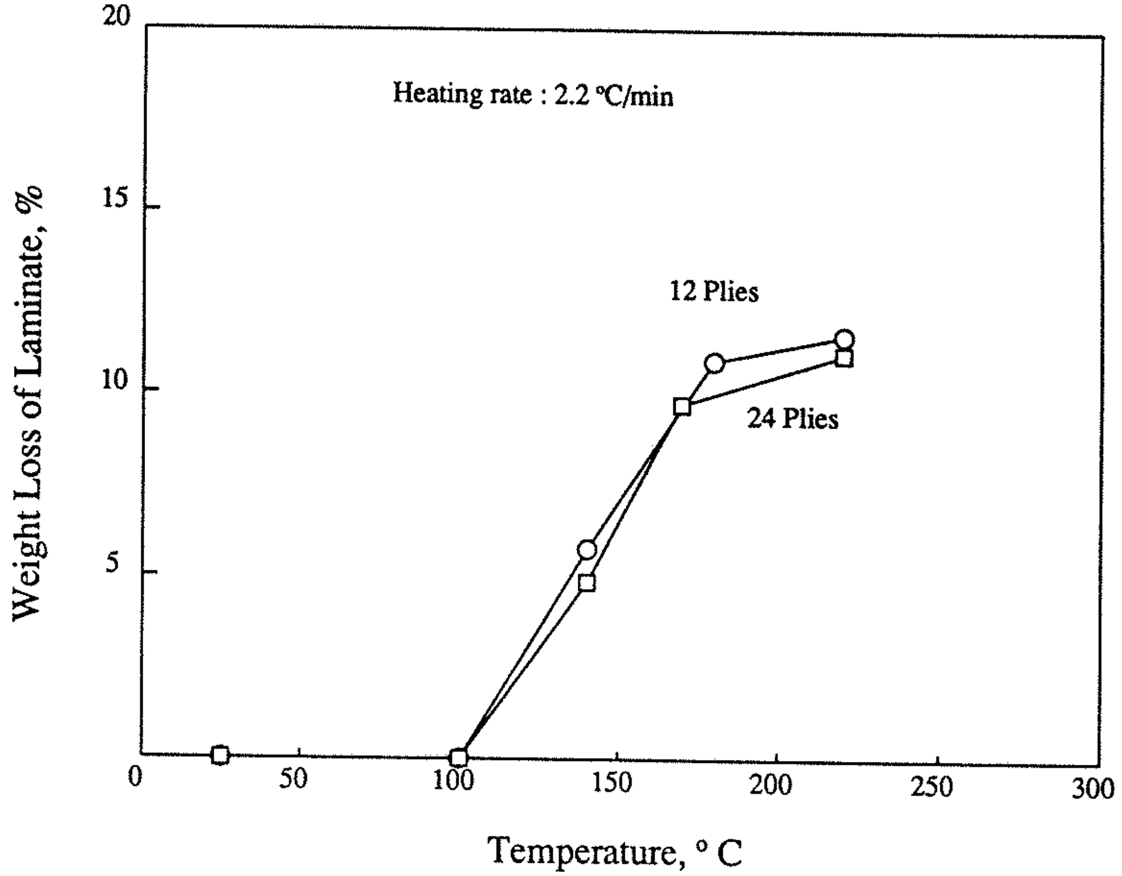

Figure 3.19: Weight loss of the Avimid K-III/IM-6 laminates of 12 plies and 24 plies as a function of temperature at the heating rate of 2.2 °C/min.

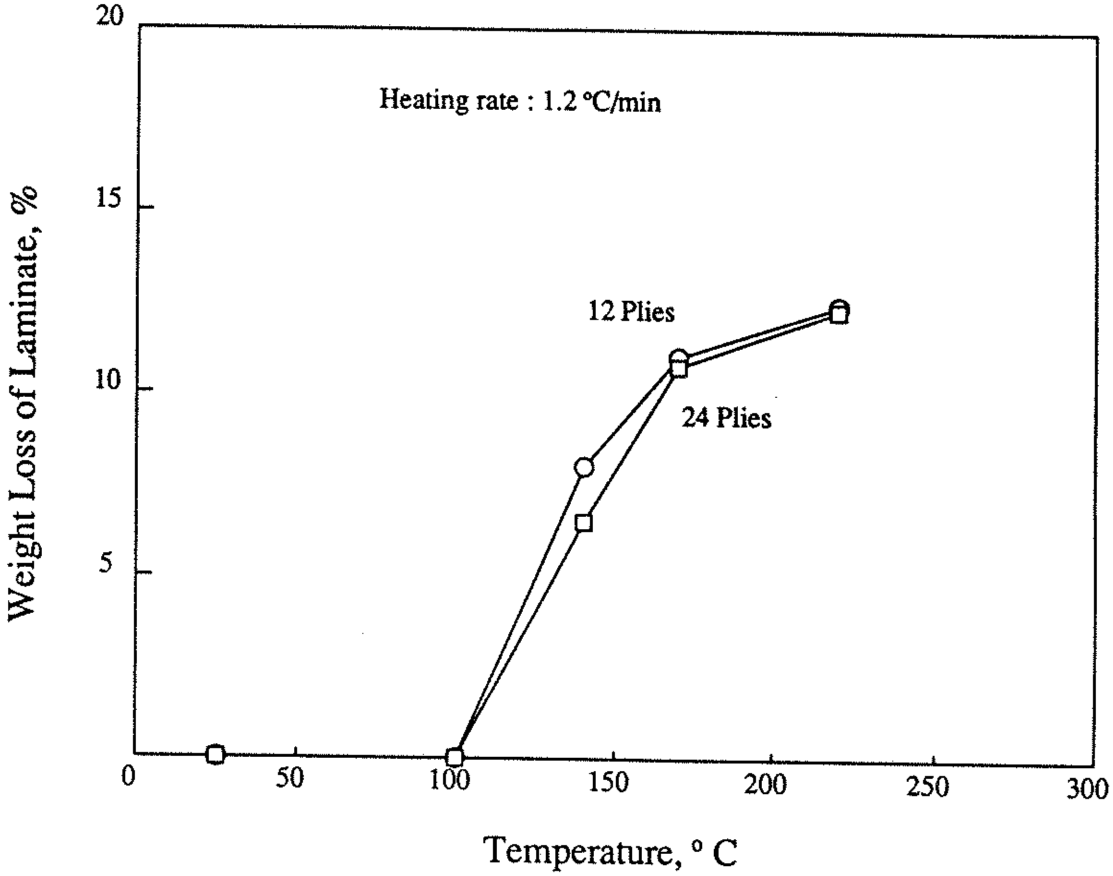

Figure 3.20: Weight loss of the Avimid K-III/IM-6 laminates of 12 plies and 24 plies as a function of temperature at the heating rate of 1.2 °C/min.

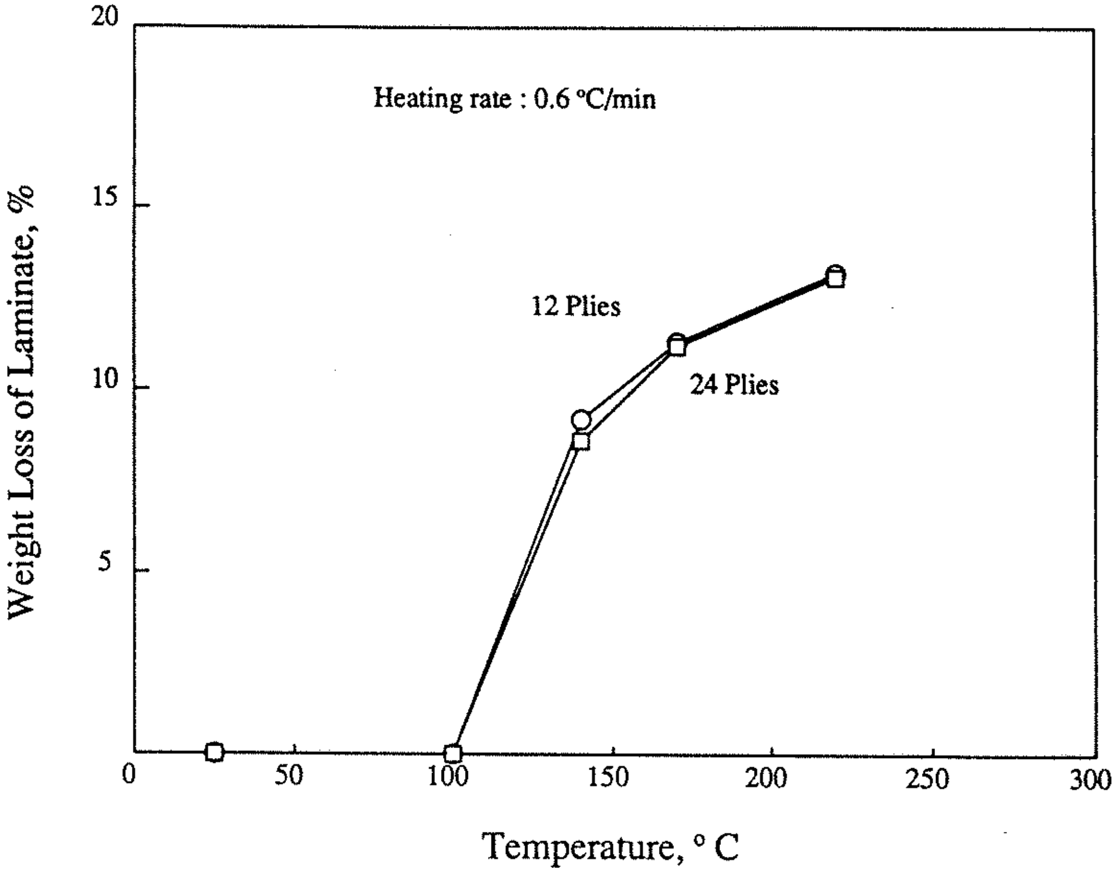

Figure 3.21: Weight loss of the Avimid K-III/IM-6 laminates of 12 plies and 24 layers as a function of temperature at the heating rate of 0.6 °C/min.

were processed with a heating rate of 0.6 °C/min and stopped at 140, 170 and 220 °C.

Figure 3.22 shows a typical gas chromatogram for a calibration solution which consists of ethanol, n-butanol and NMP. The area ratios of ethanol and NMP to n-butanol were used to build a calibration curve. Figure 3.23 shows a typical gas chromatogram for the volatile mixture which was cumulatively collected to 140 °C. By comparing the retention times with those from Figure 3.22, we can confirm that ethanol and NMP are the volatile components evaporating out of the Avimid K-III/IM-6 laminate. With the calibration curve, the area ratios of ethanol and NMP to n-butanol provide the compositions of the condensates.

Figure 3.24 shows the total and component volatile removal as a function of the tool temperature for 5.25 × 5.25 inches, 24 ply unidirectionally-aligned prepregs of Avimid K-III/IM-6 measured at a heating rate of 0.6 °C/min. The weight loss value at 360 °C is taken from the TGA experiments assuming that the evaporation of the volatiles is completely finished at 360 °C. The removal of water and ethanol which are the byproducts of the imidization reaction is found to be finished before about 180 °C. Clearly, a high boiling solvent, NMP is the only one volatile component which is still being removed even after its boiling point, 202 °C. This indicates that there is a strong resistance to NMP evaporation from the liquid phase and the mass transfer limited model for the evaporation flux is reasonably acceptable.

From the viewpoint of the polymerization chemistry of Avimid K-III, the volatile byproducts of the imidization reaction are one mole of ethanol and one mole of water for every mole of polyimide linkages formed (see Figure 2.2). How-

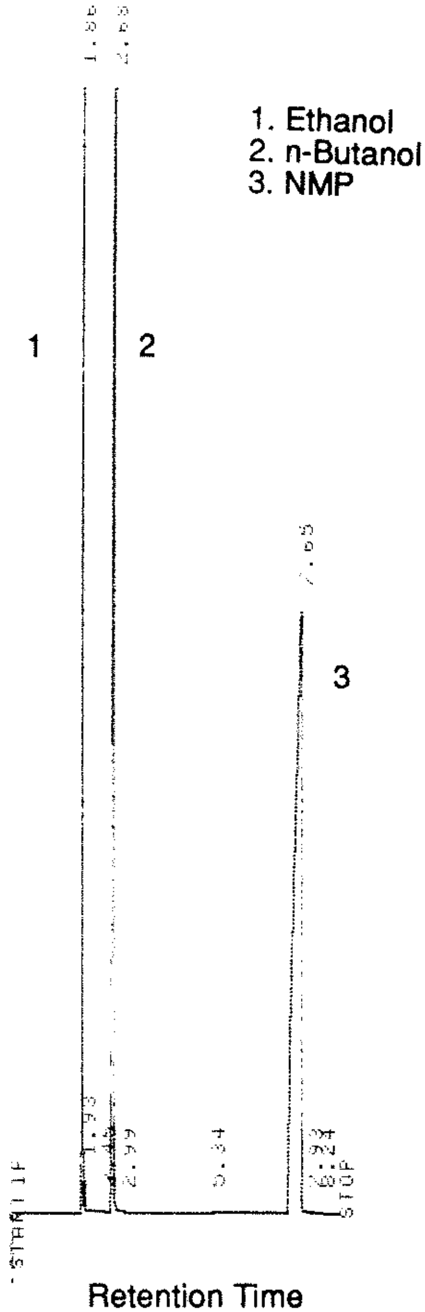

Figure 3.22: Gas chromatogram for a calibration solution containing ethanol, n-butanol and NMP.

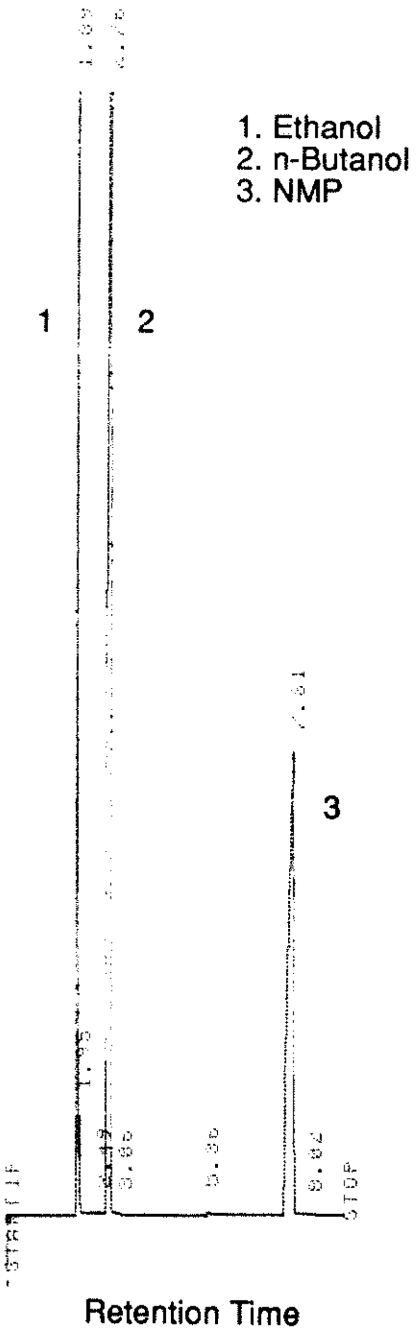

Figure 3.23: Gas chromatogram for the condensate collected from the Avimid K-III/IM-6 laminate processed to 140 °C.

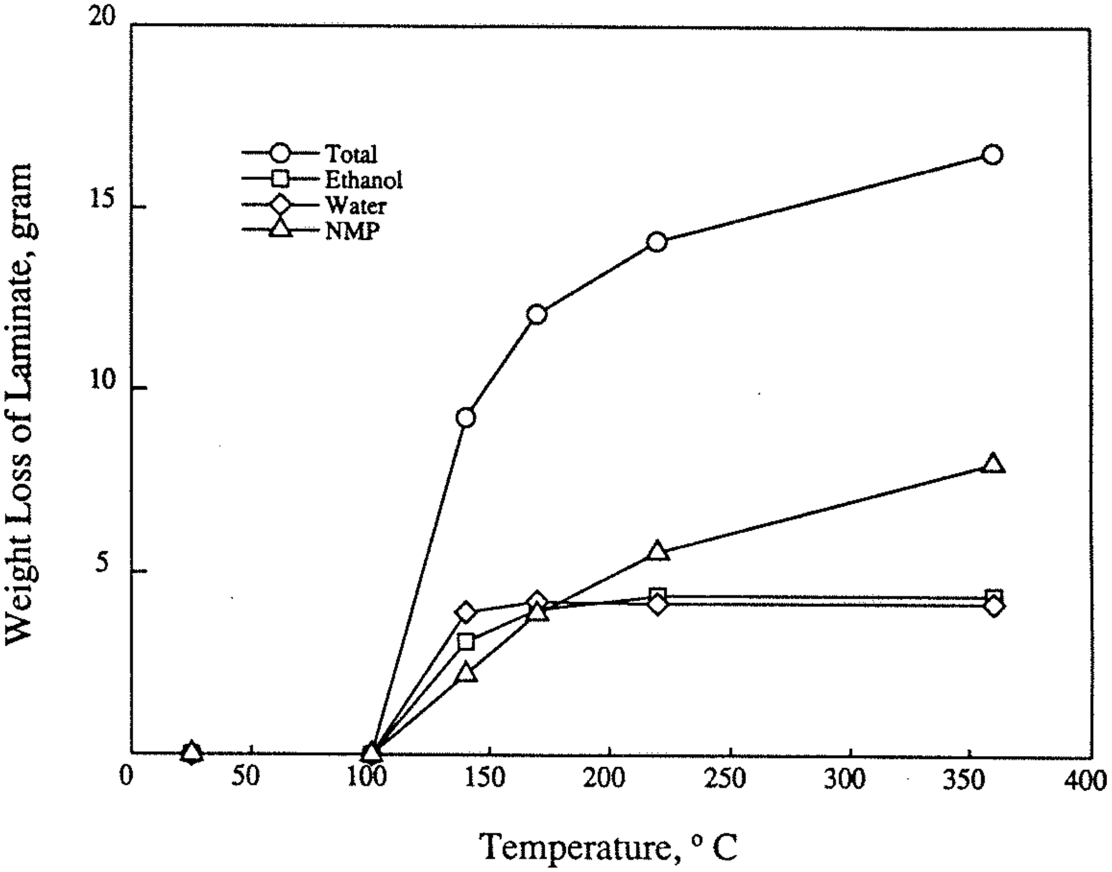

Figure 3.24: Total and component volatile removal as a function of the tool temperature for 5.25 × 5.25 inches, 24-ply unidirectionally-aligned prepregs of Avimid K-III/IM-6 measured at a heating rate of 0.6 °C/min.

ever, the mole number of water is much higher than that of ethanol as shown in Figure 3.24. This indicates that the Avimid K-III/IM-6 prepreg has hygroscopic water which is absorbed from air during a long-period storage in the refrigerator. Note that the solvent, NMP, is very hygroscopic. Because ethanol is produced only by the imidization reaction, we can calculate the amount of water produced from the reaction based on the measured ethanol content. Then, the absorbed water content of the Avimid K-III/IM-6 laminate used is found to be about 2 wt. %. Figure 3.25 is the normalized replotting of Figure 3.24 considering the effect of absorbed water, and will be used for comparing with the model predictions.

3.3.8. Temperature Measurements

The temperature as a function of time was measured at three locations inside a 24-ply Avimid K-III/IM-6 composite with J-type thermocouples. Results of the temperature measurements with a heating rate of 1.2 °C/min are shown in Figure 3.26. The temperature profiles calculated by the devolatilization submodel show [25] that the maximum temperature difference between the tool surface and the bleeder is less than 10 °C for a heating rate of 0.5 °C/min. From Figure 3.26, the maximum temperature difference is 15 °C, which is presumably due to a faster heating rate. However, it can be said that the temperature profile in the laminate is relatively flat. This justifies the model assumption [25] that the temperature difference through the laminate is small, therefore the molar fraction of each volatile can be estimated by:

$$Y_i = \frac{\dot{m}_i / M_{Wi}}{\sum_{i=1}^{3} \dot{m}_i / M_{Wi}} \tag{3.1}$$

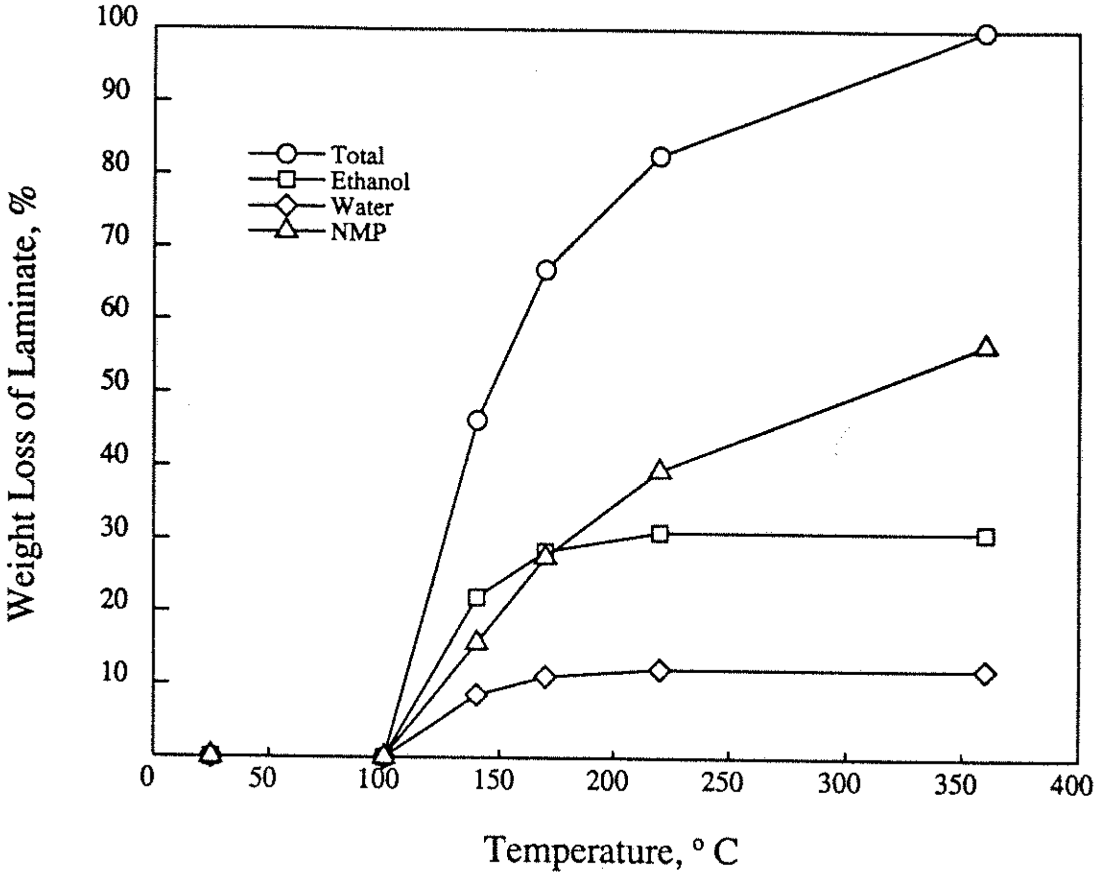

Figure 3.25: Total and component volatile removal as a function of the tool temperature considering the effect of absorbed water.

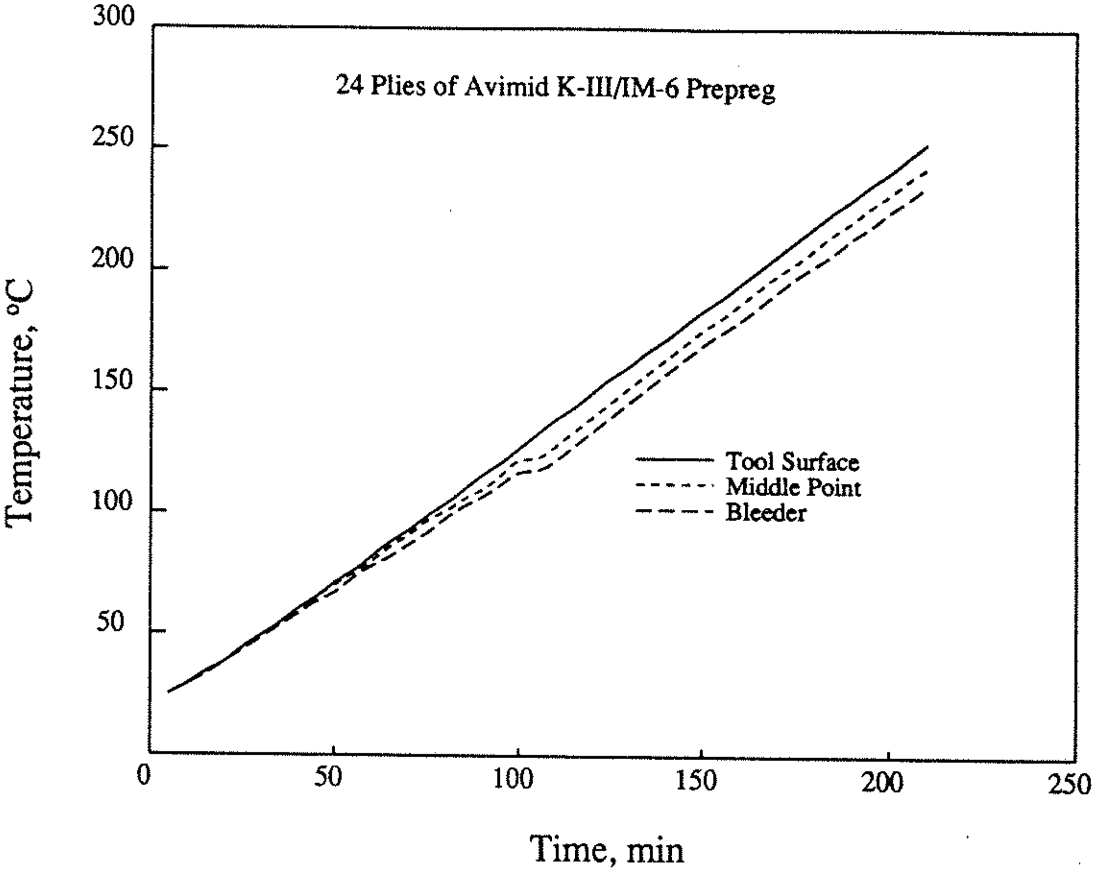

Figure 3.26: Temperature change as function of time at three positions inside a 24-ply Avimid K-III/IM-6 laminate with a heating rate of 1.2 °C/min.

where $\dot{m}_i$ is the evaporation rate of i^{th} volatile component and M_{Wi} is the molecular weight of i^{th} component.

The temperatures in the middle point and at the bleeder have inflection points at 130 °C where full vacuum was applied. This is due to the fact that on applying full vacuum a violent evaporation of the volatiles takes place which needs energy to supply the heat of vaporization.

3.4. EXPERIMENTAL VERIFICATION OF THE DEVOLATILIZATION SUBMODEL

Summarizing the devolatilization submodel explained earlier, equations have been developed for the energy balance, gas phase mass balance, liquid phase mass balance, and mass balances for water, ethanol, NMP, and the active groups in the monomer and growing polymer chains. To these seven coupled partial differential equations have been added expressions for the evaporation rate of each volatile component, for the polymer reaction kinetics, and for the volumetric mass transfer coefficient for transfer between liquid and gas phases. Additional inputs were obtained for physical properties including density, heat capacity, thermal conductivity, and viscosity.

The simulation results of the devolatilization submodel can be found elsewhere [6]. The model predicts the total and individual component volatile mass fluxes, as well as the temperature and pressure profiles through the laminate as a function of the initial laminate thickness and the temperature and pressure cycles employed during autoclave processing.

3.4.1. Input Parameter

Among the input parameters, the volumetric mass transfer coefficient is the key parameter of the devolatilization model. It is clear that the overall mass transfer coefficient, $K_m A_\beta$, should increase as the devolatilization takes place due to an increase in the interfacial area, A_β. However, when the polymerization takes place, the viscosity of the liquid builds up quickly. This reduces K_m and will cause $K_m A_\beta$ to be decreased. Figure 3.27 shows the complex viscosity of prepregs based on Avimid K-III measured at 0.5, 1, 2, and 5 °C/min heat-up rates [26]. As the heating rate is increased, the minimum viscosity temperature is shifting to higher temperature. It should be noted that the mass transfer coefficient is inversely proportional to the viscosity. Therefore, based on Figure 3.27, the overall volumetric mass transfer coefficients for the different heating rates are estimated as shown in Figure 3.28 and used as an input parameter for the model.

3.4.2. Comparisons of Model Prediction with Experimental Results

In order to verify the devolatilization model the results from the devolatilization experiments are compared with the model predictions.

A finite element collocation method based on the method of lines was utilized to solve the seven coupled partial differential equations. Several packages have been tested and the DPDE subroutine in the IMSL package (International Mathematics and Statistics Library, 1983 version) was chosen for simulation due to its

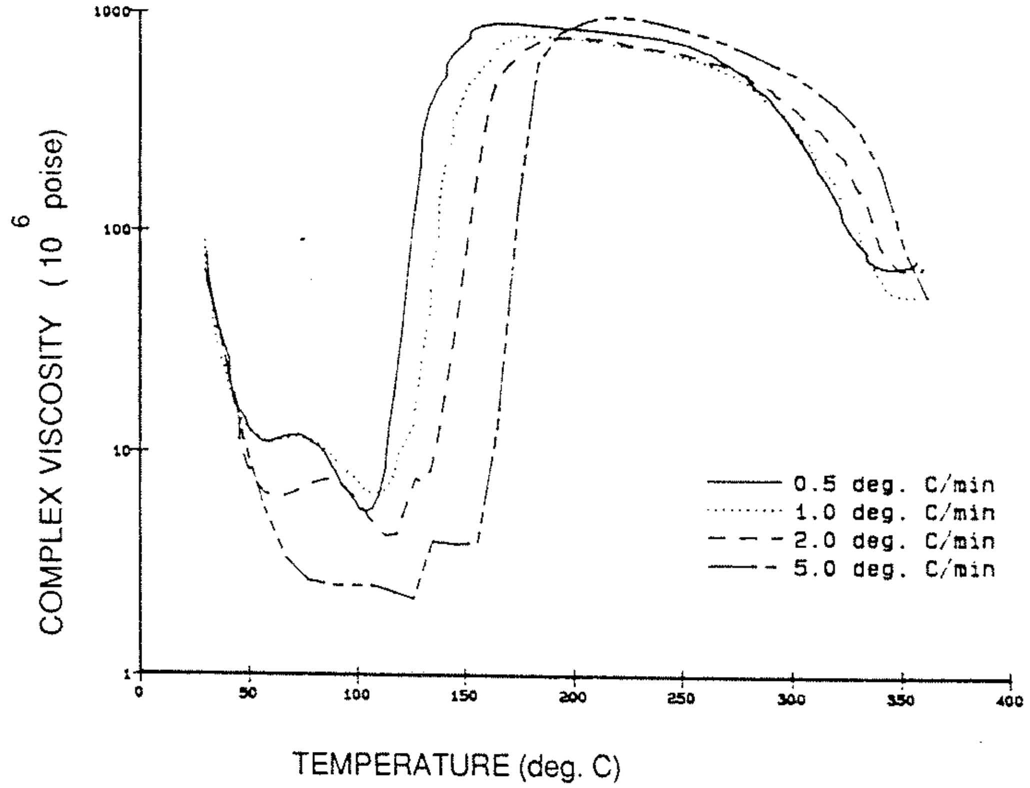

Figure 3.27: Complex viscosity of prepregs based on Avimid K-III measured at 0.5, 1, 2, and 5 °C/min heat-up rates [26].

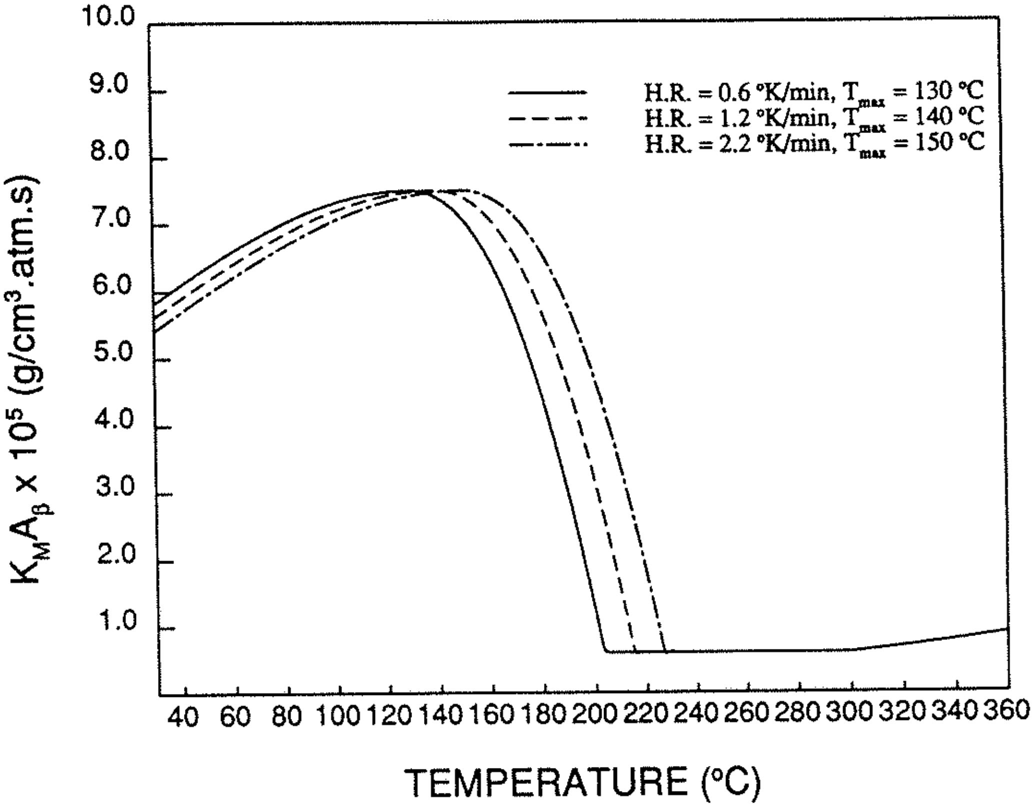

Figure 3.28: Overall volumetric mass transfer coefficients as a function of temperature and heating rate.

efficiency and accuracy. In all cases the tool surface temperature was increased continuously at a constant heating rate to 360 °C.

Figure 3.29 shows the comparison between the measured component weight losses and those predicted from the model for the 24-ply Avimid K-III/IM-6 laminate with a heating rate of 0.6 °C/min. Clearly, there is ~~an~~ good agreement between the experimental data and model predictions. Figure 3.30 also shows the comparison between the measured total weight losses and those predicted from the model for the 24-ply laminates with the three different heating rates. There is, also, an acceptable agreement between the experimental data and model predictions. As the heating rate is increased, the model underpredicts the weight losses. This is probably attributed to the fact that the volatile removal through the lateral direction of the laminate is not negligible because the size of the laminate is relatively small. It should be noted that the devolatilization model is based on one-dimensionall~~y~~ ~~developed.~~ due [illegible].

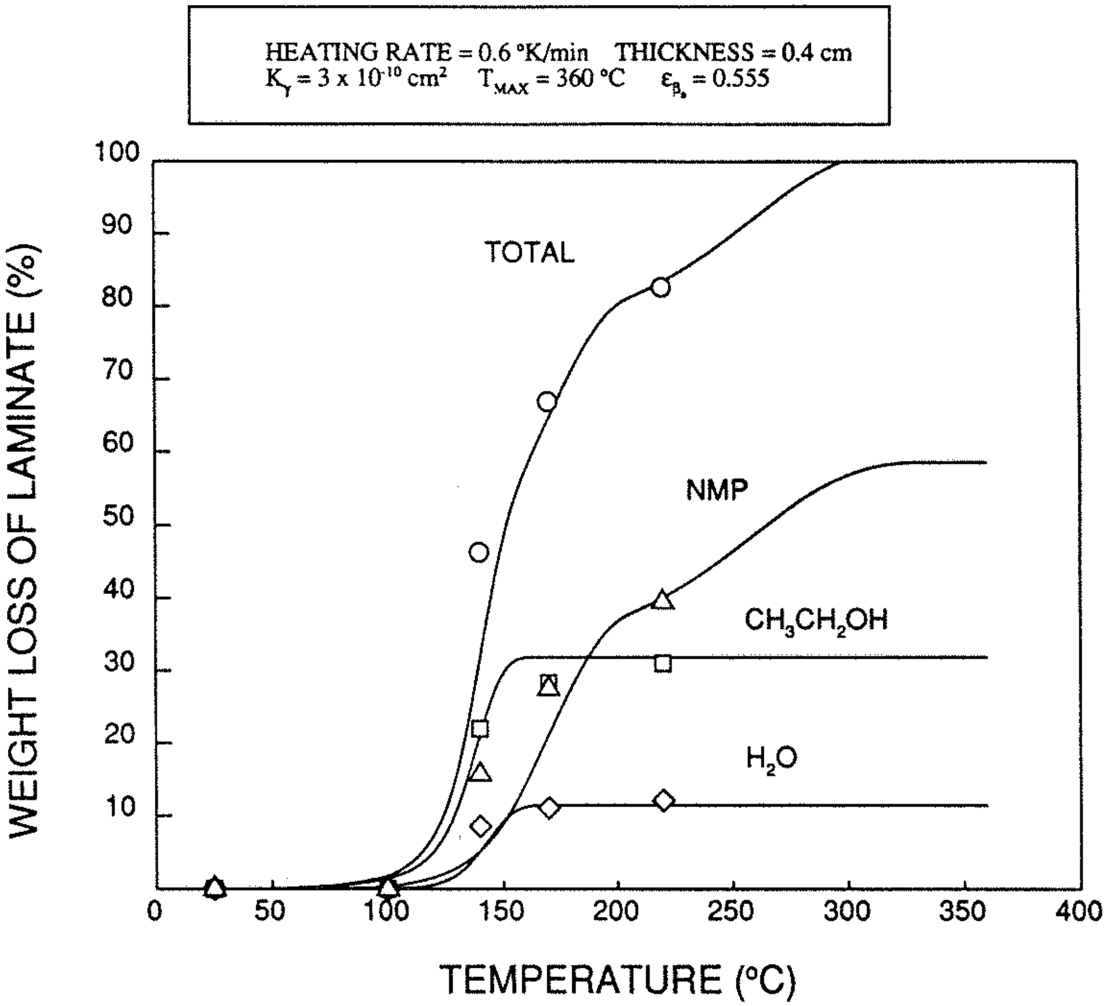

Figure 3.29: Comparison between the measured component weight losses and those predicted from the model for the 24-ply Avimid K-III/IM-6 laminate with a heating rate of 0.6 °C/min.

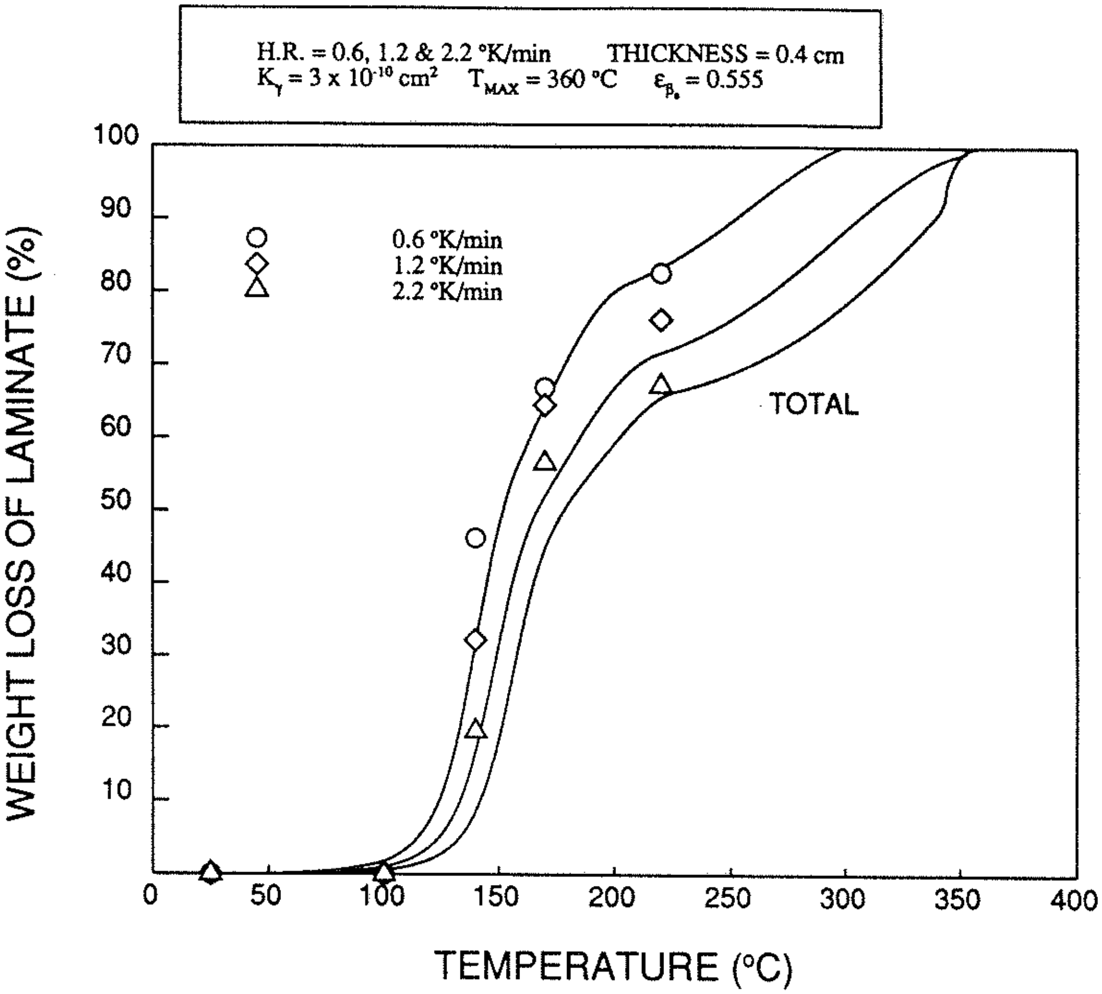

Figure 3.30: Comparison between the measured total weight losses and those predicted from the model for the 24-ply Avimid K-III/IM-6 laminate with the three different heating rates.

4. CONSOLIDATION

4.1. TWO-DIMENSIONAL FLOW CONSOLIDATION EXPERIMENTS

4.1.1. Resin Pressure Measurement Apparatus

In order to better understand the consolidation behavior, an apparatus for measuring resin pressure was constructed as shown schematically in Figure 4.1. A laboratory press was utilized, in which a rectangular consolidation cell (4.8×4.8×2 inches) made of Plexiglas was placed. The applied pressure can be determined by the weight placed on the plunger. Miniature pressure transducers (Kulite Semiconductor Products) were used whose positions in the prepregs could be selected as desired. Since the thickness of a fiber bed is relatively small at least three points along the principal direction were always chosen for the pressure measurement. The geometry of the miniature pressure transducer is shown in Figure 4.2. The transducer was protected from the fibers by an "M" type screen so that only resin pressure is sensed. The "M" type screen consists of a 5 mil thick fine metallic mesh with hole size 6 mil in diameter [27].

All of the consolidation experiments were performed on unidirectionally aligned graphite fibers impregnated with oil of constant viscosity. Silicone oil with viscos-

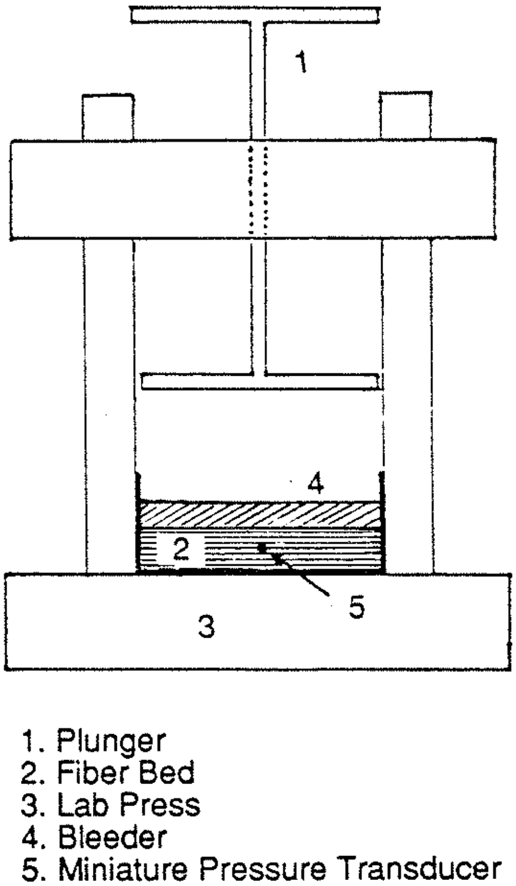

Figure 4.1: Schematic of a resin pressure measurement cell.

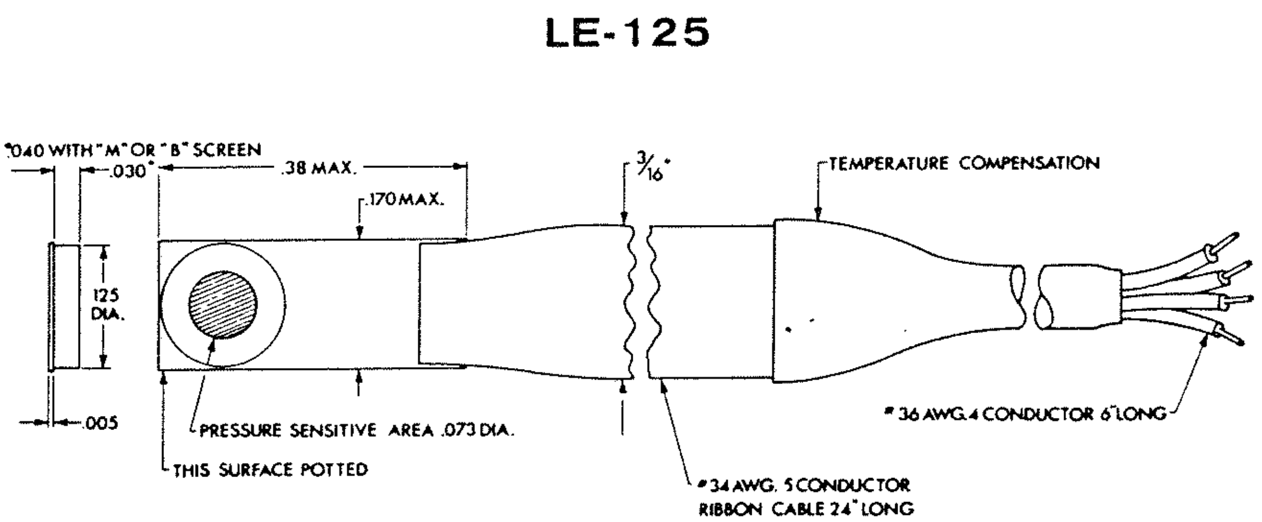

Figure 4.2: Schematic of a miniature pressure transducer.

ity of 100 centistokes was used to mimic a resin; the graphite fiber was Hercules AS4-12K. The unidirectionally aligned carbon fiber bed with the fiber volume fraction of 0.45 was prepared with a winding device which is shown in Figure 4.3.

A data acquisition system was developed to process the electrical signals from the miniature pressure transducers. A PC's Limited system 200 personal computer was used to digitally record the resin pressure measurements. The pressure transducers were connected to the PC via 3B-18 signal conditioners (Analog Devices). The signal conditioners were then attached to the universal data acquisition board which contained the A/D converter. Four data points per second for each pressure transducer were recorded and averaged.

4.1.2. Effect of Filter Paper on Resin Pressure

Four layers of filter paper were used to prepare a well aligned fiber bed of 8 mm thickness. Each filter paper was equally spaced at every 2 mm thickness. Two miniature pressure transducers were placed at the bottom and below the bleeder, respectively. When the dead weight was placed on the top of the plunger (i.e. constant load condition), the resin pressures at the two different positions were measured as a function of time.

Figure 4.4 shows the resin pressure change as a function of time for the bed with the equally spaced filter paper. It can be seen that the resin pressure at the bottom (i.e. at the tool surface) is not changed much. On the other hand, Figure 4.5 shows the resin pressure change as a function of time for the fiber bed without filter paper; all other experimental conditions being the same. Clearly, the resin pressure at the bottom decreases quickly and continuously. Thus, the

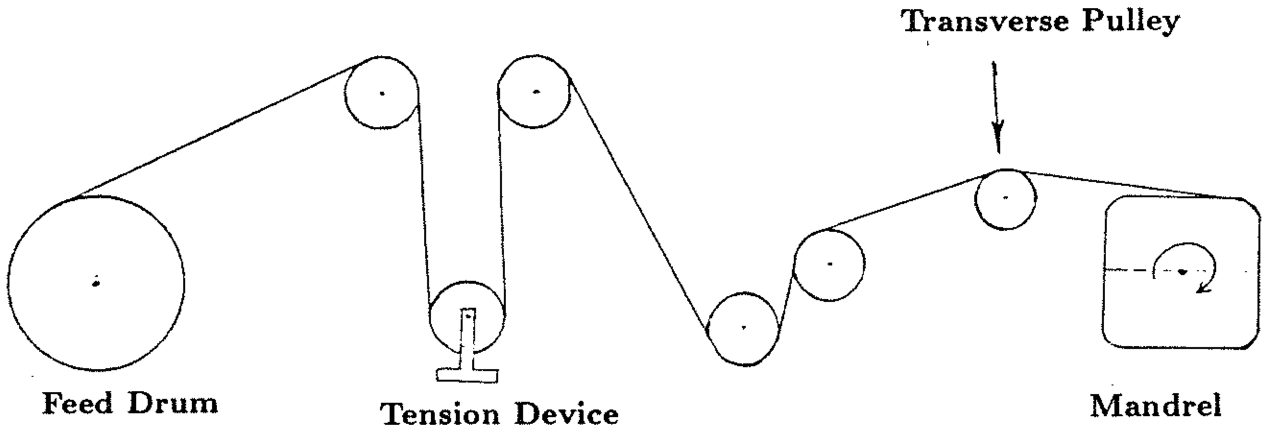

Figure 4.3: Schematic of the winding device for a unidirectionally aligned fiber.

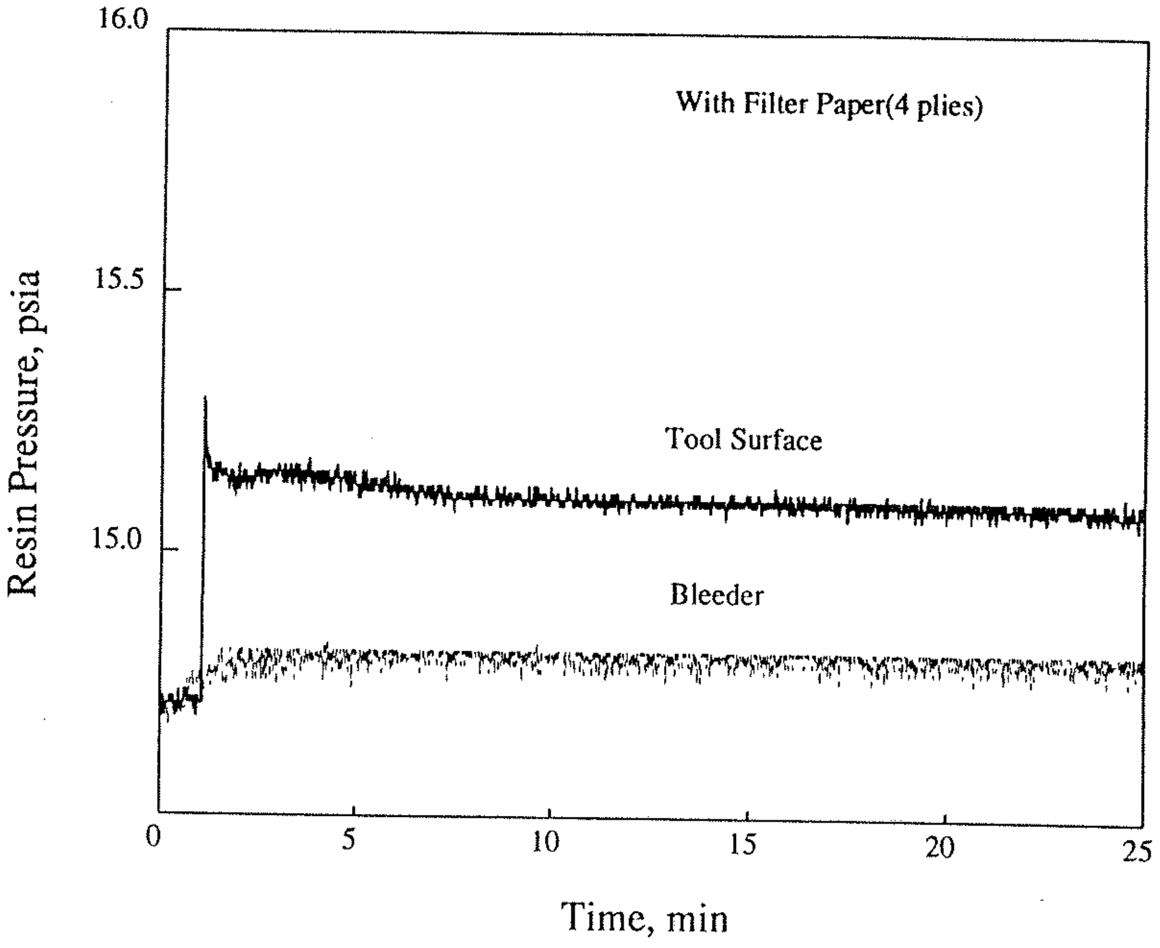

Figure 4.4: Resin pressure change as a function of time for a bed with equally spaced filter paper.

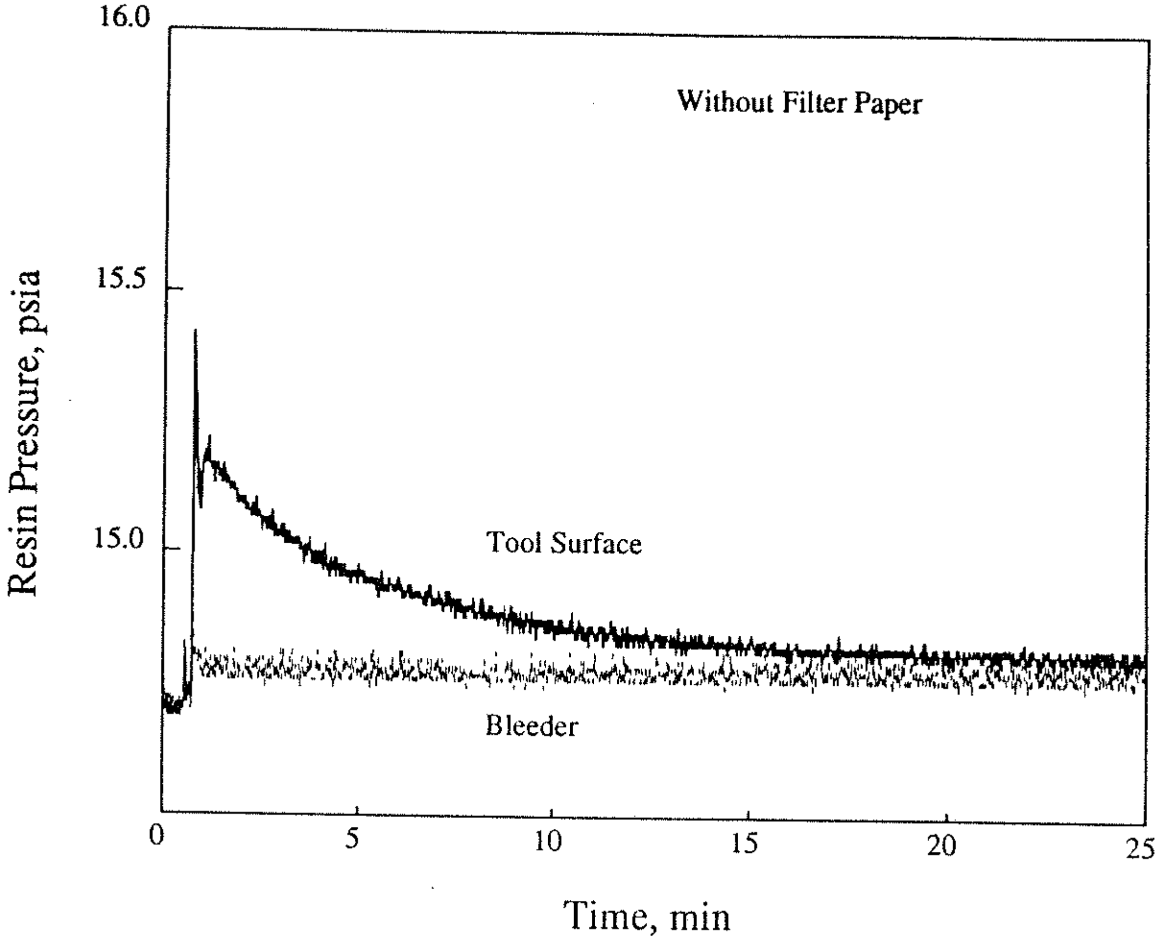

Figure 4.5: Resin pressure change as a function of time for the bed without filter paper.

filter paper influences the resin flow significantly, at least for fluids (silicone oil) of 100 centistokes viscosity. This finding suggests that filter paper should not be used in the resin pressure and/or permeability measurement experiments.

4.1.3. Effect of Bleeder Capacity

A consolidation experiment with the bleeder was performed to examine the effect of bleeder capacity. The bleeder used was Airweave N-10 (Airtech International Inc.) which is a nonwoven fabric and is lighter than a typical glass bleeder. The height of the unidirectionally aligned carbon fiber bed was 16 mm and the fiber volume fraction, V_f, was 0.45. Three miniature pressure transducers were positioned at the bottom (tool surface), middle point, and top (below the bleeder), respectively.

Figure 4.6 shows the resin pressure change as a function of time at three different positions for the case of two layers of Airweave N-10. The resin pressures at the bottom and in the middle are continuously decreasing and the boundary pressure at the bleeder-composite interface is almost constant after jumping slightly on application of the load.

In order to examine whether or not a pressure gradient in the horizontal direction (parallel to the fiber axis) occurs, the resin pressure in this direction was measured and is shown in Figure 4.7. There is a pronounced pressure gradient in the horizontal direction, which means that the bleeder ply consolidation experiment must be considered as two-dimensional flow.

In order to investigate the effect of bleeder capacity on the resin pressure,

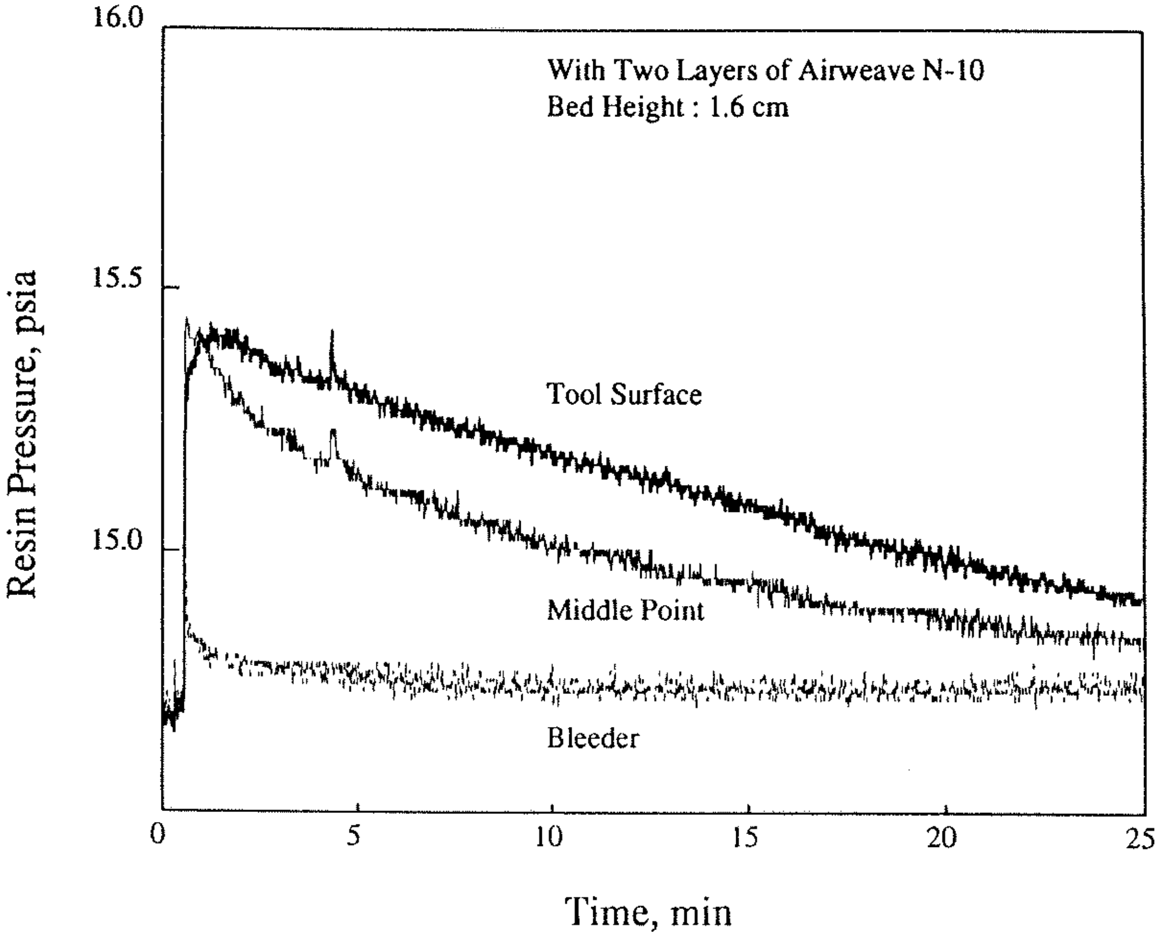

Figure 4.6: Resin pressure change as a function of time with two layers of Airweave N-10.

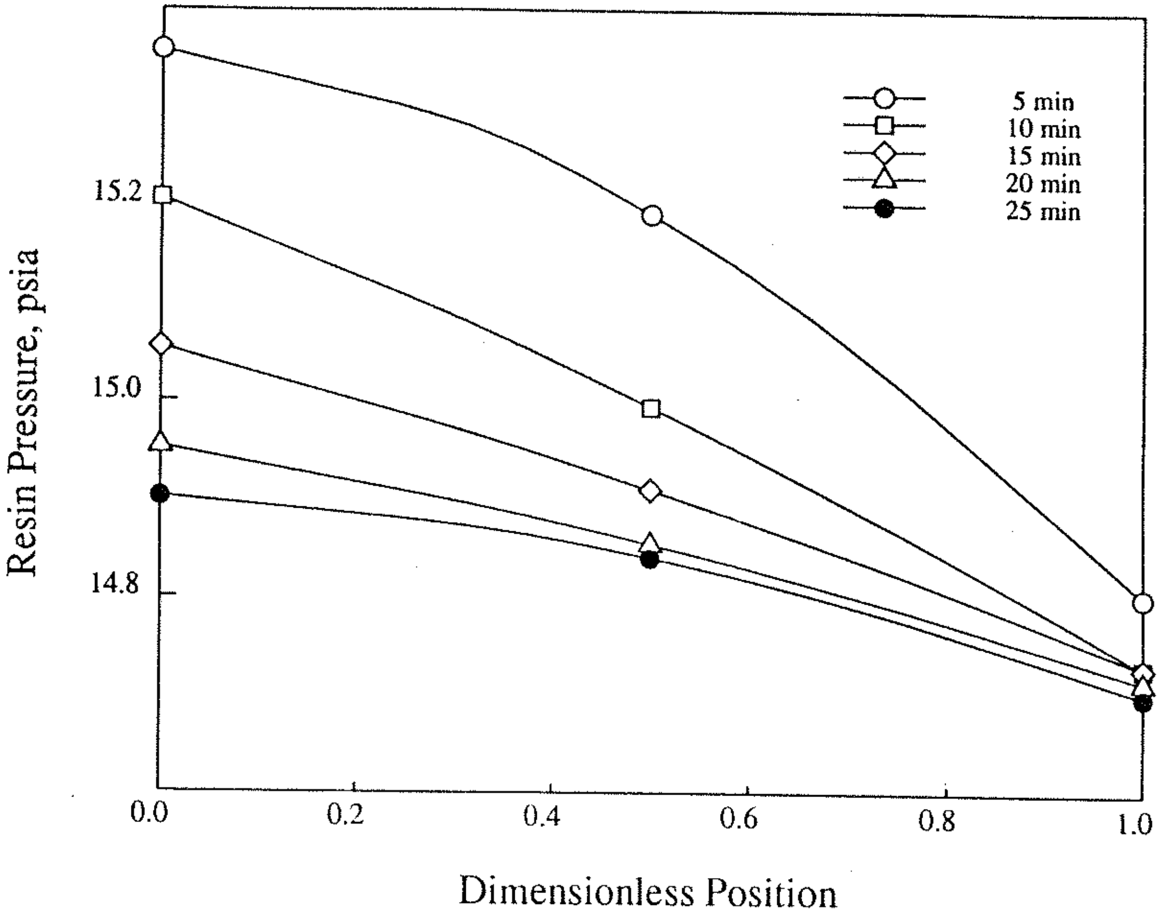

Figure 4.7: Resin pressure-position (horizontal-parallel to the fiber axis) distributions as a function of time with two layers of Airweave N-10 (position measure from centerline of the bed).

the number of layers of Airweave N-10 was reduced to one, all other parameters being the same. Figure 4.8 shows the resin pressure change as a function of time. The resin pressure at the bottom continuously decreases. However, the resin pressure in the middle of the fiber bed initially decreases and increases slightly later. This phenomenon can be explained as follows: The flow pattern was initially two-dimensional until the layer of Airweave N-10 becomes saturated with oil. When the bleeder becomes saturated, horizontal flow becomes dominant. It is also observed that as the bleeder becomes saturated the resin pressure at the bleeder-composite interface increases slightly. Figure 4.9 shows the resin pressure-vertical position distribution as a function of time. It is noteworthy that the resin pressure profiles are nonlinear. The observed maximum in the pressure profiles at larger times (the 20 and 25 minute curves) is due to a saturated bleeder which makes the horizontal flow dominant at that point in time. For horizontal flow, the pressure must be highest at mid-laminate and decrease as one goes toward each end.

In order to further examine the effect of a bleeder, no bleeder was used. This experiment can be referred to as compression molding. The resin pressure at three different positions along the vertical direction was measured as a function of time as shown in Figure 4.10. It was observed that the oil is squeezed and overflows on the caul plate when the fiber bed consolidates. The resin pressure below the caul plate is as high as that at the bottom and at the middle point, and becomes higher after 10 min. From these measurements, it is clear that the pressure gradient in the vertical direction is negligible when no bleeder is introduced. This implies that there are pressure gradients in the horizontal direction which induce the resin flow.

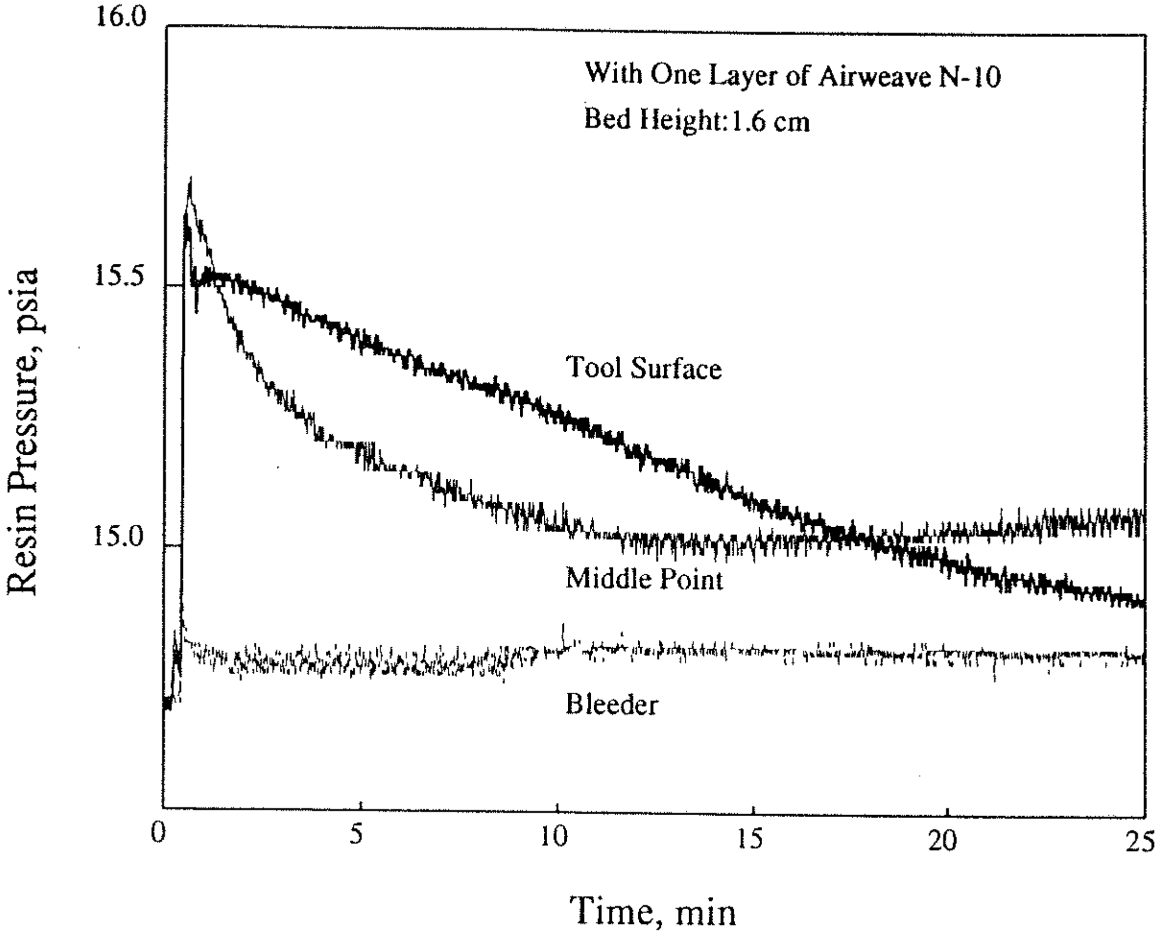

Figure 4.8: Resin pressure change as a function of time with one layer of Airweave N-10.

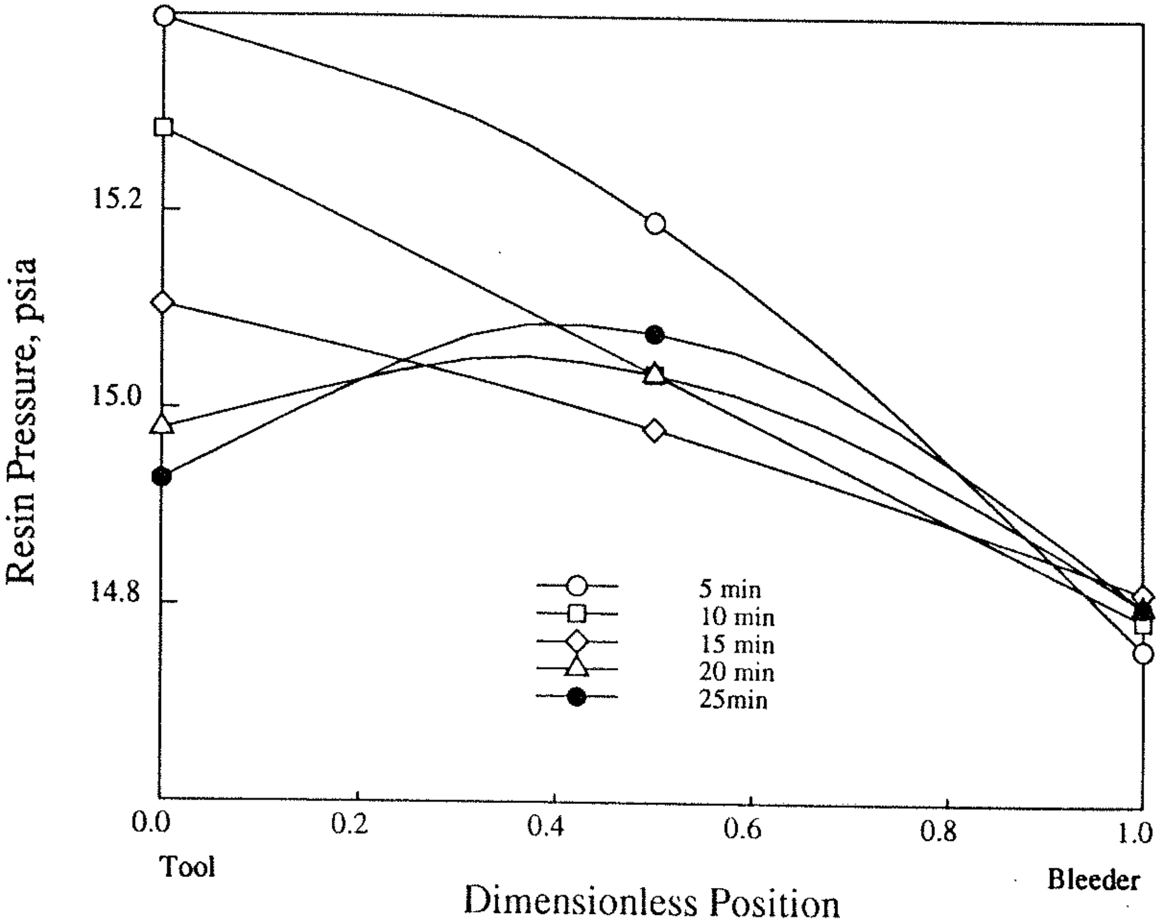

Figure 4.9: Resin pressure-position (vertical) distributions as a function of time with one layer of Airweave N-10.

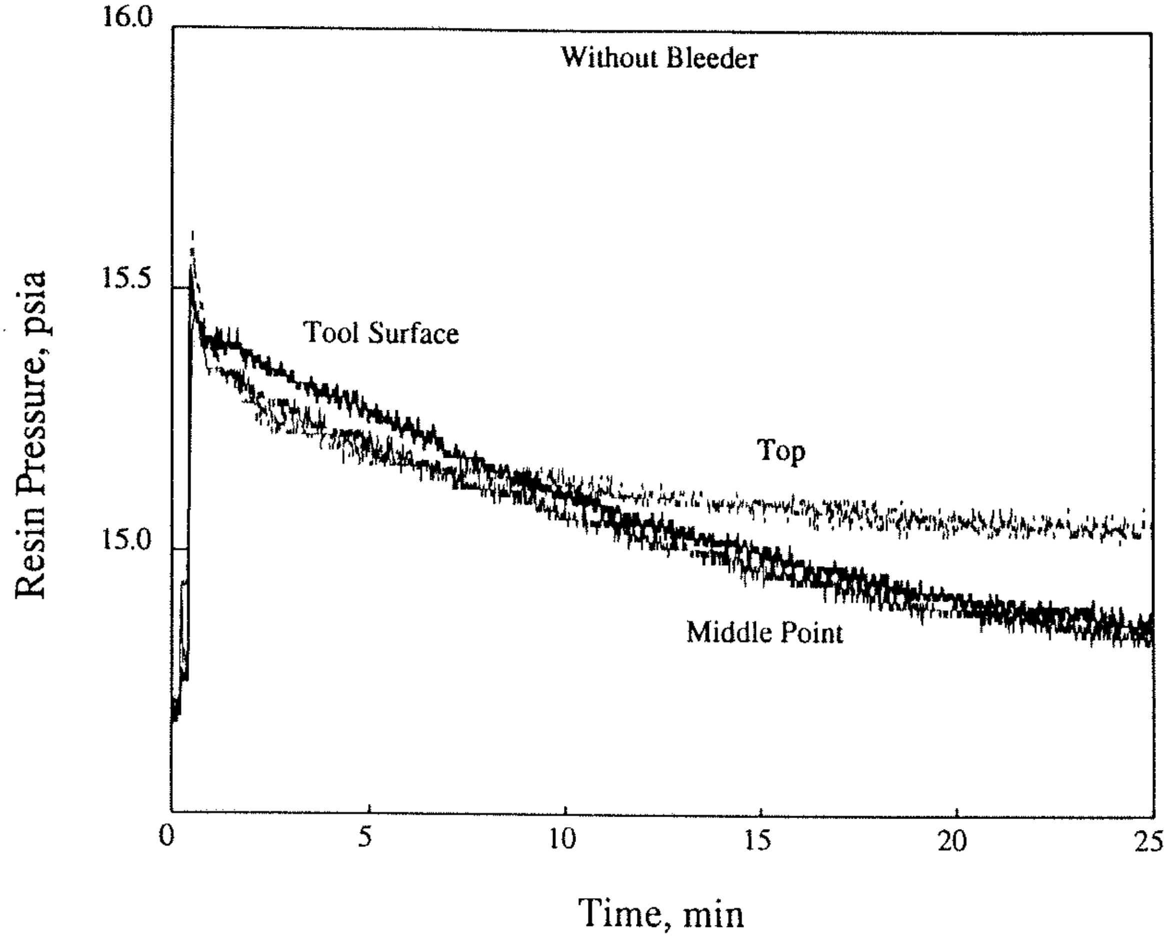

Figure 4.10: Resin pressure change as a function of time without a bleeder.

Figure 4.11 shows the resin pressure change as a function of time in the horizontal direction. As expected, there are pressure gradients in the horizontal direction and the resin pressure at the center is the largest and quickly decreases. The resin pressure at the three different positions becomes equal after 25 min. Compared with the vertical flow, the decay of the resin pressure is faster. This is due to the fact that the permeability in the horizontal direction (fiber axis direction) is nearly 20 times the permeability in the vertical direction (perpendicular to the fiber axis) [16]. This finding coincides with Murooka's work [28]. Murooka et al. measured resin pressures in the horizontal direction in the prepregs (multilayer printed circuit board) when the prepregs were compressed. They found that there are pressure gradients in the horizontal direction and the resin pressures in the prepregs continuously decrease. They also found that the resin pressure profiles were nonlinear from four-point resin pressure measurement with time.

From a comparison of Figure 4.10, Figure 4.8 and Figure 4.6, it is clear that the bleeder capacity plays an important role in determining the flow pattern. Therefore, a sufficient amount of the bleeder was used for the other experiments not to make the bleeder saturated.

4.1.4. Effect of Applied Pressure

The effect of the applied load on the resin pressure was also investigated. The consolidation pressure was increased from 0.7 psig to 1.9 psig. Figure 4.12, when compared with Figure 4.6, shows that the resin pressure decreases more quickly due to the increased load. This means that the applied load can affect the resin flow and hence the resin content profile and consolidation profile of a laminate.

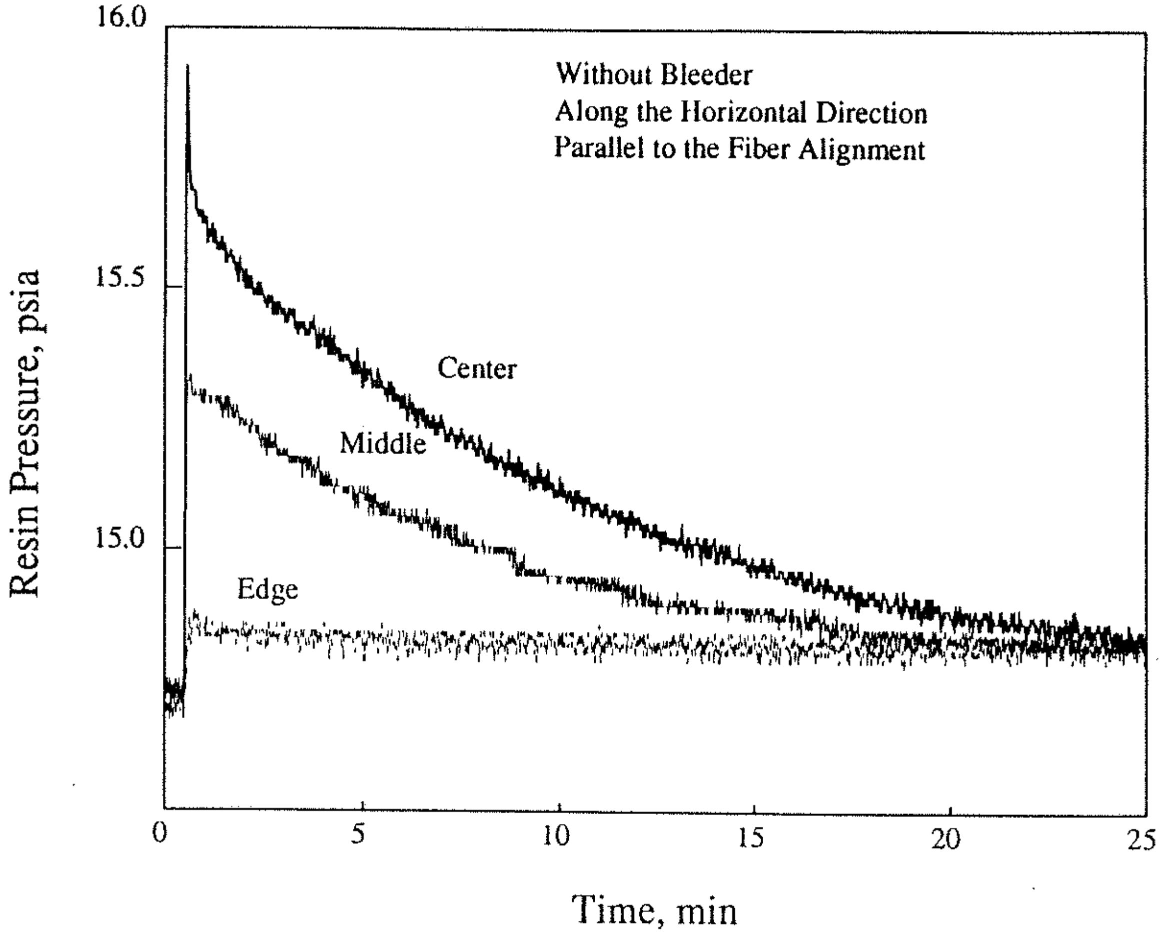

Figure 4.11: Resin pressure change in the horizontal direction as a function of time without a bleeder.

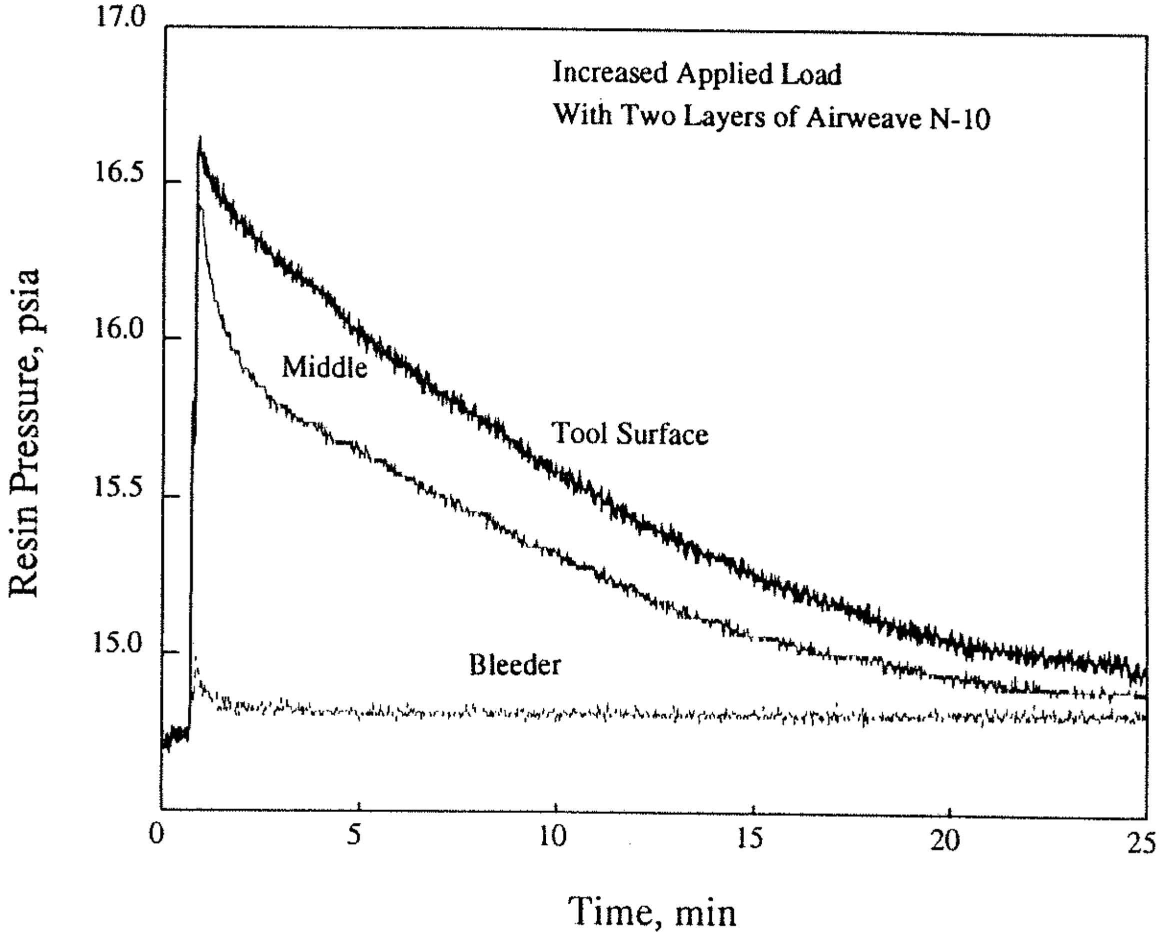

Figure 4.12: Resin pressure change as a function of time with two layers of Airweave N-10 and increased consolidation load in the vertical direction (1.9 psig).

The resin pressure profiles are also found to be nonlinear as shown in Figure 4.13.

4.1.5. Effect of Bed Thickness

The effect of fiber bed thickness on the resin pressure distribution was examined. The thickness of the fiber bed was increased from 16 mm to 24 mm. The initial fiber volume fraction was again 0.45. The resin pressure at three different positions as a function of time is shown in Figure 4.14. The locations of the pressure transducers are indicated in the insert. The resin pressure as a function of time is shown to be almost equal irrespective of position. This means that the pressure profile is relatively flat except near the boundary. Figure 4.15 shows the sharp resin pressure gradient at the bleeder-composite boundary. This implies that the vertical flow is not favorable, which can be explained in terms of large differences in directional permeability for horizontal and vertical flow. The ratio of the axial permeability to the transverse permeability is about 20. For the 16 mm thick fiber bed, the ratio of the areas available for vertical and horizontal flow is large enough to overcome the effect of different permeabilities. However, when the bed thickness is increased to 24 mm, flow in the horizontal direction becomes dominant. The ratios of the areas available for horizontal flow to vertical flow are 0.53 and 0.8 for the 16 mm and 24 mm thick bed, respectively. This result coincides with the prediction that in a thin laminate (64-ply) the vertical resin loss is significantly higher than the horizontal loss, whereas in a thick laminate (256-ply) the reverse holds true [4].

The resin pressure at the tool surface decreases even for the thick fiber bed of 0.45 fiber volume fraction, which is not predicted by the Springer-Loos model [11].

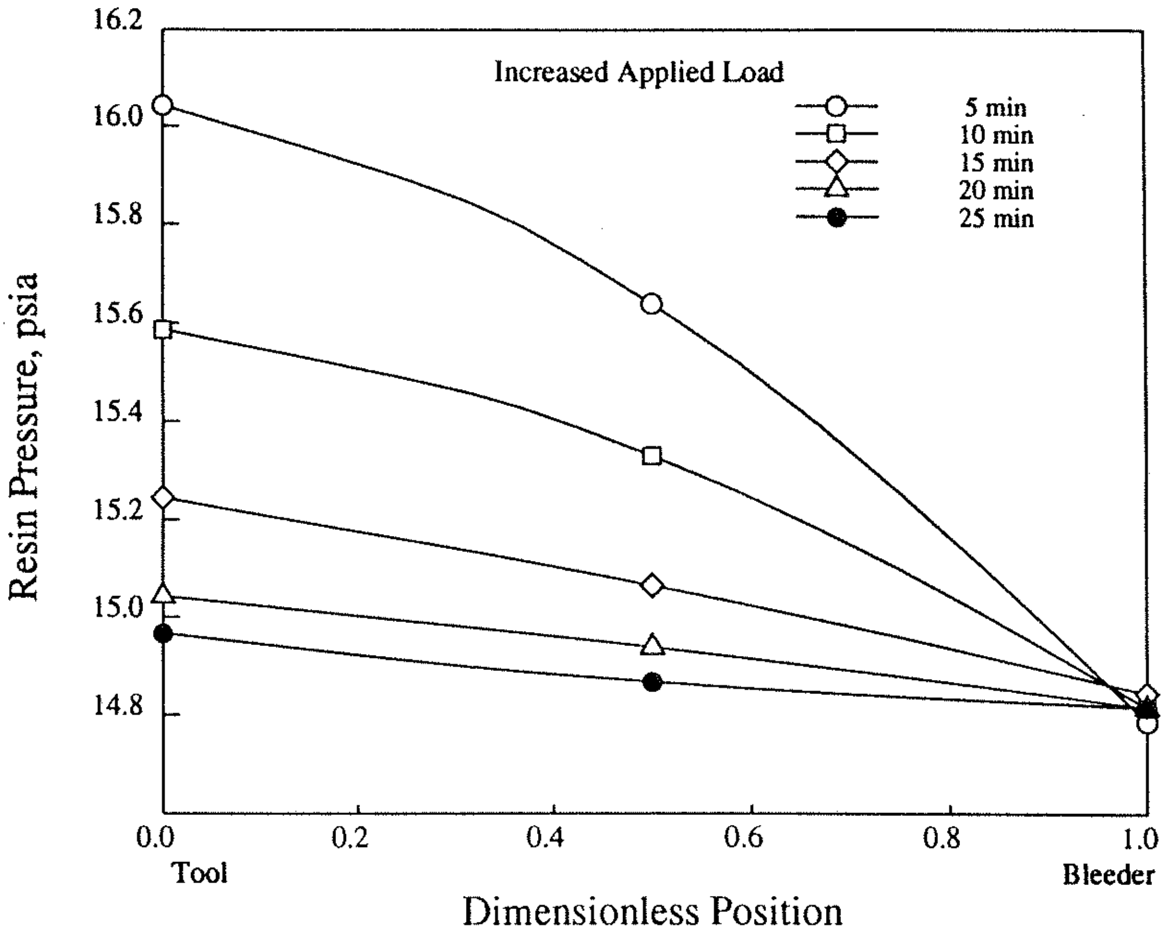

Figure 4.13: Resin pressure distributions as a function of position with two layers of Airweave N-10 and the increased consolidation load in the vertical direction.

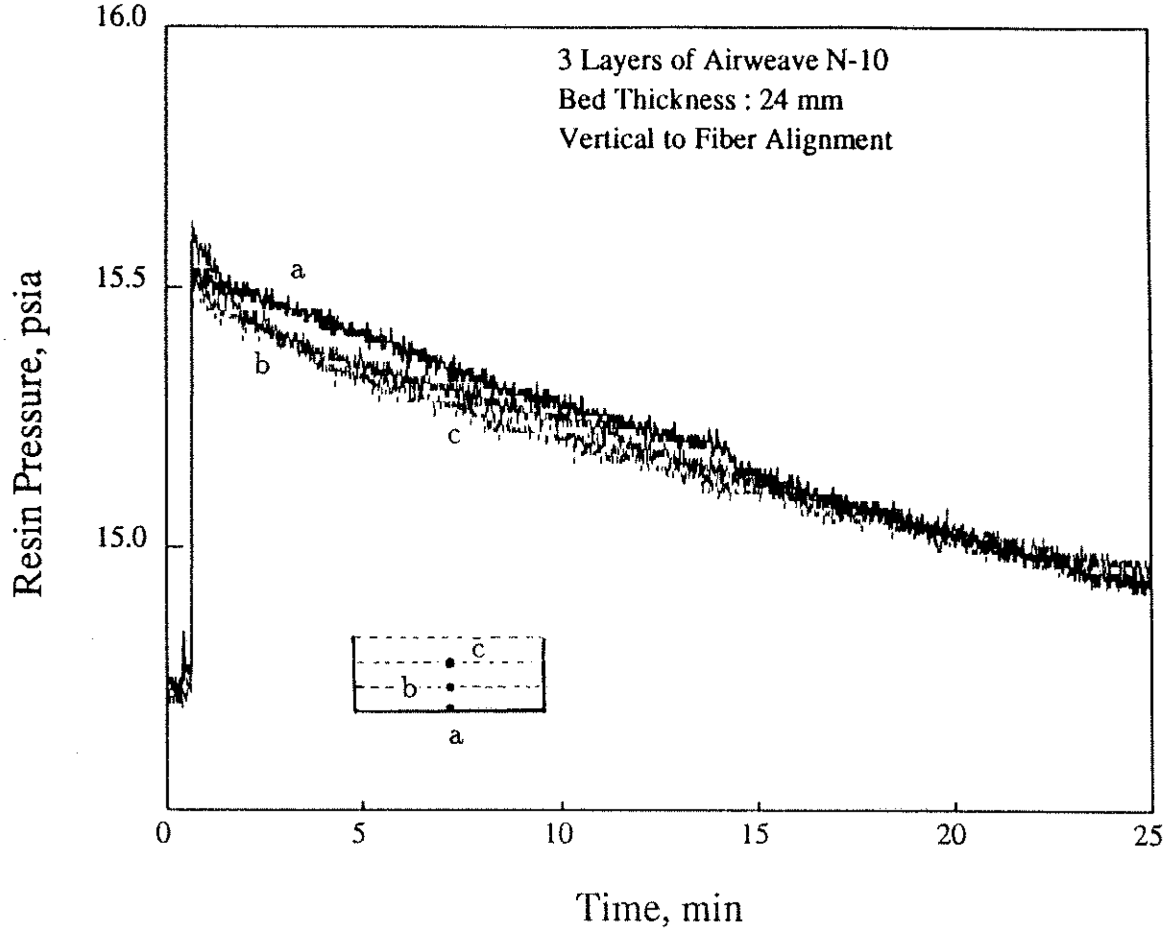

Figure 4.14: Resin pressure change as a function of time at the specified positions for the 24 mm thick bed.

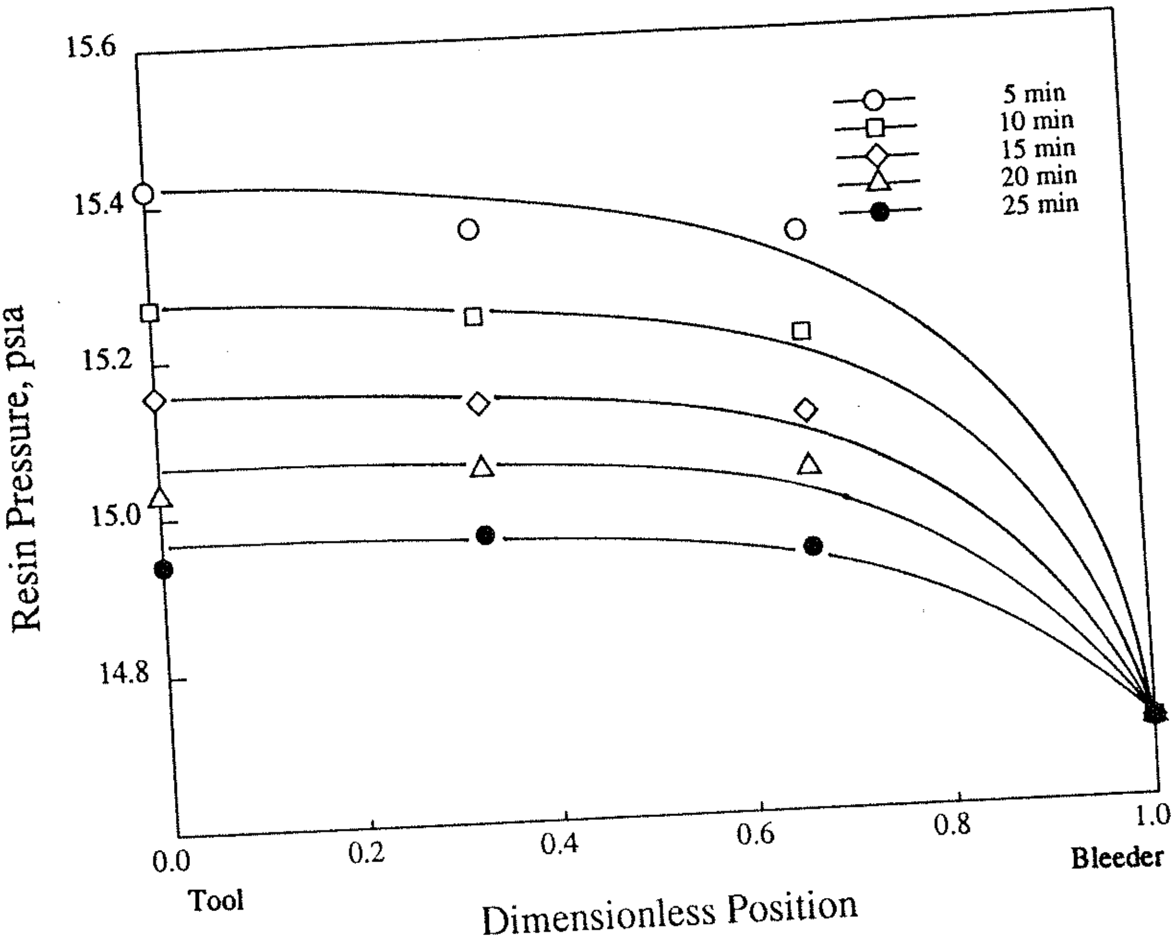

Figure 4.15: Resin pressure-position (vertical) distributions as a function of time for the 24 mm thick bed.

The reason is that the Springer-Loos model assumes that the resin pressure at the tool surface is constant for the bed with low fiber volume fraction ($V_f \leq 0.6$). However, the model of Dave et al. [3] can explain the resin pressure change data resulting from the various experimental conditions. It should be noted that the resin pressure profile governs the consolidation behavior of the laminate.

4.1.6. Effect of Bleeder Type

In order to investigate the effect of bleeder type on the boundary pressure, a woven glass bleeder was used instead of the Airweave N-10 (nonwoven type bleeder). The glass bleeder is less porous than the Airweave N-10. Figure 4.16 shows the resin pressure changes as a function of time for the bed with 24 layers of glass bleeder. It is found from monitoring resin pressure at the bleeder (i.e. at the boundary) that as long as the capacity of the bleeder is sufficient to accommodate the resin the boundary pressure remains constant irrespective of the type of a bleeder. However, 15 layers of the glass bleeder resulted in the saturation of the bleeder, which is associated with the increasing boundary pressure as shown in Figure 4.17.

In order to examine the effect of bleeder type on the resin pressure profile, two layers of Airweave N-10 were changed to 24 layers of glass bleeder, all other conditions being kept the same. A comparison of Figure 4.16 with Figure 4.6 shows that the initial resin pressures at the tool surface are not the same, even though the same piston weight is used. The resin pressure for the case of the 24-layer of glass bleeder is lower. This phenomenon can be explained as follows: When the consolidation pressure is applied on the bleeder, the mechanism of

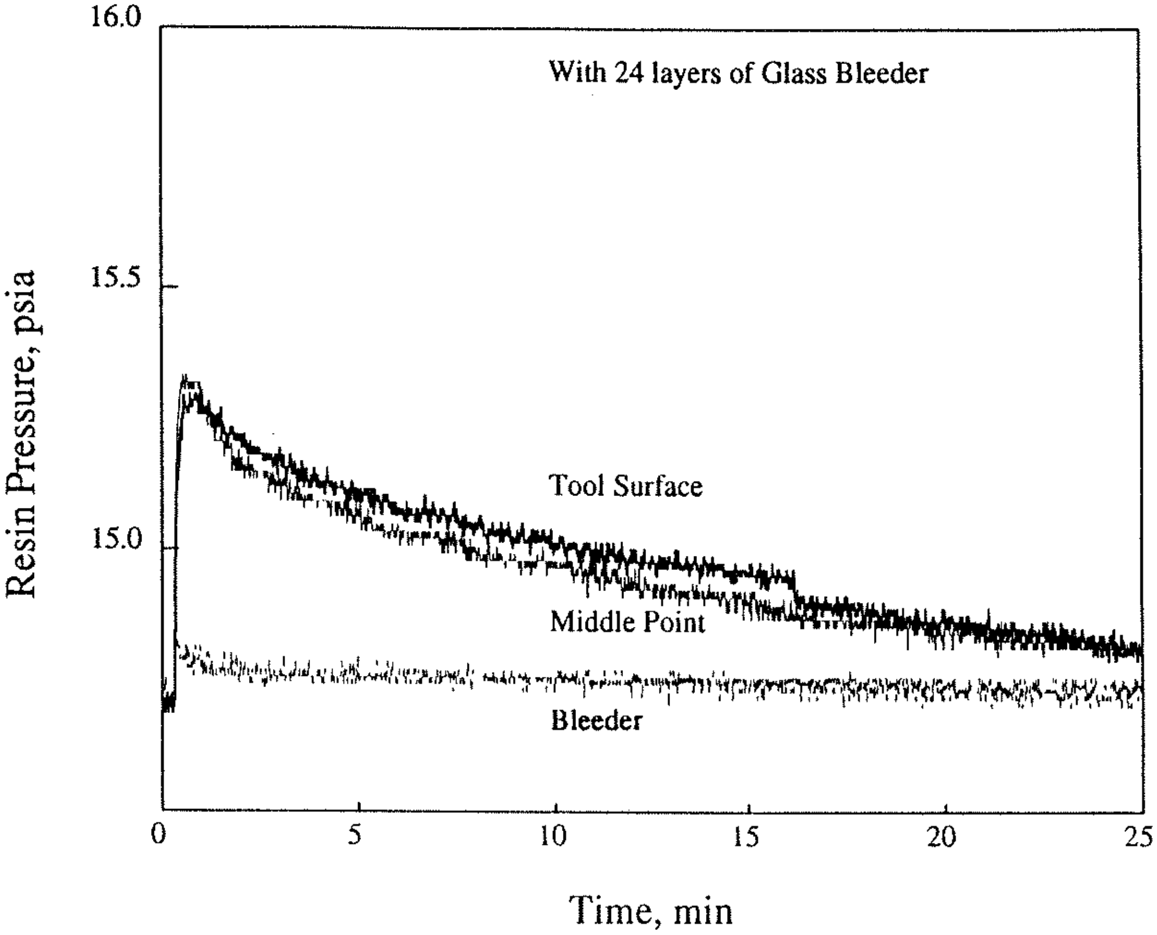

Figure 4.16: Resin pressure change as a function of time with 24 layers of a glass bleeder.

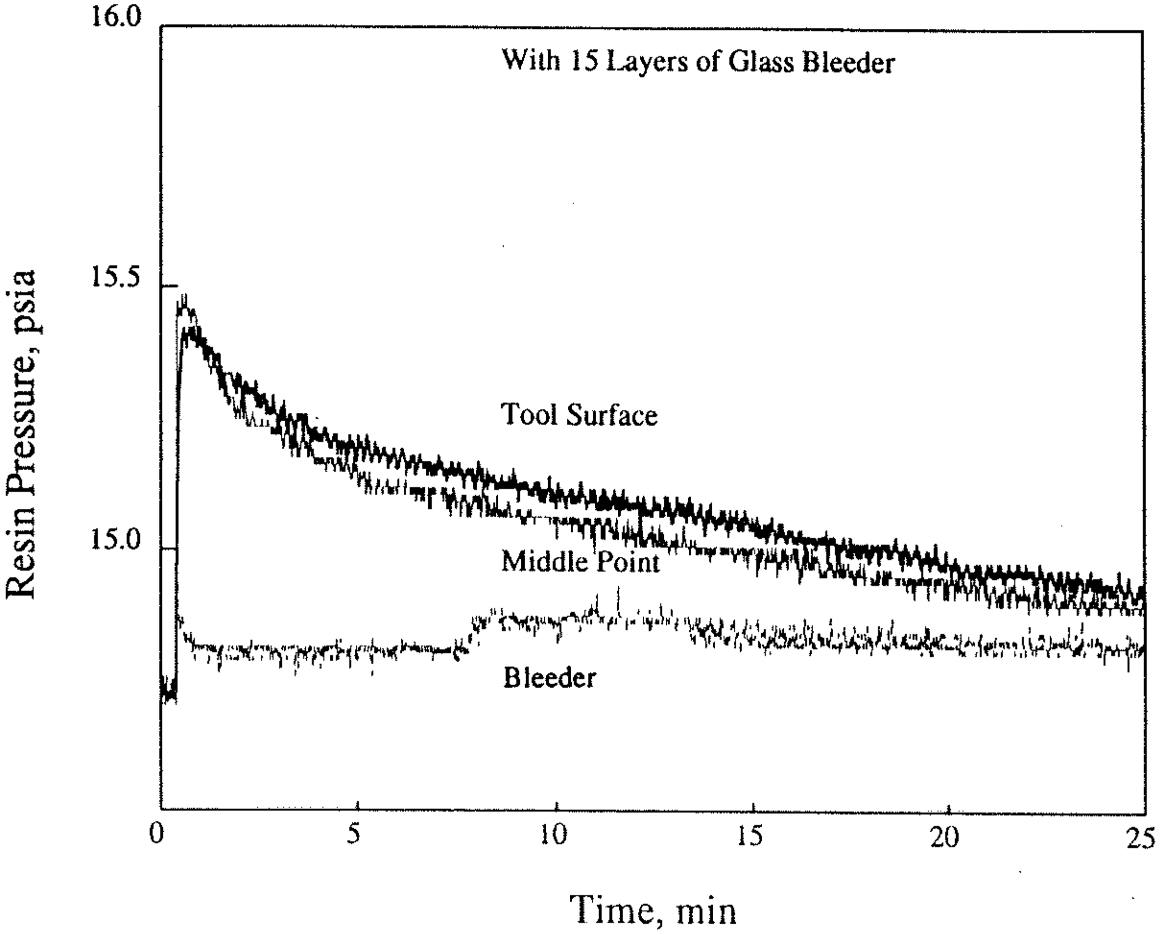

Figure 4.17: Resin pressure change as a function of time with 15 layers of a glass bleeder.

transferring the force depends on the number of the bleeder layers. When more than one layer of the bleeder is used, there is a compaction between bleeder layers. In the beginning of consolidation, there are few contact points through which the load is transferred. Then, each layer of the bleeder begins to compact and the load is increased with compaction. The compaction of the bleeder takes time and occurs simultaneously with consolidation of the fiber bed. Because during this time that it takes to compact the bleeder the carbon fiber bed is also compacted and takes some of the applied load acting as a spring, the resin pressure sensed by the pressure transducer on applying the load is lower than in absence of a bleeder.

It is also found that there are sharp gradients at the boundary in the resin pressure profile. In other words, the resin pressure profile in the vertical direction has a pronounced nonlinearity as shown in Figure 4.18.

4.2. ONE-DIMENSIONAL FLOW CONSOLIDATION EXPERIMENTS

4.2.1. Construction of the Apparatus for One-Dimensional Flow

In order to eliminate the complexity of two-dimensional flow consolidation in analyzing the resin flow phenomena, a one-dimensional flow consolidation experiment was designed and is shown schematically Figure 4.19. A unidirectionally-aligned carbon fiber bed (3 × 4 × 1 inches) was prepared and the four sides of the bed were blocked with a silicone mold-making material (Silastic HS RTV). The sides of the top surface of the bed were also masked so that the applied load

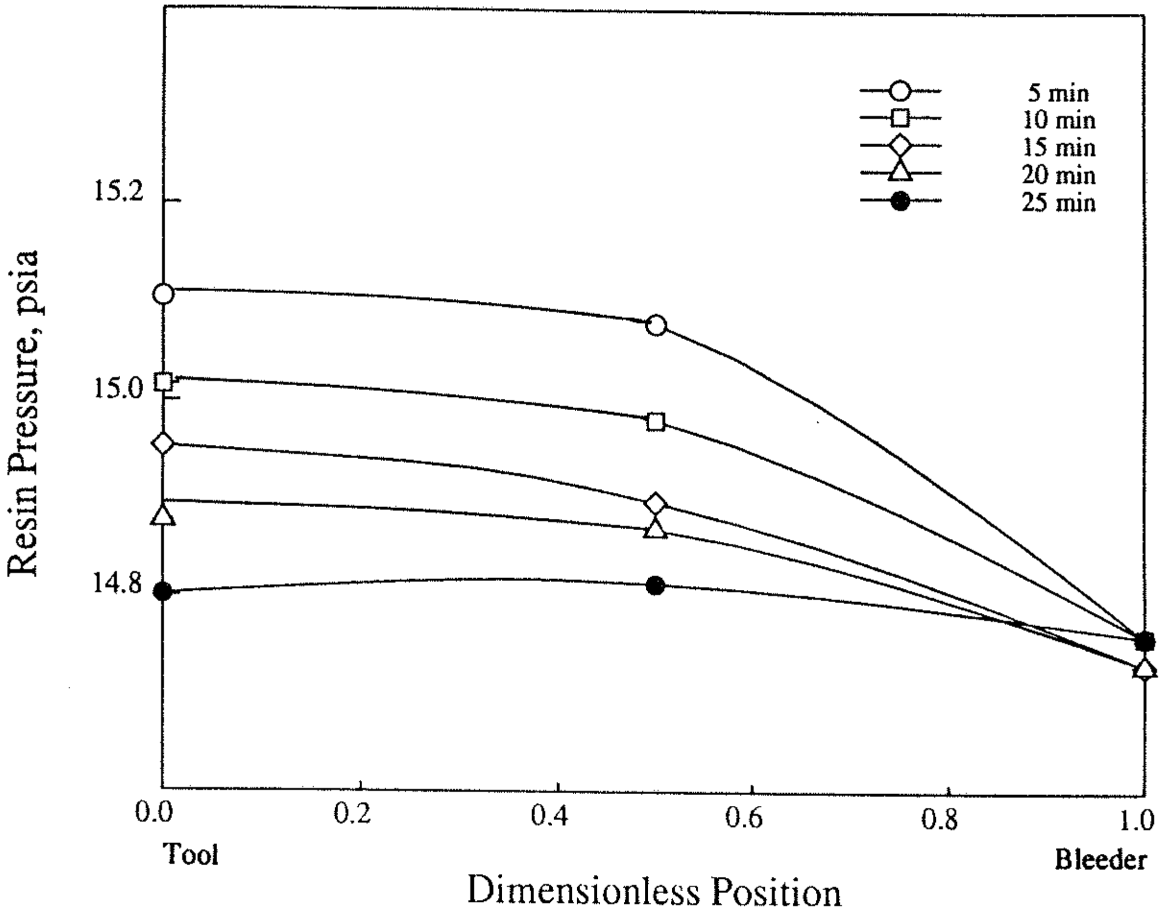

Figure 4.18: Resin pressure-position distribution as a function of time with 24 layers of a glass bleeder

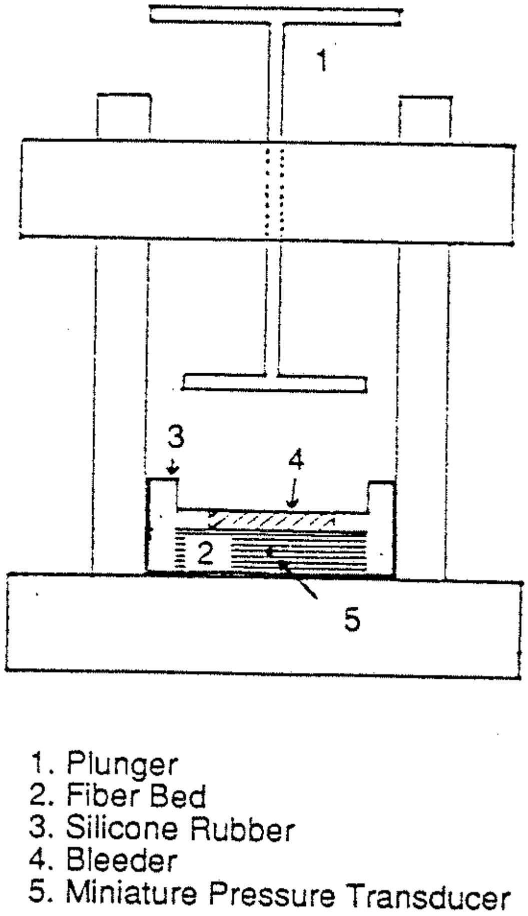

Figure 4.19: Schematic of a resin pressure measurement cell for one-dimensional flow.

can be exerted on the mask to block a horizontal flow. The apparatus shown in Figure 4.19 was used to monitor the resin pressures and examine the boundary conditions including bleeder capacity for the one-dimensional flow situation.

4.2.2. Effect of Bleeder Capacity

Figure 4.20 shows the resin (oil) pressure change at three different positions as a function of time for one-dimensional flow into two layers of Airweave N-10 bleeder cloth. A dead load of 1 psig was applied. The resin pressure at the tool surface stays unchanged for about 10 min and then begins to decrease very slowly because horizontal flow is blocked. The boundary pressure at the bleeder-composite interface is almost constant, which means that the bleeder has not been saturated and is still capable of absorbing resin (oil) flowing out of the bed.

Figure 4.21 shows the resin pressure-position profile as a function of consolidation time. The resin pressure profiles are relatively flat near the tool surface and steep at the boundary. In other words, the pressure gradient becomes larger as the bleeder is approached. This implies that the resin (oil) flow is greatest at the bleeder-composite interface. These results can explain why the measured per-ply thickness after consolidation depends on the position in the laminate. Kim et al. [29] studied the compaction behavior of thick laminates during autoclave cure using a thickness monitoring system. They measured the absolute compaction of each ply for a 96-ply laminate and found that the thickness per ply decreased as the bleeder (bag) was approached. It should be noted that the Springer-Loos model [8] can predict the number of plies compacted, but it cannot explain why the thickness per ply changes continuously with position. Again, the resin pressure

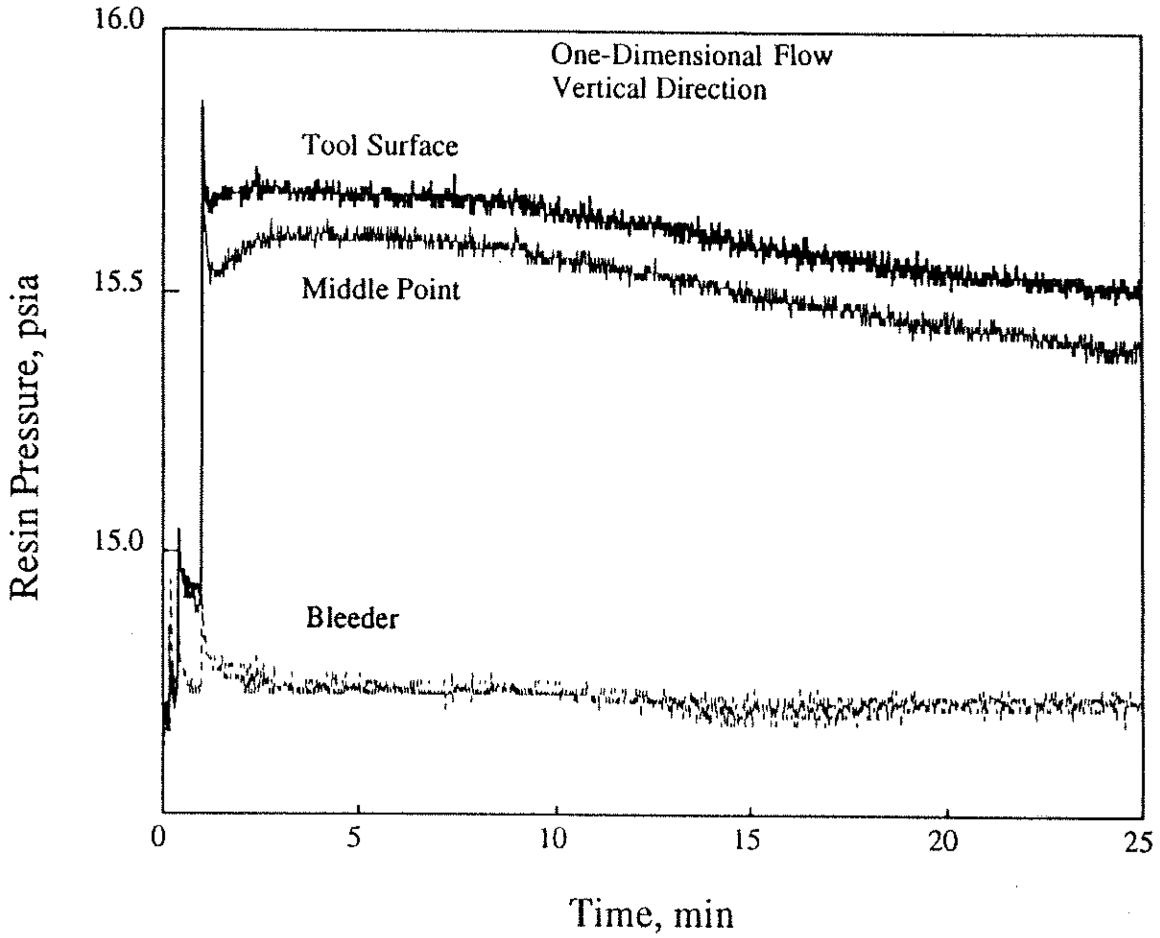

Figure 4.20: Resin pressure change as a function of time for one-dimensional flow consolidation

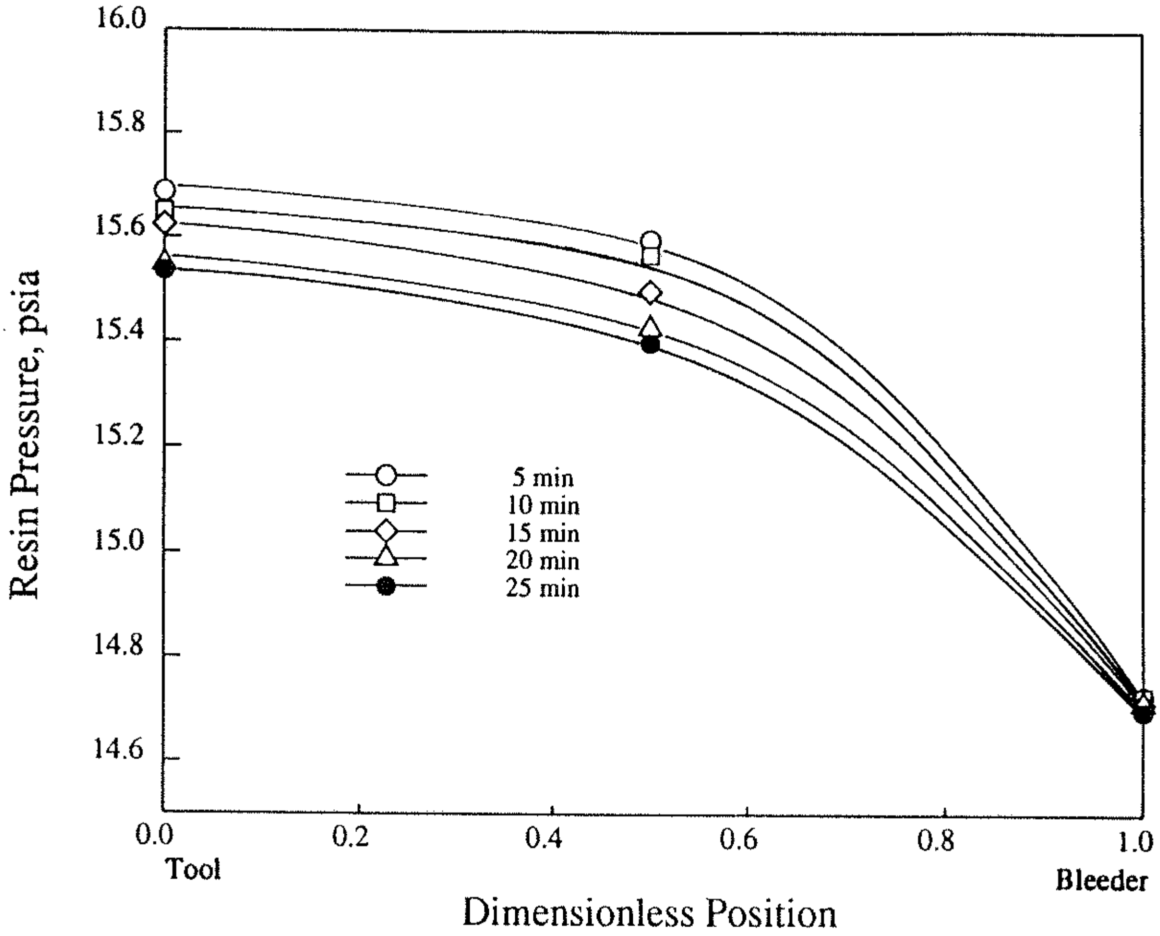

Figure 4.21: Resin pressure-position distributions as a function of time for one-dimensional flow consolidation.

profiles are nonlinear and the pressure gradient at the bleeder boundary decreases with time.

In order to investigate the effect of bleeder capacity, only one layer of bleeder cloth was used. Figure 4.22 shows the resin pressure change with time. The boundary resin pressure instantaneously increases to 15.8 psia and stays unchanged, indicating a saturated bleeder. The resin pressure decay at the tool surface and in the middle of the laminate is very slow because the resin flow has been effectively cut off by the saturated bleeder. The resin pressure profiles are flat as shown in Figure 4.23. The pressure gradient at the boundary is small compared with the case of no saturation of bleeder.

4.2.3. Effect of Applied Pressure

The effect of the consolidation pressure on the resin pressure was briefly examined. Two layers of Airweave N-10 were used to prevent saturation of the bleeder. The applied pressure was increased from 1.0 psig to 2.1 psig. Figure 4.24 shows that the resin pressure decreases more quickly when compared with Figure 4.20. However, compared with two-dimensional flow consolidation (see Figure 4.12), the rate of resin pressure decay is much lower. Figures 4.25 and 4.21 indicate that the nonlinearity in the resin pressure profile becomes more severe as the applied load is increased.

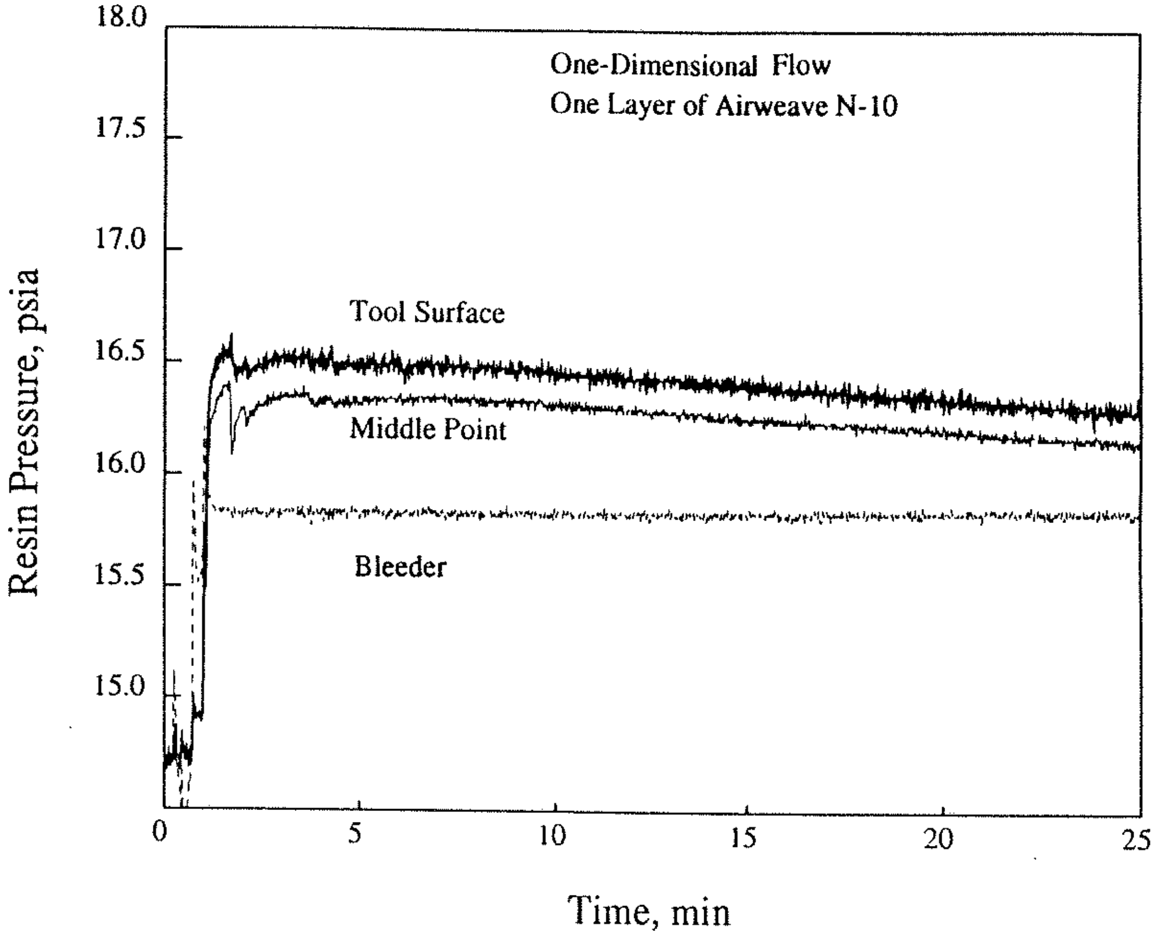

Figure 4.22: Resin pressure change as a function of time for the bed with a saturation of the bleeder.

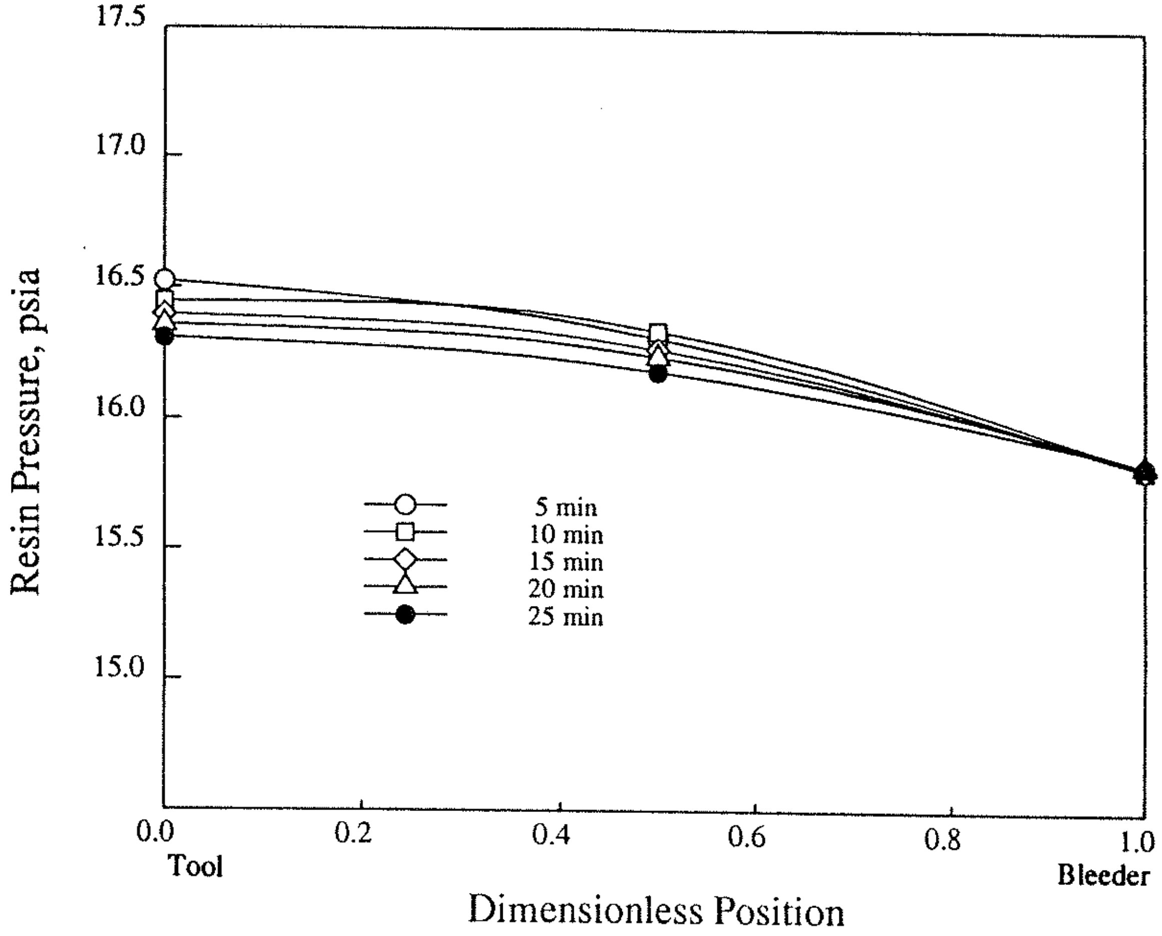

Figure 4.23: Resin pressure-position distributions as a function of time for the bed with a saturation of the bleeder.

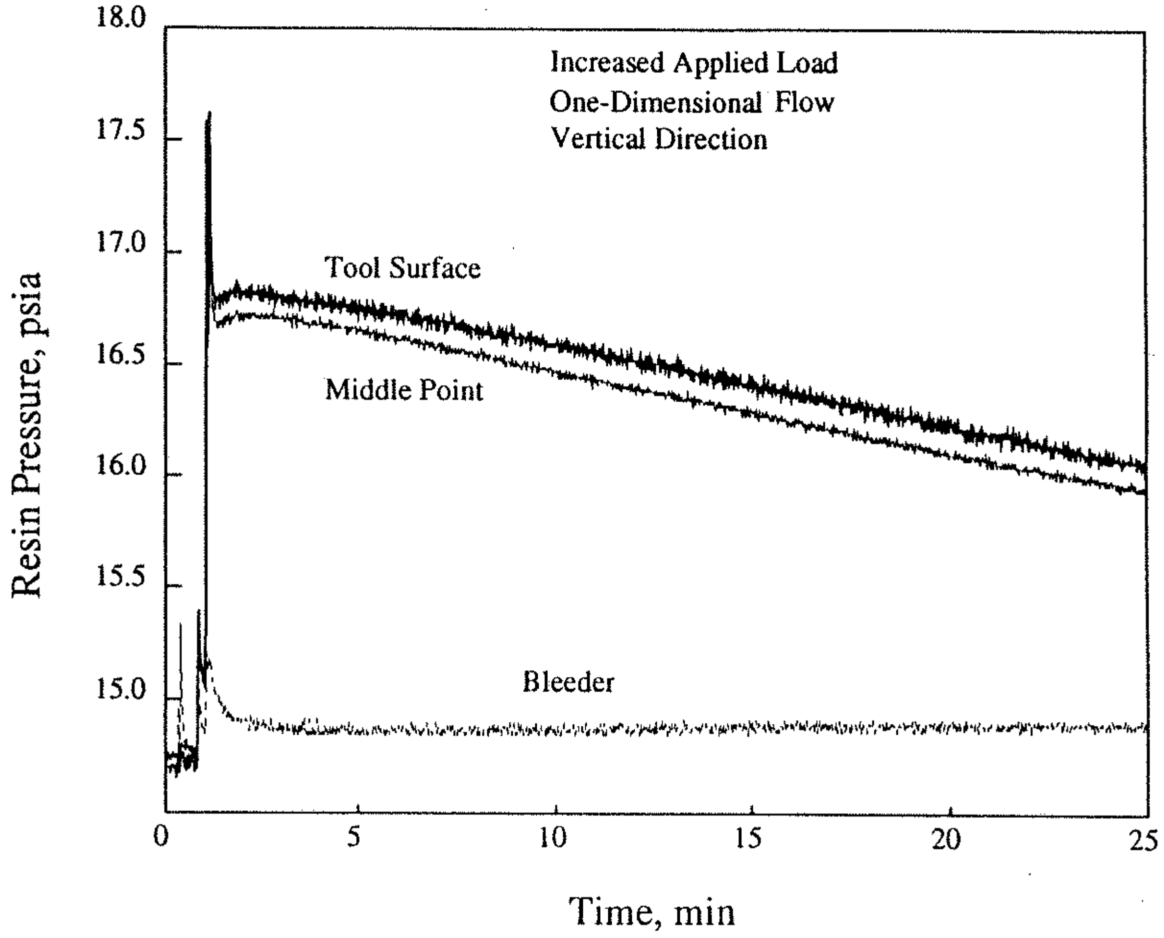

Figure 4.24: Resin pressure change as a function of time with the increased consolidation load.

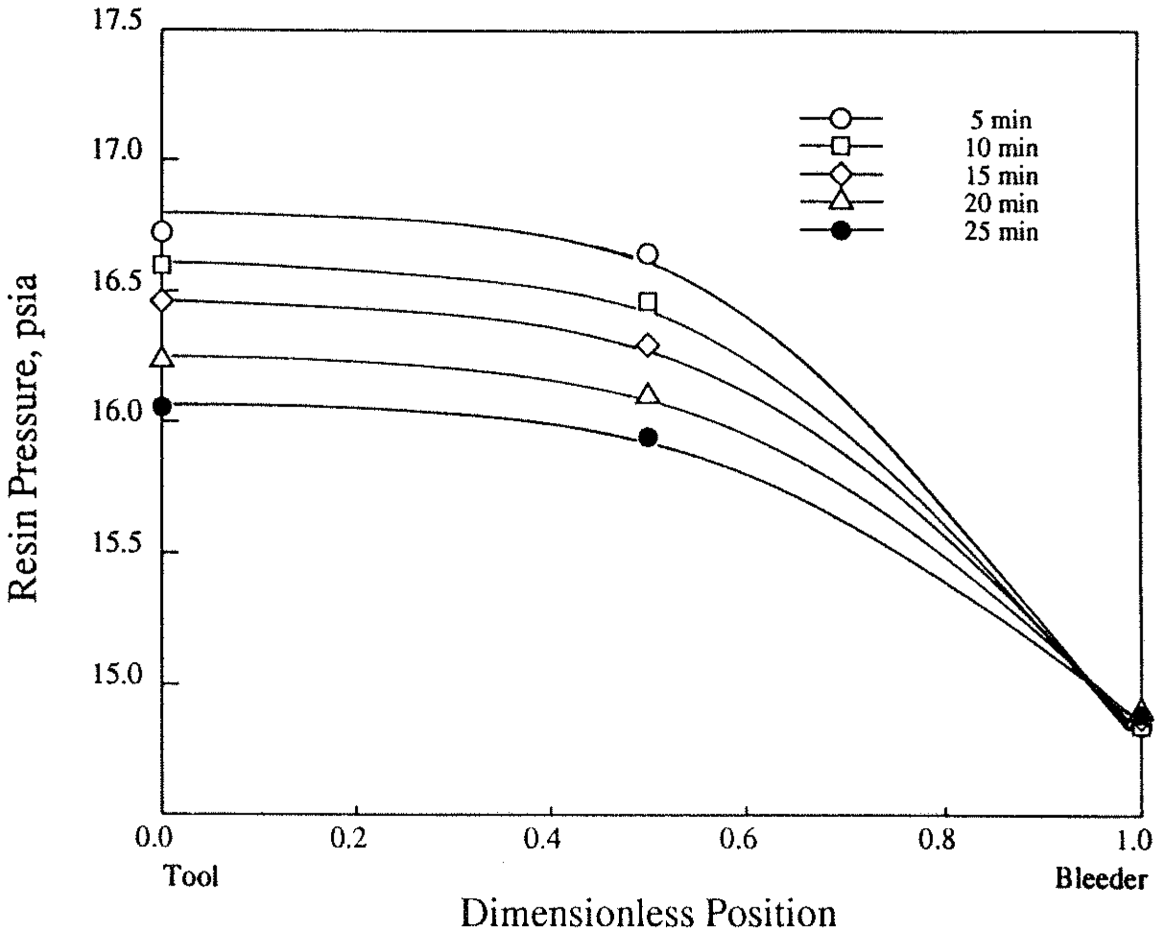

Figure 4.25: Resin pressure-position distributions as a function of time with the increased consolidation load.

4.2.4. Effect of Bleeder Type

The effect of bleeder type on the resin pressure was also tested. Sixteen layers of glass bleeder were used instead of two layers of Airweave N-10. The resin pressure change data shown in Figure 4.26 can be explained in the same manner as in two-dimensional flow consolidation. That is to say, the number of glass bleeder used affects the mechanism of transferring the load. See section 4.1.6 for further details.

4.3. EXPERIMENTAL VERIFICATION OF THE CONSOLIDATION SUBMODEL

4.3.1. Mathematics of the Resin Flow Model

The resin flow model of Dave et al. [3] is based on the following interpretation of the physical phenomena. When a porous fibrous bed, completely saturated with incompressible fluid (resin), is subjected to compression during processing, the phenomenon of flow through the fibrous bed due to consolidation is similar to the situation when a water-saturated soil is subjected to compressive stresses [30, 31]. For both the fibrous bed as well as the water-saturated soil, the volume decrease is due almost entirely to a decrease in the liquid content, the volume decreases of the solid constituents and the liquid in the pores being negligible.

For the case of one-dimensional consolidation of a porous medium, the stress

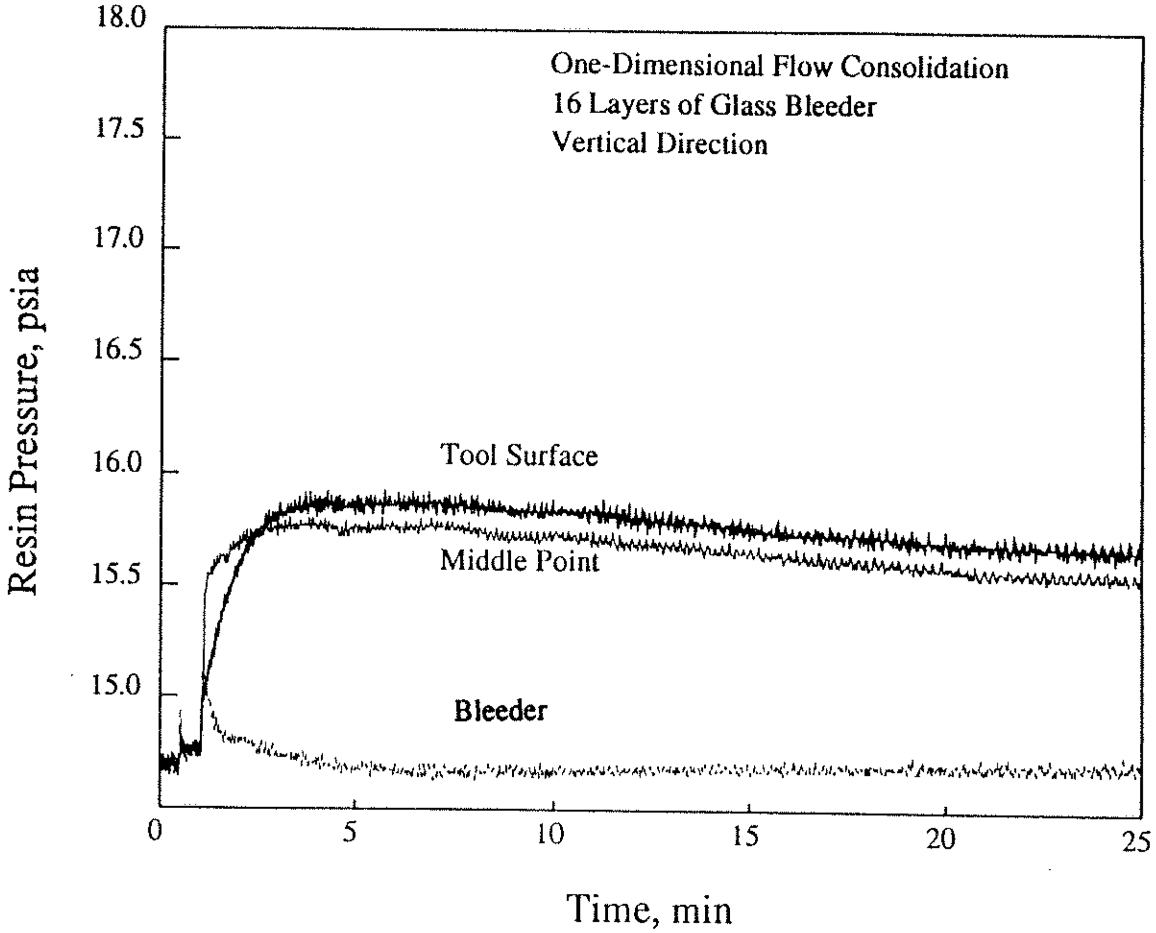

Figure 4.26: Resin pressure change as a function of time with 16 layers of glass bleeder

during consolidation is given by the following equilibrium equation:

$$\sigma = p + p_r \tag{4.1}$$

where σ is the total externally applied stress, p is the effective stress, i.e. the stress borne by the spring-like skeletal structure of the porous bed, and p_r is the hydraulic pressure of the fluid in the porous medium.

The following assumptions are also needed to finalize the model according to consolidation theory [30, 31, 32] : i) the porous fiber bed is completely saturated with resin, ii) the individual fibers and resin are incompressible, iii) the resin flow equation follows Darcy's Law, iv) the porous fiber bed is homogeneous, v) the velocity and stress-strain increases are small and the situation is quasistatic, vi) body forces such as self weight can be neglected.

The generalized situation of resin flow through a porous fiber bed is now represented by one-dimensional consolidation with three-dimensional flow. The ~~most~~ frequently used governing differential equation for satisfying the consolidation of a porous bed within a given time interval with three-dimensional flow and a one-dimensional confined compression condition (no boundary motion in x or y directions) is given by [32]:

$$\frac{1}{\eta m_v}[k_x(\frac{\partial^2 p_r}{\partial x^2}) + k_y(\frac{\partial^2 p_r}{\partial y^2}) + k_z(\frac{\partial^2 p_r}{\partial z^2})] = \frac{\partial p_r}{\partial t} - \frac{\partial \sigma}{\partial t} \tag{4.2}$$

where k_x, k_y, k_z = specific permeabilities in the x, y, and z directions, which depend on the stress level, η =viscosity of the resin in the porous fiber bed, p_r = hydraulic resin pressure within the pores, t = time, and m_v = coefficient of volume change.

The numerical solution can be obtained by simultaneously solving the above equation of continuity, with the initial and boundary conditions specified, and the following equations: 1) the equilibrium equation (eq. (4.1)), 2) an experimentally obtained relationship between the void ratio, e (void/solid) and effective stress for the skeletal fibrous bed of the composite, 3) the equation for the coefficient of volume change, m_v, 4) experimentally determined relationships for the specific permeabilities (k_x, k_y, k_z) as functions of fiber diameter and length, void ratio and shape factor, and 5) a relationship for resin viscosity as a function of the extent of reaction and temperature.

The developed model provides resin pressure profiles, resin flow, the degree of consolidation, laminate thickness and residual resin as a function of laminate thickness and the particular temperature-pressure-time cycle used. It is found that the resin pressure gradients in both the vertical and horizontal directions are not linear.

4.3.2. Numerical Technique

In order to verify the consolidation submodel, the one-dimensional resin flow equation was solved numerically by a Finite Element Collocation method to predict the resin pressure resulting from the various experimental conditions. The IMSL (International Mathematics and Statistics Library) software package DPDES was used to integrate the ODE's which arise from the method of lines solution of a PDE system in one space variable.

4.3.3. Input Parameters

In order to verify the resin flow model (consolidation submodel) based on soil consolidation theory, the stress-strain relation, i.e., the relationship between the resin ratio and the effective stress, and the specific permeabilities in the vertical and horizontal directions are needed. It should be noted that both the stress-strain relation and the specific permeability are dependent on the fiber volume fraction (or resin ratio).

For the stress-strain relation, it is known [4] that there are three distinct effective stress ranges in which different deformation behavior of the graphite fibers is demonstrated. In the low range of the effective stress (≤ 5 psi), which is applicable to this one-dimensional flow consolidation experiment, the fiber bed has a linear behavior which may be termed as "immediate or distortion settlement" behavior. The immediate settlement occurs concomitantly with load application, primarily as a consequence of distortion within the packed fiber bed. The resin ratio, e, is linearly proportional to the effective stress, p.

Two different one-dimensional consolidation experiments were selected for the model comparison. The stress-strain relations for the two chosen one-dimensional flow consolidation experiments were linear due to the low effective stress. Therefore, the slope and the intercept of the linear relation were determined for the two cases from the initial and final resin ratios, and the applied load. The relation for the experiment resulting in Figure 4.20 is shown in Equation (4.3) and Equation (4.4) shows the relation for the experiment resulting in Figure 4.24.

$$e = -0.46p + 1.0 \tag{4.3}$$

$$e = -0.30p + 1.0 \tag{4.4}$$

Then, the coefficient of volume change was calculated as follows:

$$m_v = -(\frac{de}{dp})/(1+e) \tag{4.5}$$

The values of input parameters used for the calculation are determined as follows: The initial resin ratios are 1.0 and 1.0, and the final resin ratios are 0.54 and ~~0.7~~ 0.37 for the two cases, respectively. The transverse permeability, k_z, was determined based on the experimental results of Lam and Kardos [16] and calculated from equation (4.6):

$$k_z = \frac{D_f^2 e^3}{16K_z(1+e)} \tag{4.6}$$

where D_f is the diameter of the fiber (= 0.003 inch) and K_z is Kozeny constant (= 11).

4.3.4. Comparisons of Model Prediction with Experimental Results

The various governing equations available in the literature for one-dimensional consolidation with one-dimensional flow have recently been reviewed [33]. By starting from first principles, the correct equation was derived as:

$$\frac{\partial p_r}{\partial t} - \frac{\partial \sigma}{\partial t} = \frac{(1+e)^2}{\eta a_v} \frac{\partial}{\partial z} \left(\frac{k_z}{1+e} \frac{\partial p_r}{\partial z} \right) \tag{4.7}$$

$$I.C. \quad t = 0, \quad p_r = \sigma_0 \ for \ all \ z \tag{4.8}$$

$$B.C.\ 1 \quad z = 0, \quad \frac{\partial p_r}{\partial z} = 0 \tag{4.9}$$

$$B.C.\ 2 \quad z = L, \quad p_r = p_{r,bc} \tag{4.10}$$

It was found that the differences in resin pressure predicted by equation (4.7) and other formulations are considerable and that equation (4.7) gives the best accuracy [33]. It was also shown that it is necessary to transform the coordinate system to a moving one, i.e., moving with the height of the shrinking laminate.

Therefore, equation (4.7) was selected and simulated with a moving boundary condition to compare with the measured resin pressure. In order to implement the moving boundary at the top of the laminate ($z = h$), the following variable transformation was introduced:

$$\xi = z/h(t) \tag{4.11}$$

$$t' = t \tag{4.12}$$

From (4.11) and (4.12)

$$\frac{\partial}{\partial t} = -\frac{\xi}{h}\frac{dh}{dt}\frac{\partial}{\partial \xi} + \frac{\partial}{\partial t'} \tag{4.13}$$

$$\frac{\partial}{\partial z} = \frac{1}{h}\frac{\partial}{\partial \xi} \tag{4.14}$$

Substituting (4.13) and (4.14) in equation (4.7) and replacing t' by t, we end up with equation (4.15).

$$\frac{\partial p_r}{\partial t} = \frac{\xi}{h}\frac{dh}{dt}\frac{\partial p_r}{\partial \xi} + \frac{(1+e)^2}{\eta a_v h^2}\left[\frac{\partial}{\partial \xi}\left(\frac{k_z}{1+e}\frac{\partial p_r}{\partial \xi}\right)\right] + \frac{\partial \sigma}{\partial t} \tag{4.15}$$

$$I.C.\quad t = 0,\quad p_r = \sigma_0 \; for\;\; all\;\; \xi \tag{4.16}$$

$$B.C.\ 1\quad \xi = 0,\quad \frac{\partial p_r}{\partial \xi} = 0 \tag{4.17}$$

$$B.C.\ 2\quad \xi = 1,\quad p_r = p_{r,bc} \tag{4.18}$$

The final form, equation (4.15), was numerically solved with the technique mentioned earlier and the resulting pressure compared with the measured resin pressure.

Figure 4.27 shows the comparison between the measured resin pressure change in the vertical direction and that predicted from the resin flow model, i.e., equation (4.15). The input parameters used for the model predictions are shown in Figure 4.27. It can be said that there is an acceptable agreement between the measured and predicted resin pressure in the vertical direction. Figure 4.28 shows a comparison between the measured resin pressure in the vertical direction with increased applied load and that predicted from the resin flow model. The agreement is even better in this case. The agreement can also be seen in Figure 4.29 where the resin pressures at different consolidation times are plotted as a function of vertical position in the laminate.

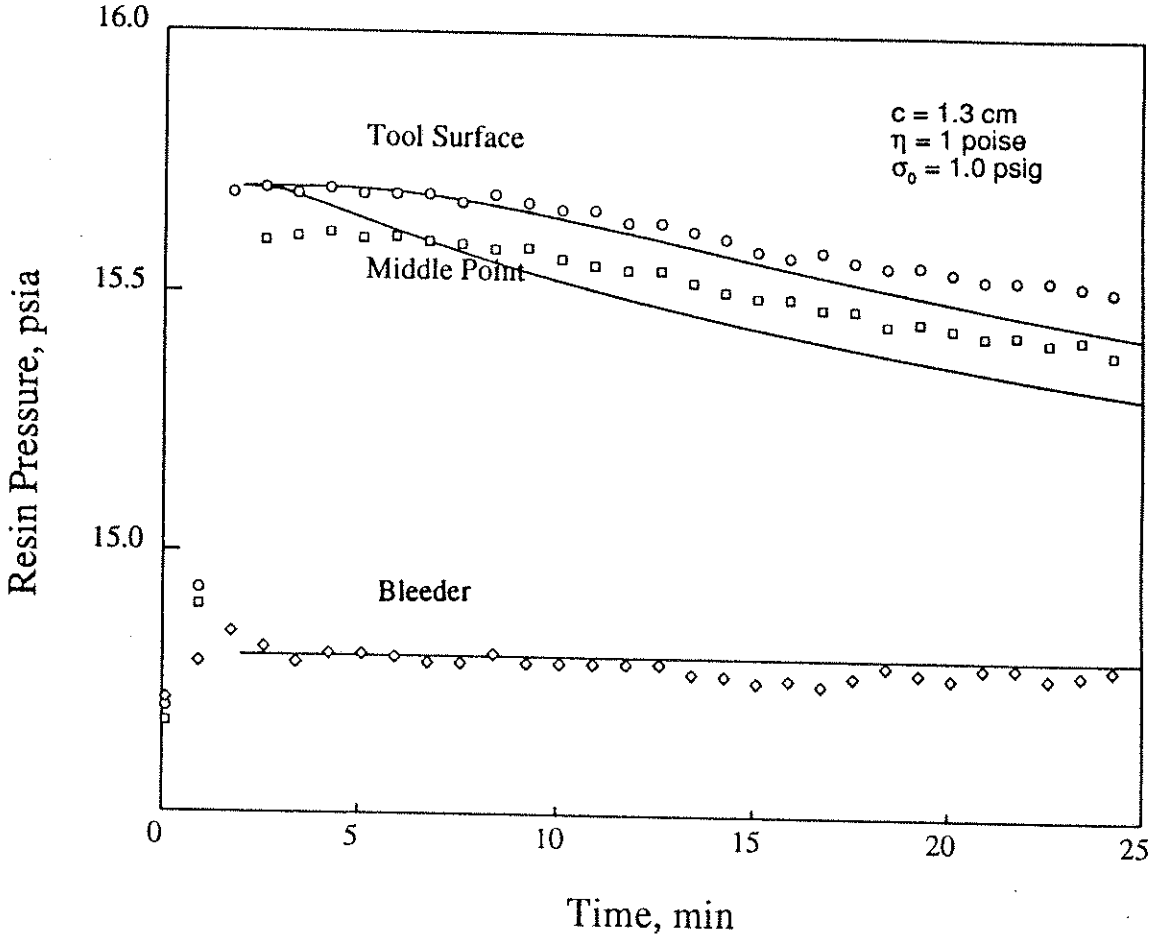

Figure 4.27: Comparison between the measured resin pressure change in the vertical direction and that predicted from the modified Dave et al. resin flow model (solid lines-model; symbols-experiment).

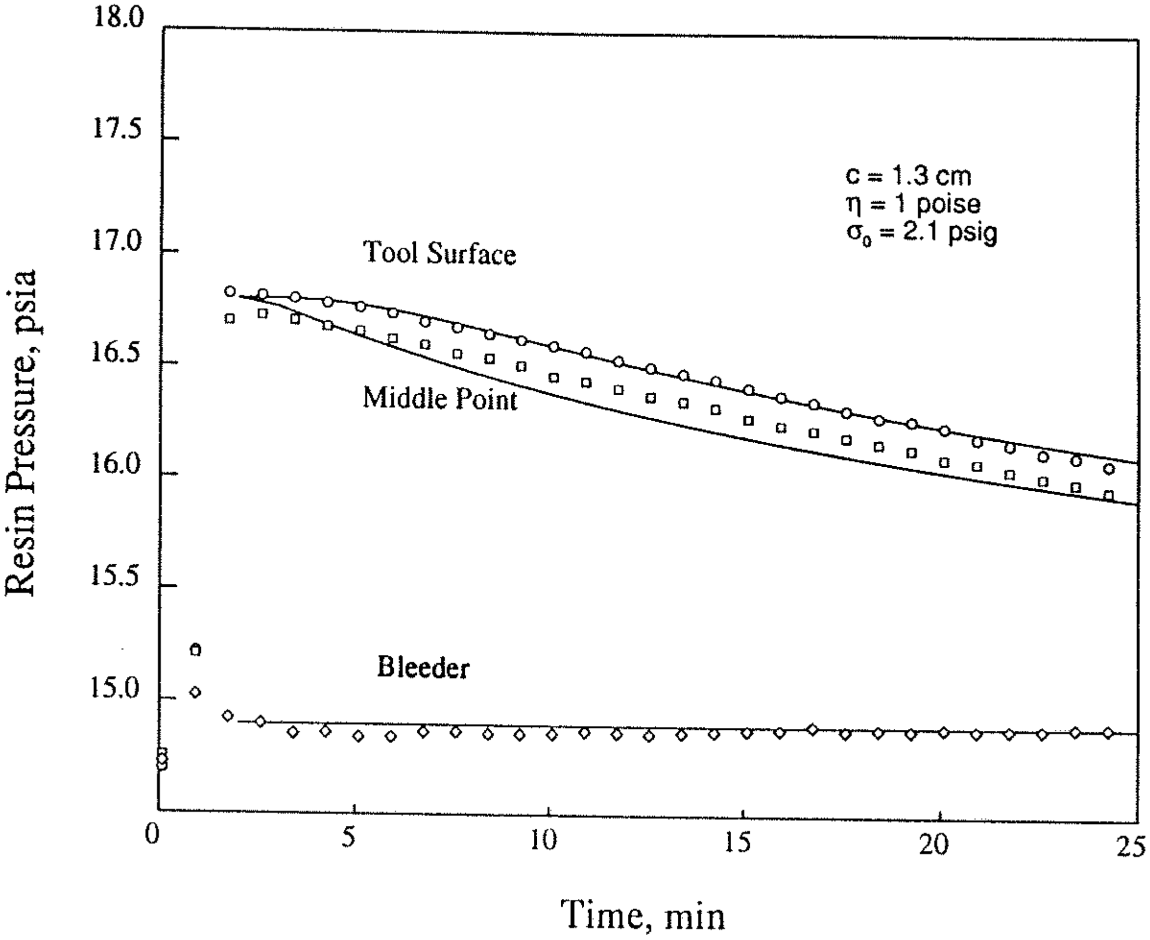

Figure 4.28: Comparison between the measured resin pressure change in the vertical direction and that predicted from the modified Dave et al. resin flow model with increased load (solid lines-model; symbols-experiment).

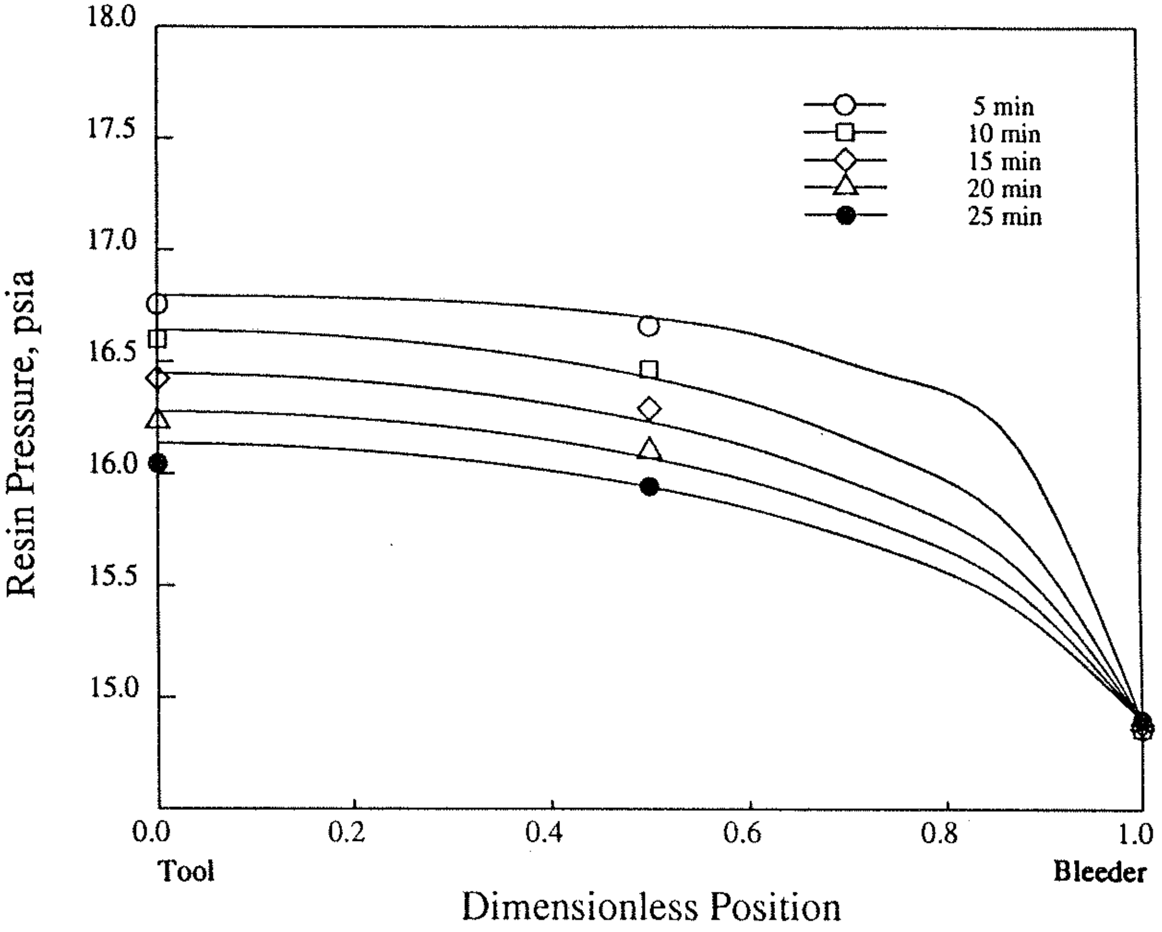

Figure 4.29: Comparison between the measured resin pressure distributions in the vertical direction and that predicted from the modified Dave et al. resin flow model with increased load (solid lines-model; symbols-experiment).

5. CONCLUSIONS AND RECOMMENDATIONS

5.1. DEVOLATILIZATION

- Differential scanning calorimetry (DSC) studies show that the crystallinity and morphological structure of the polyimide based on the Avimid K-III resin are strongly dependent upon the heating rate.

- Polarized light optical microscopy studies confirm the existence of the crystallites formed in the Avimid K-III resin during the processing and also show that the Avimid K-III neat resin is not an optically isotropic material at room temperature.

- Optical microscopy studies also show that the cracks are growing and are interconnected to serve as a path through which the evaporating volatiles can migrate in the laminate. The needle-shaped cracks running in the fiber direction are formed in the processing of the Avimid K-III/IM-6 prepregs.

- Bulk density measurements show that the bulk density of the laminates decreases (i.e., the crack density increases) as the processing temperature is increased.

- The devolatilization process is strongly dependent upon the heating rate. The dependency of the devolatilization process on the heating rate increases as the laminate thickness is increased.

- Temperature measurements show that the temperature profile in the laminate is relatively flat (i.e., the maximum temperature difference between the tool surface and the bleeder is less than 15 °C). Applies to [illegible] thickness

- The devolatilization model is experimentally verified by measuring the total and component volatile fluxes as a function of processing temperature. The devolatilization model accurately predicts the total and individual component volatile mass fluxes, as well as the temperature and pressure profiles through the laminate as a function of the initial laminate thickness and temperature and pressure cycles employed during autoclave processing. Therefore, this model can be utilized to simulate the devolatilization process and to develop a state-of-the-art composite manufacturing system.

- A lower heating rate is better in processing a thicker laminate. Also, a complete removal of the high-boiling point solvent needs a slow heating rate.

5.2. CONSOLIDATION

- The resin pressure profiles in the vertical and horizontal direction are found to be nonlinear. The resin pressure profile for a thicker fiber bed is more nonlinear.

- The bleeder capacity plays an important role in determining the resin flow pattern (vertical or horizontal).

- The resin flow model based on soil consolidation theory and experimentally verified. The resin flow (consolidation) model accurately predicts resin pressure profiles, resin flow, the degree of consolidation and laminate thickness. Therefore, this model can be utilized to simulate the consolidation process and to develop a state-of-the-art composite manufacturing system.

- The resin flow model of Dave et al. is constructed based on the assumption that the porous fiber bed is completely saturated with resin. This means that as soon as the consolidation pressure is applied on the bleeder, resin pressures of all the points in the bed including the tool surface immediately increase to the corresponding applied pressure except at the bleeder-composite interface. However, when several layers of the bleeder are used, the resin pressure can not sense the total magnitude of the applied consolidation load because of the time that bleeder layers take to be compacted. Now, this finding can be extended as follows: If a fiber bed is not saturated due to the number of prepregs laid up, the applied pressure will not be immediately transferred down to the tool surface. That is to say, there is an analogy between the bleeder layers and prepreg layers. Therefore, the resin pressures in the unsaturated prepreg bed will be lower than the applied pressure even at the beginning of the consolidation. This will cause the resin flow at the boundary to be small and result in a composite which does not have enough resin loss. It is, therefore, recommended that a saturated prepreg bed is necessary to better predict the resin flow with the resin flow model of Dave et al. The saturated prepreg bed might be achieved with a proper lay-up and/or debulking.

- The resin pressure measurements indicate that the bleeder capacity is very important in determining the resin flow pattern. The bleeder capacity is a key factor to determining whether or not the bleeder will be saturated. A saturated bleeder can effectively cut off the resin flow. However, the bleeder capacity should be considered in conjunction with the consolidation pressure since a bleeder with an unsaturated condition for a given applied load can possibly be saturated with a higher consolidation load. The applied consolidation pressure should be first determined considering the required final resin content in the composite. This can be easily done with a help of the stress-strain relationship for a selected resin/fiber system. Then, the bleeder capacity can be automatically calculated since the initial and final resin content in the composite are already specified. The bleeder capacity, of course, should be large enough to absorb all the resin coming out of the laminate.

- Once the bleeder capacity is determined, a question arises as to what kind of bleeder could be used. The number of bleeder layer can be easily calculated if a certain type of the bleeder is selected because we know the capacity of one layer of the selected bleeder. It should be noted that if more than one layer of the bleeder is used, the resin flow will be changed due to the different load transferring mechanism. Therefore, the bleeder type should be selected considering the fact that as the capacity of one layer of the selected bleeder is smaller, the number of layers used will be increased.

- If a two-dimensional resin flow is allowed for the consolidation of a thick composite, the horizontal flow will be dominant because of a higher permeability. This will cause too much resin flow out of the laminate. Therefore, it is recommended that the horizontal flow be blocked using dams to properly control the resin flow of a thick composite. The selection of both the bleeder type and magnitude of the applied pressure should be carefully determined for a thick composite. This is due to the fact that as the composite is thicker, the resin flow profile becomes more nonlinear.

6. ACKNOWLEDGMENT

I would like to express my sincere gratitude to my dissertation advisors, Professor John L. Kardos and Professor Milorad P. Duduković for their invaluable guidance and advice during this research.

I would like to express my appreciation to Mr. M. B. Hsu for providing helpful discussions on the experiments, and to Dr. Y.B. Yang for his assistance in performing the computer simulations.

I wish to express my thanks to Sunkyong Industries for the financial support for my family and for providing a hot-stage optical microscopy facility. I also wish to acknowledge support for this work by the Air Force Wright Aeronautical Laboratories, Materials Laboratory, Wright Patterson AFB, under Contract No. F33615-85-C-5046.

I am grateful to my parents, Myungil and Youngsoon, and my wife, Myungaeh, and my children, Eunsil and Eunsuk. This dissertation is dedicated to them.

7. NOMENCLATURE

a_v : coefficient of compressibility ($-\frac{de}{dp}$), psi^{-1}
ρ_m : averaged density for the composite, g/cm^3
C_{pm} : averaged heat capacity for the composite, cal/(g °K)
ρ_γ : gas density, gmol/cm^3
$C_{p\gamma}$: heat capacity of gas, cal/(g °K)
D_f : diameter of the fiber, in
V_γ : gas velocity, cm/min
ΔH_{vap} : enthalpy of vaporization, cal/gmol
$\dot{m}$: species evaporation flux, g/(min cm^3)
k_{eff} : effective thermal conductivity, cal/(cm min °K)
k : specific permeability, cm^2
h : heat transfer coefficient, cal/(cm^2 min °K)
K_γ : permeability of gas, cm^2
K_z : Kozeny constant
μ_γ : viscosity of gas, poise
P : gas pressure, atm
p : effective stress, psi
p_r : resin pressure, psi
α : extent of reaction
ϵ : volume fraction
η : viscosity of the resin, poise
R : gas constant, 82.05 (atm cm^3)/(gmol °K)
R_A : reaction kinetics
Y : mole fraction of gas component
$K_m A_{\beta\gamma}$: volumetric mass transfer coefficient, min/cm^2
γ : activity coefficient
P^{sat} : saturation vapor pressure, atm
Re : Reynolds number
C : concentration in the liquid phase, gmol/cm^3
ρ_β : liquid density, g/cm^3
M_W : molecular weight
ϕ : volume fraction
T : temperature, °K

L : fiber bed thickness
t : time, min
σ : total externally applied stress, psi
ξ : dimensionless thickness
m_v : coefficient of volume change, psi^{-1}
e : void ratio (resin ratio)

subscript

i : i^{th} component
σ : solid phase
β : liquid phase
γ : gas phase
vac : vacuum
∞ : ambient condition
$_0$: initial condition
A : functional group such as amine, acid, and hyroxyl
x : x direction
y : y direction
z : z direction
bc : boundary condition

8. BIBLIOGRAPHY

[1] H. H. Gibbs, "K-Polymer: A New Experimental Thermoplastic Matrix Resin for Advanced Structural Aerospace Composites," *SAMPE J.,* 37, Sep./Oct. (1984)

[2] H. H. Gibbs, "Processing Studies on K-Polymer Composite Materials: Part I - Prepregs Based on K-II Polyimide," *SAMPE J.,* 22, Jul./Aug. (1985)

[3] R. Dave, J. L. Kardos, and M. P. Duduković, "A Model for Resin Flow During Composite Processing: Part 1 - General Mathematical Development," *Polymer Composites,* 8, 29 (1987)

[4] R. Dave, J. L. Kardos, and M. P. Duduković, "A Model for Resin Flow During Composite Processing: Part 2 - Numerical Analysis for Unidirectional Graphite/Epoxy Laminates," *Polymer Composites,* 8, 123 (1987)

[5] S. Whitaker, "Simultaneous Heat, Mass and Momentum Transfer in Porous Media: A Theory of Drying," in *Advances in Heat Transfer,* vol. 13, Academic, New York, (1977)

[6] Y.B. Yang, J.L. Kardos, I.S. Yoon, S.J. Choi, and M.P. Duduković, "Management of Volatiles During Processing of Condensation Polyimide Composites," *Proceedings of the American Society for Composites, Fourth Technical Conference,* Western Hemisphere Publ., Blacksburg, VA, p36-45, (Oct. 3-5, 1989)

[7] G. S. Springer, "Resin Flow During the Cure of Fiber Reinforced Composites," *Journal of Composite Materials,* 16, 400 (1982)

[8] A. C. Loos and G. S. Springer, "Curing of Epoxy Matrix Composites," *Journal of Composite Materials,* 17, 135 (1983)

[9] R. A. Brand, G. C. Brown and E. L. McKague, "Processing Science of Epoxy Resin Composites," Air Force Contract No. F33615-80-C-5021, Final Report, AFWAL, August 1980 to December 1983, January 1984

[10] F. C. Campbell, A. R. Mallow, B. L. Boman and G. A. Blase, "Computer-Aided Curing of Composites," Air Force Contract F33615-83-C-5088, Seventh Quarterly Interim Technical Report, January 1986

J. F. Rabek "Experimental Methods in Polymer chemistry," John Wiley and Sons, New York, (1980

[11] J. Tang, W. I. Lee and G. S. Springer, "Effects of Cure Pressure on Resin Flow, Voids, and Mechanical Properties," *Journal of Composite Materials,* 21, 421 (1987)

[12] T. G. Gutowski, "A Resin Flow/Fiber Deformation Model for Composites," *SAMPE Quarterly,* 16(4), 58 (1985)

[13] T. G. Gutowski, T. Morigaki and Z. Cai, "The Consolidation of Laminate Composites," *Journal of Composite Materials,* 21(2), 172 (1987)

[14] T. G. Gutowski, Z. Cai, J. Kingery and S. J. Wineman, "Resin Flow/Fiber Deformation Experiments," *SAMPE Quarterly,* 17(4), 54 (1986)

[15] T. G. Gutowski, Z. Cai, S. Bauer, D. Boucher, J. Kingery and S. Wineman, "Consolidation Experiments for Laminate Composites," *Journal of Composite Materials,* 21, 650 (1987)

[16] R. Lam and J. L. Kardos, "The Permeability and Consolidation of Graphite Fibers During Processing of Composites," *Proc. Pol. Mat. Sci. Eng. (ACS),* 57, 532 (1987)

[ ]

[17] A. R. Wedgewood and D. C. Grant, "Autoclave Processing of Condensation Polyimide Composite Based on Prepregs of Avimid K," *34th International SAMPE Symposium,* 34, 1 (1989)

[18] E. D. Wachsman and C. W. Frank, "Effect of Cure History on the Morphology of Polyimide: Fluorescence Spectroscopy as a Method for Determining the Degree of Cure", *Polymer,* 29, 1191 (1988)

[19] J. T. Hartness, "An Evaluation of a High Temperature Thermoplastic Polyimide Composite", *32nd International SAMPE Symposium,* 32, 154 (1987)

[20] F. S. Cheng, J. L. Kardos and T. L. Tolbert, "One Way to Strengthen Graphite/Polycarbonate Composites," *SPE Journal,* 26, 62, (August 1970)

[21] P. Cebe, "Non-Isothermal Crystallization of Poly(Etheretherketone) Aromatic Polymer Composite," *Polymer Composite,* 9(4), 271 (August 1988)

[22] W. T. Whang and S. C. Wu, "The Liquid Crystalline State of Polyimide Precursors," *Journal of Polymer Science: Part A: Polymer Chemistry,* 26, 2749 (1988)

[23] S. A. Johnson and N. K. Roberts, "New Insights into Chemistry and Processing of Condensation Curing Graphite/Polyimide Composites, *32nd International SAMPE Symposium,* 32, 868 (1987)

[24] R. Randall, "Process Development: Autoclave Curing of a Condensation Polyimide/Carbon Fiber Prepreg," *20th International SAMPE Technical Conference,* 531, (Sept. 27-29, 1988)

[25] J. L. Kardos, M. P. Duduković, Yubo Yang and I. S. Yoon, "Part II: Condensation Reaction Void Modeling" in "Processing Science of Thermoplastic Composites", J. E. Kurz and J. L. Kardos, Air Force Contract *No. F33615–85–C–5046*, Final Technical Report, Air Force Materials Laboratory, Wright-Patterson AFB, 1 January 1987 – 31 December 1989.

[26] A. R. Wedgewood, "Autoclave Processing of Condensation Polyimide Composites Based on Prepregs of Avimid K-III", *19th International SAMPE Technical Conference*, 19, 420 (1987)

[27] *Kulite Miniature IS^R Silicon Diaphragm Pressure Transducer Catalog (bulletin KS-1000)*, Kulite Semiconductor Products, Inc., Ridgefield, New Jersey

[28] H. Murooka, M. Kyooi and H. Murakami, "Voids in Multilayer Printed Circuit Boards by Thermal Pressing Adhsion: A Study of the Causes," *Proceedings of ANTEC,* 47, 382 (1989)

[29] T. W. Kim, E. J. Jun and W. I. Lee, "Compaction Behavior of Thick Composite Laminates During Cure," *Proceedings of Annual International SAMPE Symposium,* 34, 15 (1989)

[30] D. W. Taylor, "Fundamentals of Soil Mechanics," J. Wiley and Sons, New York, (1948)

[31] K. Terzaghi, *Akad. Wiss. Wein. Mathem. Nuturw. Kl.,* Abt. IIa, 132 (1923)

[32] T. W. Lambe and R. V. Whitman, "Soil Mechanics," J. Wiley and Sons, New York, (1969)

[33] R. Srivastava, S. Munjal and M. P. Duduković, *Unpublished results*

9. VITA

Biographical items on the author of the dissertation, Mr. In Seon Yoon.

1. Born on January 5, 1957.
2. Attended Seoul National University, Seoul, Korea from March, 1975 to February, 1979. Received the degree of Bachelor of Science in Chemical Engineering (Cum Laude) in February, 1979.
3. Attended Korea Advanced Institute of Science and Technology, Seoul, Korea from March, 1979 to February, 1981. Received the degree of Master of Science in Chemical Engineering in February, 1981.
4. Attended Massachusetts Institute of Technology, Boston, U.S.A. from January 1983, to December, 1983. Received the Certificate in Center for Advanced Engineering Study.
5. Research Engineer, Research & Development Center, Sunkyong Industries, Suwon, Korea from March, 1981 to August, 1986. Promoted to Senior Research Engineer in February, 1985.
6. Attended Washington University in St. Louis from September, 1986 to the present date. Awarded a Fellowship in the academic year 1986-1987.
7. Research Assistant at Materials Research Laboratory at Washington University since September 1987 to the present date.
8. Membership in Professional Societies. SPE, SAMPE.

May 1990